論文 / 著書情報
Article / Book Information

題目(和文)	酸化マグネシウム／水系ケミカルヒートポンプのための伝熱促進複合材料に関する研究
Title(English)	A Study on Heat Transfer-Enhanced Composites for a Magnesium Oxide/Water Chemical Heat Pump
著者(和文)	マッシミリアーノ ザメンゴ
Author(English)	Massimiliano Zamengo
出典(和文)	学位:博士(工学), 学位授与機関:東京工業大学, 報告番号:甲第9477号, 授与年月日:2014年3月26日, 学位の種別:課程博士, 審査員:加藤 之貴,池田 泰久,高橋 実,竹下 健二,矢野 豊彦
Citation(English)	Degree:Doctor (Engineering), Conferring organization: Tokyo Institute of Technology, Report number:甲第9477号, Conferred date:2014/3/26, Degree Type:Course doctor, Examiner:,,,,
学位種別(和文)	博士論文
Type(English)	Doctoral Thesis

A Study on Heat Transfer-Enhanced Composites for a Magnesium Oxide/Water Chemical Heat Pump

Doctoral thesis – Academic year 2013-2014

Author: **Massimiliano Zamengo**

Supervisor: **Assoc. Prof., Dr. Yukitaka Kato**

Department of Nuclear Engineering

Graduate school of Science and Engineering

Tokyo Institute of Technology

Table of contents

Massimiliano Zamengo, Y. Kato Laboratory, RLNR, Tokyo Institute of Technology

A Study on Heat Transfer-Enhanced Composites for a Magnesium Oxide/Water Chemical Heat Pump

Chapter 1

Introduction

1. INTRODUCTION

1.1. Background of research

1.1.1. Demand of primary energy for industry

The worldwide growing demand of energy is raising concerns about sustainability. Especially in the developing countries, industrialization and business opportunities are rapidly shifting the populations into a different lifestyle, which requires as much energy as in the developed ones. Industry is a sector which is a large primary energy consumer. The energy consumption will account for about 30% of the total demand of primary energy [1]. A better utilization of primary energy would be beneficial to the whole system and will ensure a sustainable development of societies.

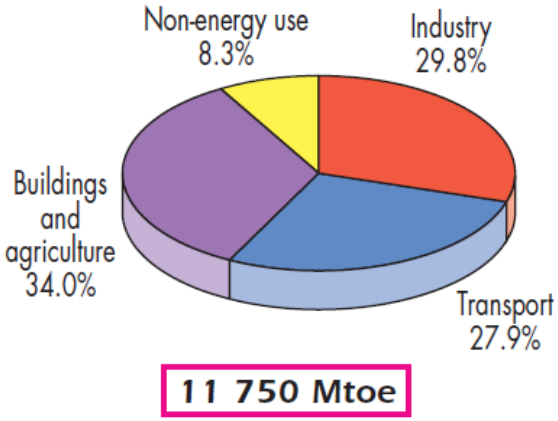

Fig. 1.1 Total final consumption of primary energy by sector in 2035 (with actual policies) [1]

1.1.2. Industrial cogeneration and energy management

Combined heat and power generation allows to utilize primary energy with very high efficiency, in some cases even over 80% in enthalpy base. Such a technology is already well common for some industries, like steel making, oil refining, production of chemicals and so on. Those industries are characterized by a different profile of energy utilization, which depends generally on the production process, with peaks of demand variable with time. It may happen that some amounts of heat cannot be used, or there is a mismatch between electricity and heat loads demanded. This is exemplified on Fig.1.2. In such cases, heat is usually rejected and wasted in the environment. It is possible to operate the combined heat and electricity generation at partial load, however its efficiency would be decreased (it is maximum at the design condition of 100% load). In the future, in order to harvest, store and reutilize surplus amounts of heat, a heat storage technology is necessary. This technology would be suitable for avoiding operating the combined generator at partial loads with lower efficiency. During low demand, heat would be stored and reutilized later during the peak demand. Moreover, wishing to decrease the utilization of fossil fuels as sources of primary energy, a new generation of cogenerators would be based on nuclear reactors. As it may become complicated to modify the thermal power output of a nuclear reactor, the possibility to let it operate at steady state and utilize a heat buffer would be advantageous.

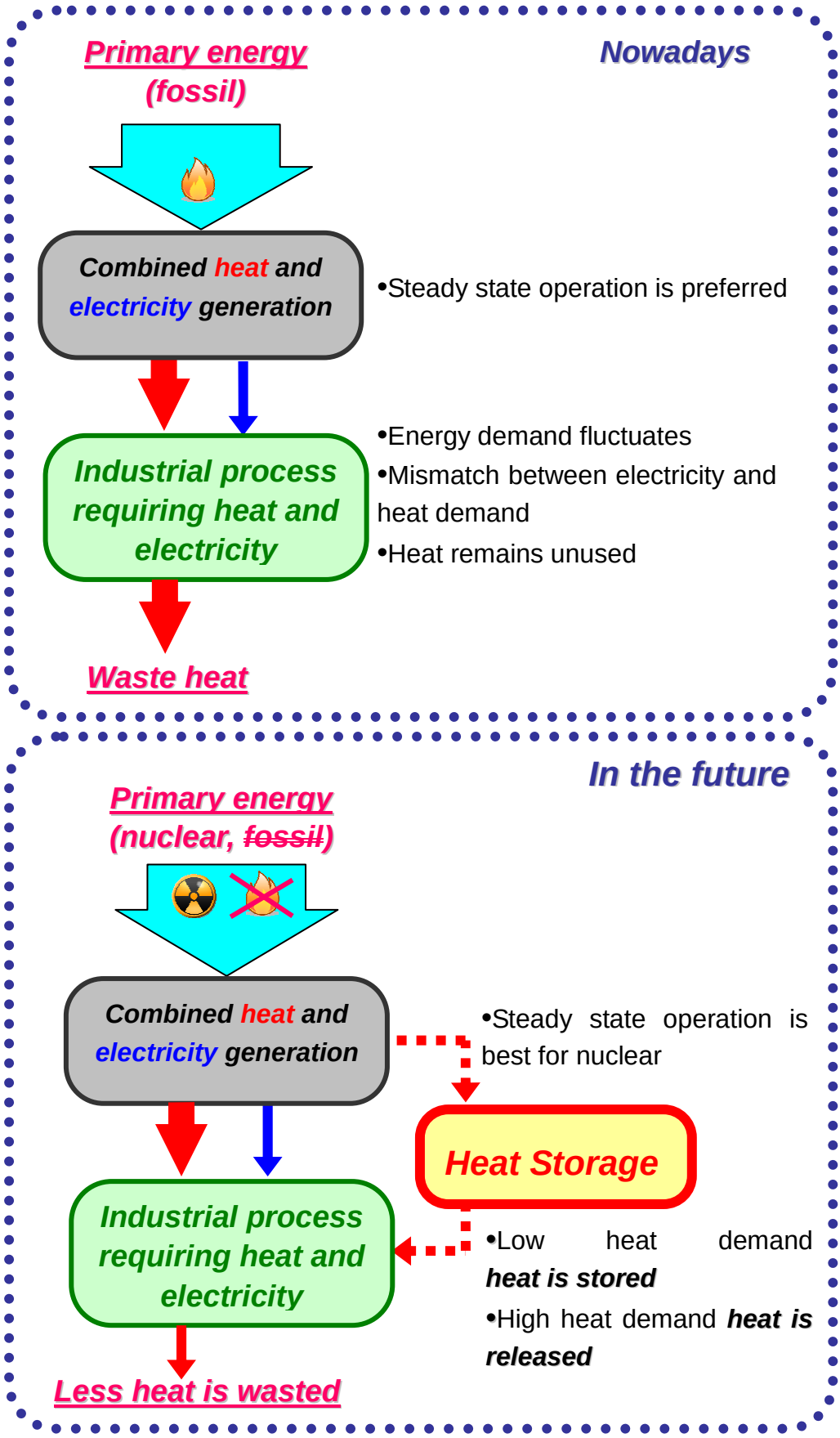

Fig. 1.2 Example of industrial clusters and energy management of thermal and electrical energy

1.1.3. Small nuclear reactor and combined heat and power for the industry

Smaller sized nuclear reactors were instrumental during the pioneering days of commercial nuclear power to facilitate the development and demonstration of early reactor technologies and to establish operational experience for the fledgling nuclear power industry. Deliberately small reactors offer substantial benefits in safety, security, operational flexibilities and economics, and they are well positioned to figure prominently in the second nuclear era (Ingersoll, 2009) [2]. *Small nuclear cogenerating reactors may be suited to support existing process heat markets since their smaller sizes align well with the capacity requirements of process industries. Recently, there has been a renewed interest in small and medium-sized reactors (SMR) due to their low carbon generation, simpler design, more affordable economics, job creation, and possibility for new international market opportunities. These concepts are being pursued to support small utilities, countries with financing or infrastructure constraints, distributed power markets, and process heat customers. SMR designs developed some decades ago were not successful since the economy of size was the prevailing approach for nuclear power production. In a future energy mix with more small scale and intermittent production from renewable energy systems (RES), SMRs have the potential to become an important player. SMRs may be better suited for the flexible operation needed to balance RES variability. The heat demand over a range of temperatures for various European industries is presented in Fig. 1.3. About 60% of the heat demand is for low (<100℃) to moderate temperatures (100–400℃). The processes with the highest temperature demands can be found in the basic metal, chemical (both heat supply and as feedstock), and non-metallic minerals branches*. (J.Carlsson, 2012) [3], (P. G. Kosky, 1981) [4].

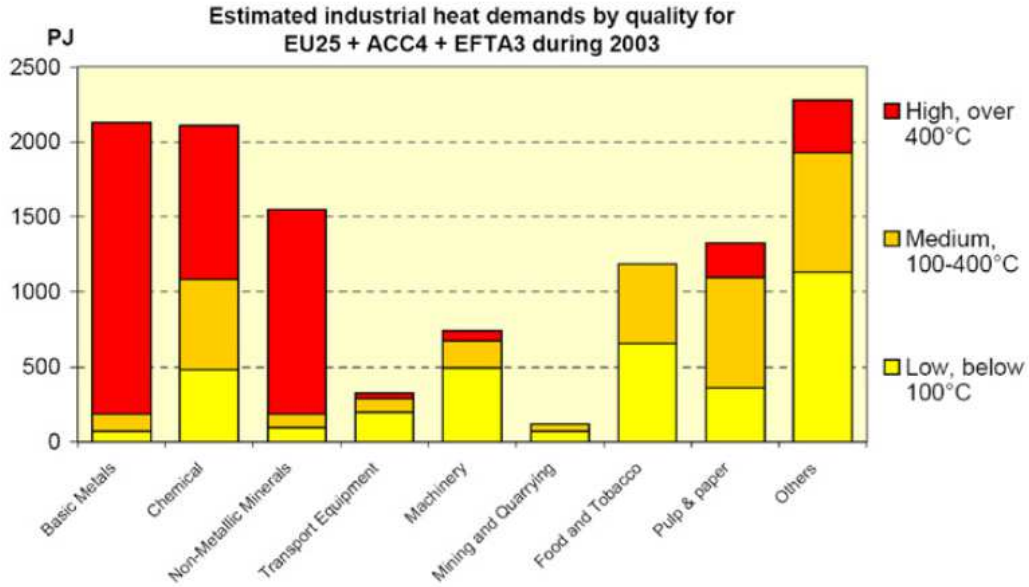

Fig. 1.3 Industrial heat demands estimated by temperature and manufacturing branch for 32 countries (EU27+EFTA+Croatia+Turkey) in Europe. (The figure is based on experience from the German industry reported in (AGFW, 2005) and applied on an IEA database for the target area (EUROHEATCOOL, 2006) [3]).

The possibility to utilize a heat storage technology in a cogenerating nuclear power station would

make easier to manage the load variations caused by the instabilities derived from production cycles or balancing the RES variability, actively contributing to the operations of a 'smart grid'. This is particular advantageous because nuclear power station are generally more suitable for operation at steady state rather than load following.

1.2. Chemical heat storage

1.2.1. Principle of chemical heat storage

Chemical heat storage is a relatively young research field but it is recently attracting the interest of industry. One of the main difficulties is given by the materials, their properties, energy density (heat that can be stored per unit mass or volume), durability, human health and environmental issues

The theory of chemical heat storage and chemical heat pump (CHP) were discussed since the '70, at first as storage of solar heat [5] and later for refrigeration purposes [6]. Since then, many progresses have been done, but these technologies are not well industrialized yet.

The general principle of chemical heat pump cycle is given in Fig.1.4. It is a four-temperature cycle based on a reversible chemical reaction and can operate two kinds of transformations, as shown on the Clausius-Clapeyron plots on Fig. 1.4(a) and 1.4(b). The lines represent the equilibrium of the chemical reaction and of water evaporation. Those are expressed by:

$$\ln K = \ln\left(\frac{P}{P_0}\right) = -\frac{\Delta H}{RT} + \frac{\Delta S}{R} \qquad (1)$$

where K is equilibrium constant, P the equilibrium pressure, ΔH and ΔS are the enthalpy change and entropy changes by reaction, respectively.

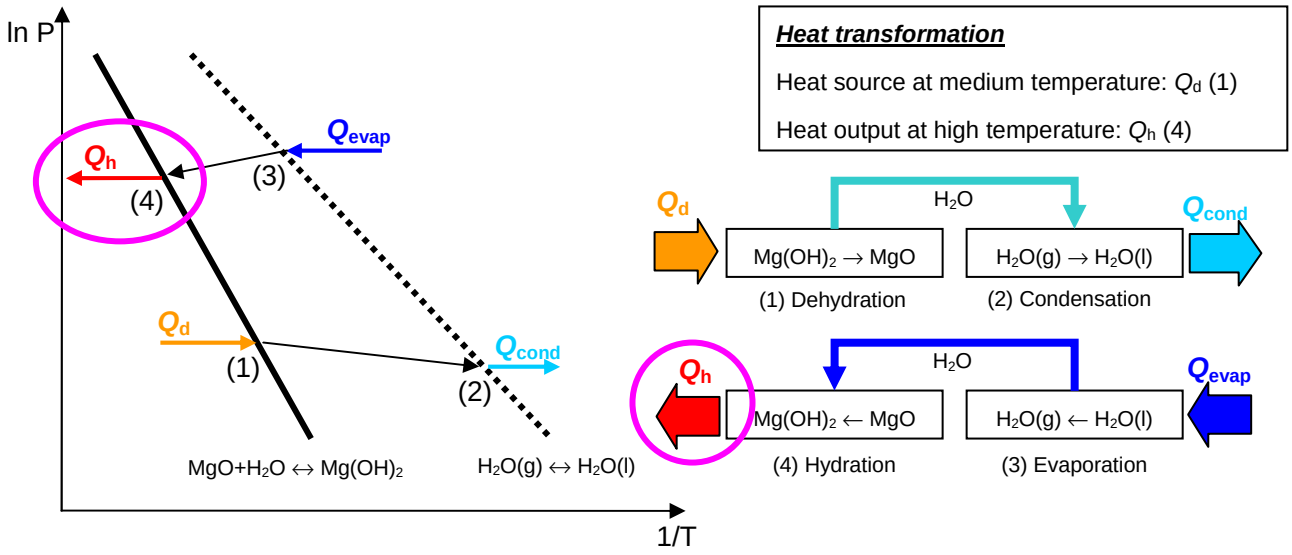

Fig. 1.4(a) Utilization of chemical heat pump principle for heat transformation (from middle to high temperature)

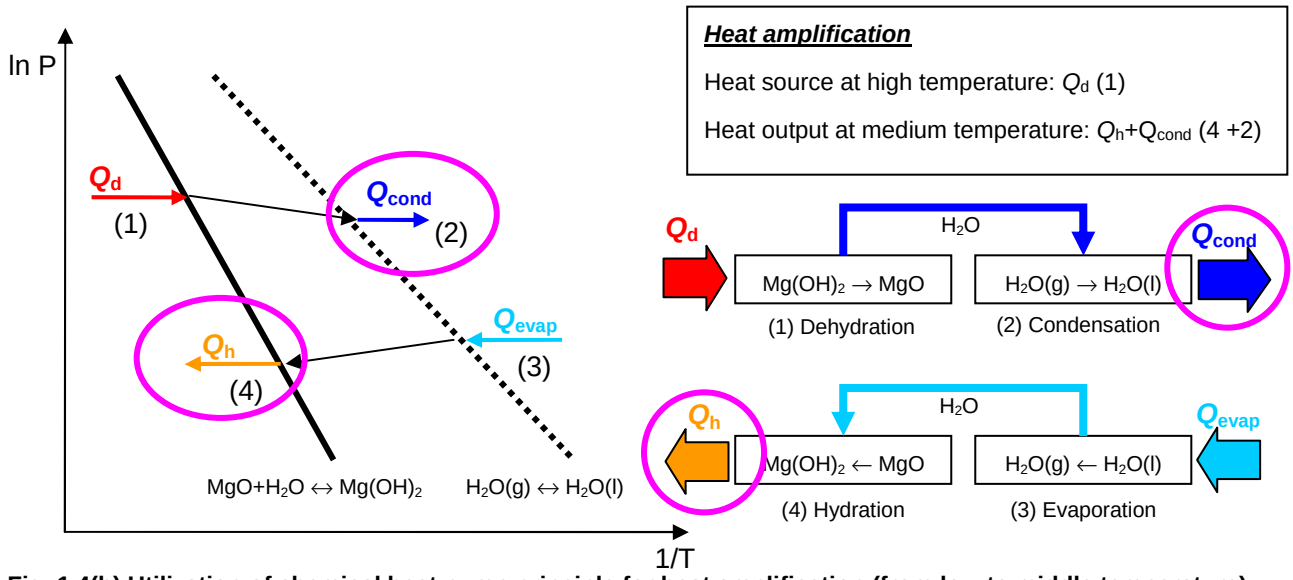

Fig. 1.4(b) Utilization of chemical heat pump principle for heat amplification (from low to middle temperature)

Fig. 1.4 The principles of the chemical heat pump showed on Clausius-Clapeyron diagrams

In this work the chemical heat pump is based on Magnesium Oxide (MgO) and Water (H_2O) adsorption and desorption reaction, but the principle is valid also for other couples of materials, like Calcium Oxide (CaO) and H_2O [7] or Cobalt Chloride ($CoCl_2$) and ammonia (NH_3) [8]. Fig.1.4(a) shows that it is possible to operate the "heat transformation" from medium temperature to high temperature. Fig.1.4(b) shows how to operate the "heat amplification" from low temperature to medium temperature. In both the figures, the new utilizable outputs are highlighted with a purple circle.

For the MgO-H_2O CHP system, the equilibria are expressed as follows:

$$MgO(s) + H_2O(g) \leftrightarrow Mg(OH)_2(s) \qquad \Delta H°_r = -81.0 \text{ kJ mol}^{-1} \qquad (2)$$

$$H_2O(g) \leftrightarrow H_2O(l) \qquad \Delta H°_{pc} = -41.0 \text{ kJ mol}^{-1} \qquad (3)$$

The leftward reaction in (2) is the Magnesium hydroxide ($Mg(OH)_2$) dehydration. Fig. 1.5 shows the operation mode of the MgO-H_2O chemical heat pump with example operation temperatures. It is an endothermic reaction and corresponds to the heat-storage mode of the CHP system, as shown in Fig. 1.5(a). The rightward reaction in (2) is MgO hydration. It is an exothermic reaction and corresponds to the heat-output mode of the CHP system, as shown in Fig. 1.5(b).

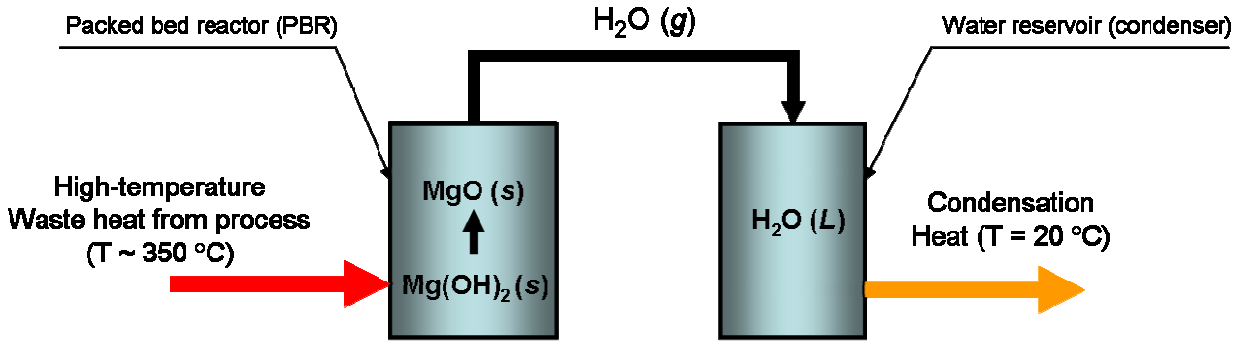

Fig. 1.5 (a) The dehydration reaction of the packed bed reactor CHP (heat storage mode)

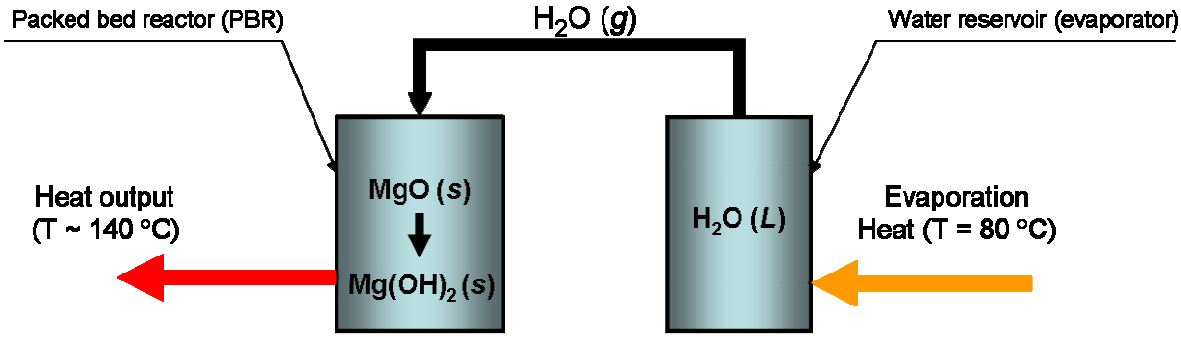

Fig. 1.5(b) The hydration reaction of the packed bed reactor CHP (heat output mode)

Fig. 1.5 The operation mode of the MgO-H_2O chemical heat pump with example operation temperatures

The dehydration reaction occurs at temperature higher than 350°C. Therefore, its application is attractive for the recovery of waste heat in industrial processes [9] such as steel making [10], or for the storage of heat and load leveling in thermal power stations, whether fuelled by fossil fuels [11], nuclear [12], or solar energies [13-14]. Another possible application on a smaller scale involves the use of this material for thermal storage to simultaneously minimize the energy consumption and pollutants from automobile engines during cold starts [15]. Because it is a chemical reaction, the ΔH^{o}_{1} (1,390 kJ kg^{-1}) is relatively high compared to other common energy storage materials, named phase changing materials (PCM), for which the ΔH corresponds to the heat of phase change from solid to liquid and vice versa. Examples of PCM are inorganic salts (like KNO_3, $MgCl_2$ and many others). In general, the latent heat of fusion for these materials ranges between 150 and 400 kJ kg^{-1} [16]. The operability of $Mg(OH)_2$ as a chemical heat storage material and chemical heat pump operation was investigated by Kato [17]. The experimental investigation was conducted on several apparatuses [18-19]. The studies included the

determination of reaction kinetics of hydration and durability to cyclic dehydration and hydration [20-21]. The thermochemical performance was determined on packed bed experiments [22], in which it was possible to operate the hydration at a pressure larger than what possible on a thermo gravimetric apparatus.

All of the solid – gas couples for the reaction have similar energy efficiency. We can define it as

$$\eta = \frac{\sum Q \text{ as input in the system}}{\sum Q \text{ as output in the system}} \qquad (1.1)$$

For understanding the values of efficiency achievable, the following scheme in Fig. 1.6 will be used are reference.

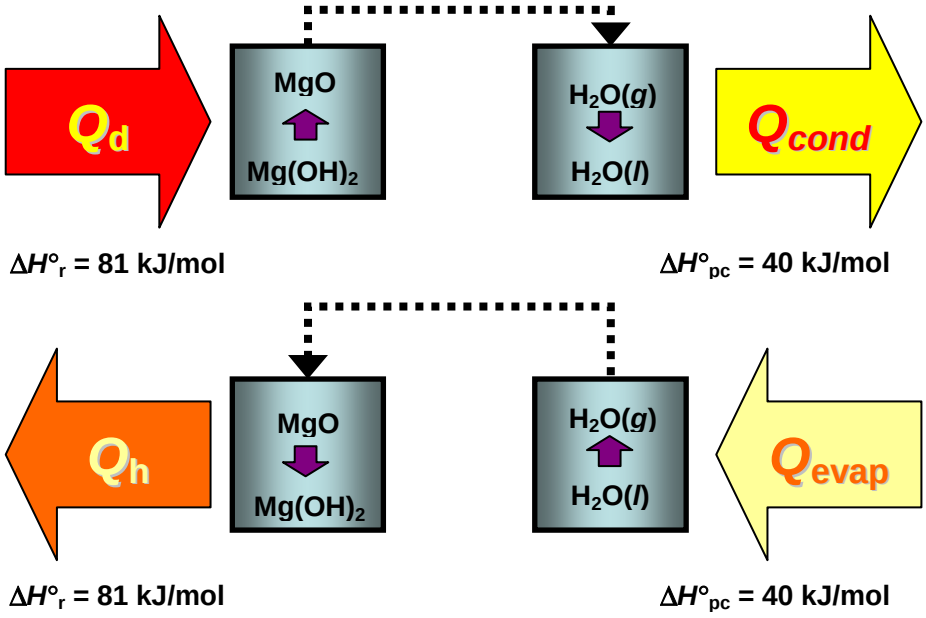

Fig. 1.6 Scheme for evaluation of the MgO-H_2O chemical heat pump efficiencies

For example, it might be possible to reutilize or not the condensation heat during the heat storage mode. Moreover it is necessary to supply the evaporation heat Q_{evap} at a temperature $T_{evap} > T_{cond}$. Depending on the industrial process, those Q_{cond} and Q_{evap} might be required or available, respectively. In the worst case they are respectively not used or supplied by a different source. When introducing the numerical values of $Q_d = -Q_h = +81$ kJ mol^{-1} or $Q_{cond} = -Q_{evap} = -40$ kJ mol^{-1}, the values on table 1.1 are obtained. Depending on the availability of Q_{evap} and the possibility to utilize Q_{cond}, the efficiency can vary from 1.5 (real heat pump mode) to 0.67.

Table 1.1 Values of efficiency of the chemical heat pump system under several conditions of heat recovery

	Q_{cond} is used	***Q_{cond} is not used***
Q_{evap} is available as waste heat	$\eta = \frac{Q_h + Q_{cond}}{Q_d} = 1.5$	$\eta = \frac{Q_h}{Q_d} = 1$
Q_{evap} is not available as waste heat	$\eta = \frac{Q_h + Q_{cond}}{Q_d + Q_{evap}} = 1$	$\eta = \frac{Q_h}{Q_d + Q_{evap}} = 0.67$

1.2.2. Development of material for chemical heat storage

Despite the potentials already mentioned, chemical heat storage is still difficult to be utilized in a practical application because of two heat transfer issues. Those are the low value of thermal conductivity of $Mg(OH)_2$ and MgO and the contact resistance between material and heat exchanger surface. Heat transfer mechanisms between packed bed reactor and heat exchanger for chemical heat pump are exemplified in Fig. 1.7, respectively for particle-type packed bed (a) and blocky type packed bed (b):

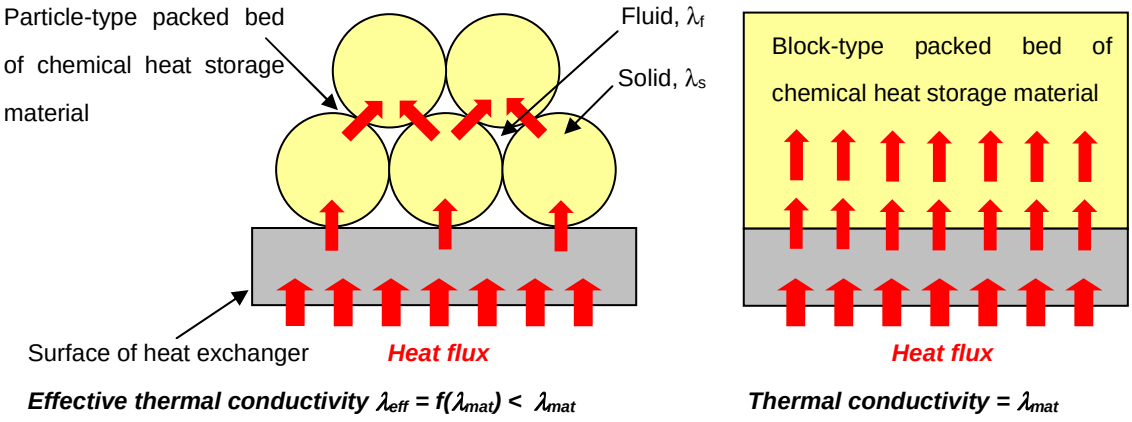

Fig. 1.7 Heat transfer mechanism between packed bed reactor and heat exchanger for chemical heat pump: (a) particle reactant, (b) Block-type reactant.

When heat transfer in bed of particles is considered, it will depend on the value of *effective* thermal conductivity, λ_{eff}. Its value depends on several parameters, which are mainly the thermal conductivity of solid phase material, λ_s, the thermal conductivity of the fluid between the particles, λ_f, and the void fraction, ε. There exist in literature many methods and equations for determining the effective thermal conductivity of packed beds, which include also other parameters, like the shape of the particles constituting the bed in Fig. 1.7 (a). Another limitation to heat transfer is given by the contact resistance between particles of the bed and the wall of the heat exchanger. A continuous tight contact would be preferable for an optimal supply or removal of heats of reactions. It is therefore necessary to develop:

1. a material with high thermal conductivity λ
2. to shape the material in order to achieve a continuous contact with heat exchanger's surface.

However, even if we increase the thermal conductivity of the material, the effective thermal conductivity might be still small. The void between particles must be reduced. As a consequence, the energy density (material per unit volume) would also be increased. The possibility to create a bulk composite with suitable gas permeability would allow including all the features required for a practical application in Fig. 1.7 (b).

Expanded graphite (EG) is a commonly employed material to enhance the heat transfer properties of chemical heat pump materials. Many researchers [23-25] mixed their original reagents with EG or other carbon materials (active carbons of carbon fibers). Porous blocks were manufactured and tested into experimental apparatuses, as in [26-27]. Some researchers prefer to maintain a high porosity in order to enhance the reactivity, but in this way thermal conductivity and heat storage capacity cannot achieve large values. On the other hand, a strong compression of the composite would increase the thermal conductivity of material almost hundred of times, but the operation at low pressure would be impractical because of the low gas permeability [28]. In other words, mass diffusion into a compressed block would be difficult and the performance of the system too poor. The optimization of mixing ratio between EG and density of material is required.

1.3. Objective

1.3.1. Development of a new composite material

In this work, a mixing method for the preparation of a $Mg(OH)_2$/EG composite was developed. This material was called EM from the initials of Expanded graphite and Magnesium hydroxide. The feasibility of different kind of EM mixtures (stability of performance and durability) was evaluated experimentally. Requirements of the preparation method are production simplicity, possibility to be suitable for a mass production and non hazardousness for the environment. This research aimed to develop a high performance material which could be used in practical application. It is required that such a material has the ability to respond promptly to load variations, therefore exchange large quantities of heat in a short time. It is therefore necessary to improve the heat transfer properties. Another key-point is the possibility to create stable figures (tablets or blocks) which can fit different configurations of heat exchangers. Last but not least, the heat storage capacity has to be large in order to reduce the size of equipment, therefore the cost, and become more attractive for a practical utilization and further development.

1.3.2. Experimental investigations and characterization of the EM composites

From a cross comparison of reaction rate constant and energy storage capacity, it was determined which is the optimal mixing mass ratio for the preparation of EM. It was also understood that it was necessary to further increase the heat storage capacity of the system, because the presence of EG decreased the volume available for $Mg(OH)_2$ in the reactor. This improvement was achieved by

tight packing the EM tablets in the reactor. As a final step, dehydration and hydration were investigated in a compressed block of EM having the same size of the reactor. Thermal conductivity of chemical heat storage materials were also measured in function of density and mass mixing ratio.

1.3.3. Numerical analysis of heat transfer with chemical reactions

The discussion of the experimental results was supported by a numerical analysis. A bi-dimensional numerical heat transfer model written in FORTRAN was complied and compared with experimental results. After verifying its good prediction of results (temperature and reacted fraction), it was possible to utilize it for local investigations in the packed bed reactor. This tool resulted useful to understand how heat transfer could enhance the chemical reaction by an improved distribution of heat in the packed bed.

1.3.4. Combination of chemical heat storage with a Rankine cycle of a small nuclear power station

The possibility to have an energy storage device in a nuclear thermal power station would make easier to manage the load variations caused by:

- the instabilities derived from the mismatch of electricity and heat demand in cogeneration systems;
- the instabilities derived from the utilization of renewable sources.

From the experimental results of heat storage capacity and heat power output, it was possible to estimate the amounts of $Mg(OH)_2$ and EM required for the peak shaving of electricity in a nuclear power station. A Rankine cycle in the power station has been modified to include a chemical heat storage reactor. The range of admissible variation of electrical power output from the steam turbine was estimated from the enthalpy and mass balances under the heat storage and heat output operation modes, respectively.

1.3.5. Research originality

This is the first attempt to use a composite of $Mg(OH)_2$ and EG in a compressed form. Previous studies on such a composite were conducted on a small scale (thermo-gravimetric experiment on uncompressed composite, sample mass of approximately 40 mg, Kim et al. [29]). The apparatus used in this work has a larger scale than in [29] (the mass of the packed bed is approximately 40 g). In this way it was possible to investigate the behavior of the composite in an environment nearer to the practical utilization. The compression of the composite in figures of tablets allowed increasing the thermal conductivity and the heat storage capacity of the system. Differently from thermo-gravimetric experiments, it was possible to investigate the hydration reaction at pressure larger than atmospheric.

1.4. Structure of thesis

In **Chapter 1**, the background of the research was explained. The principles of MgO / H_2O chemical heat pump was explained in detail. Several examples of application of this technology are

introduced, in particular the management of heat for industrial clusters using cogeneration systems. The main issues of the technology (energy density, thermal conductivity, contact resistance with heat exchangers' surface, gas permeability) were introduced. The object of this work is the development of a new composite of $Mg(OH)_2$ and expanded graphite (EG), characterized by an enhancement of thermal conductivity.

In **Chapter 2**, the experimental apparatus and procedures will be explained. The main investigation has been conducted using a packed bed reactor apparatus. Thermo gravimetric apparatus was used for studying the reaction kinetics and evaluate the reaction rate constants. Other properties as specific heat capacity and thermal conductivity were measured with a differential scanning calorimeter (DSC) and a quick thermal conductivity meter, respectively. The definition of thermochemical performance parameters, like heat storage capacity/gross heat output/mean heat output rate, will also be given.

In **Chapter 3**, the materials used in the experiments will be described. Then, the preparation method of EM composite will be explained. SEM photographs will help to demonstrate the effective attachment between $Mg(OH)_2$ and EG. It will be shown the originality and strength points of the compressed EM, like mold ability, high thermal conductivity and endurance to repetitive cyclic reactions.

In **Chapter 4**, the results obtained from the packed bed reactor experiments (dehydration and hydration) will be shown. From the evaluation of performances it was identified which was the optimal mixing ratio. It will be demonstrated that thermal conductivity and heat storage capacity/output could be increased by different configurations of the packed bed materials. Hydration performance was evaluated also for pressures higher than what is achievable by using the thermo-balance apparatus.

In the first part of **Chapter 5**, it will be set up a problem of transient heat conduction with heat sink (heat storage) for numerical simulation of the dehydration experiment in the packed bed reactor. At first, the properties of materials (thermal conductivity and specific heat capacity) in the dehydrated state will be shown in order to write the equations of property change in function of the advancement of the chemical reaction. Then, the equations of heat transfer will be formulated, together with the explanation of the method used for the calculations. A comparison between experimental results and numerical simulations will be presented. It will be finally analyzed the reaction advancement and thermochemical performance in correspondence of some representative positions in the packed bed reactor.

In **Chapter 6**, the utilization of the chemical heat storage for thermal load leveling in power station will be discussed. It will be described a model of a system including the Rankine cycle of a nuclear power plant and a chemical heat storage reactor. The analysis will be done by using experimental data of heat storage and heat output from the packed bed reactor experiments. The electrical power variation and thermal energy stored will be quantified and it will be concluded that EM can contribute effectively in the thermal load leveling.

In **Chapter 7**, the results will be summarized and the conclusions of this research will be stated.

.

1.5. References

[1] Key world energy statistics 2013, International Energy Agency, http://www.iea.org/publications/freepublications/publication/KeyWorld2013_FINAL_WEB.pdf,

[2] D.T. Ingersoll, Deliberately small reactors and the second nuclear era, Progress in Nuclear Energy, 51 (2009) 589-603

[3] J.Carlsson, D. E. Shropshire, A. van Heek, M. A. Fütterer, Economic viability of small nuclear reactors in future European cogeneration markets, Energy Policy, 43 (2012), 396–406

[4] P. G. Kosky, J. W. Flock, C.s M. Mc Farland, Nuclear process heat-application to fuels and chemical production, Nuclear Engineering and Design 66 (1981) 343-355

[5] H. W. Prengle Jr, C.H. Sun, Operational chemical storage cycles for utilization of solar energy to produce heat or electric power, Solar Energy, 18 (1976), 561-567

[6] W. Wongsuwan, S. Kumar, P. Neveu, F. Meunier, A review of chemical heat pump technology and applications, Applied Thermal Engineering, 21 (15) (2001), 1489-1519

[7] S. Fujimoto, E. Bilgen, H. Ogura, CaO/Ca(OH)$_2$ chemical heat pump system, Energy Conversion and Management, 43 (7) (2002), 947-960

[8] J. Trudel, S. Hosatte, M. Ternan, Solid–gas equilibrium in chemical heat pumps: the NH_3–$CoCl_2$ system, Applied Thermal Engineering, 19 (1999), 495-511

[9]J. Yagi, T. Akiyama, Storage of thermal energy for effective use of waste heat from industries, Journal of Materials Processing Technology, 48 (1995), 793-804

[10] R.C. McKenna, J.B. Norman, Spatial modelling of industrial heat loads and recovery potentials in the UK, Energy Policy, 38 (10), (2010), 5878-5891

[11] M.K. Drost, Z.I. Antoniak, D.R. Brown, S. Somasundaram, Central station thermal energy storage for peak and intermediate load power generation, Energy, 17 (2), (1992), 127-139

[12] H. Fenech, R.J. Saunders, Application of heat storage reservoirs to improve the performance of Brayton cycle nuclear power plants with atmospheric heat rejection, Annals of Nuclear Energy, 16 (4) (1989), 203-209

[13] M. Wierse, R. Werner, M. Groll, Magnesium hydride for thermal energy storage in a small-scale solar-thermal power station, Journal of the Less Common Metals, 172–174 (3) (1991), 1111-1121

[14] S. Kuravi, J. Trahan, D. Yogi Goswami, M.M. Rahman, E.K. Stefanakos, Thermal energy storage technologies and systems for concentrating solar power plants, Progress in Energy and Combustion Science, 39 (4) (2013), 285-319

[15] K. Darkwa, P.W. O'Callaghan, Green transport technology (GTT) analytical studies of a thermochemical store for minimizing energy consumption and air pollution from automobile engines, Applied Thermal Engineering, 17 (7) (1997), 603-614

[16] B Zalba, J Marin, L Cabeza, H Mehling, Review on thermal energy storage with phase change: materials, heat transfer analysis and applications, Appl. Therm. Eng., 23 (2003), pp. 251–283

[17] Y Kato, N Harada, Y Yoshizawa, Kinetic feasibility of a chemical heat pump for heat utilization of high-temperature processes, Applied Thermal Engineering, 19 (1999), pp. 239–254

[18] Y. Kato, F. Takahashi, A. Watanabe, Y. Yoshizawa, Thermal analysis of a magnesium oxide/water chemical heat pump for cogeneration – Applied Thermal Engineering 21 (2001) 1067-1081

[19] Y. Kato, N. Yamashita, Y. Yoshizawa, Study of chemical heat pump with reaction system of magnesium oxide/water, Kagaku Kogaku Ronbunshu, 19 (1993), 1213-1216

[20] Y. Kato, N. Yamashita, K. Kobayashi, Y. Yoshizawa, Kinetic study of the hydration of magnesium oxide for a chemical heat pump, Applied Thermal Engineering, 16 (11) (1996), 853-862

[21] Y. Kato, K. Kobayashi, Y. Yoshizawa, Durability to repetitive reaction system for a heat pump, Applied Thermal Engineering, 18 (3–4) (1998), 85-92

[22] Y. Kato, Y. Sasaki, Y. Yoshizawa, Thermal performance measurement of a packed bed reactor of a magnesium oxide/water chemical heat pump, Journal of Chemical Engineering of Japan, 36 (7) (2003), 833-839

[23] K. Fujioka, K. Hatanaka, Y. Hirata, Composite reactants of calcium chloride combined with functional carbon materials for chemical heat pumps, Applied Thermal Engineering, 28 (2008), 304-310

[24] M. Bonnissel, L. Luo, D. Tondeur, Compacted exfoliated natural graphite as heat conduction medium, Carbon, 39 (2001), 2151-2161

[25] G. Cacciola, G. Restuccia and L. Mercadante, Composites of activated carbon for refrigeration adsorption machines –Carbon, 33,9 (1995), 1205-1210

[26] S. Mauran, P. Prades, F. L'Haridon, Heat and mass transfer in consolidated reacting beds for thermochemical systems, Heat Recovery Systems & CHP, 13 (4) (1993), 315-319

[27] S. Mauran, H. Lahmidi, V. Goetz, Solar heating and cooling by a thermochemical process. First experiments of a prototype storing 60 kWh by a solid/gas reaction, Solar Energy 82 (2008), 623-636

[28] H.B. Lu, N. Mazet and B. Spinner, Modelling of gas-solid reaction--coupling of heat and mass transfer with chemical reaction, Chemical Engineering Science, 51, 15 (1996), 3829-3845

[29] S. T. Kim, J. Ryu, Y. Kato, Optimization of magnesium hydroxide composite material mixed with expanded graphite and calcium chloride for chemical heat pumps, Applied Thermal Engineering, 50, 1, (2013), 485-490

Massimiliano Zamengo, Y. Kato Laboratory, RLNR, Tokyo Institute of Technology

A Study on Heat Transfer-Enhanced Composites for a Magnesium Oxide/Water Chemical Heat Pump

Chapter 2

Experimental apparatus and procedure

2. EXPERIMENTAL APPARATUS AND PROCEDURE

2.1. Introduction

In this Chapter, the experimental apparatuses will be described in their details. The procedures and the experiment conducted will also be illustrated. They allowed investigations on the kinetic of chemical reactions and direct measurement of thermal properties.

2.2. Packed bed reactor apparatus

2.2.1. The apparatus

The experimental apparatus used for the experiments on packed beds of chemical heat storage material is shown in Fig.2.1 and 2.2. It consisted of a reaction chamber and water reservoir, connected by heated pipes and stop valves. The reactor containing the packed bed of chemical heat storage material (packed bed reactor, PBR) was placed at the center of the chamber, as shown in Figs. 2.3 and 2.4. In addition, Fig.2.3 shows the position of the seven thermocouples (K-type, sheath diameter of 1 mm) that were positioned in the PBR to measure temperature changes during reactions. Their small size and short response time is suitable for measuring the temperature variation of the chemical reactions under investigation. Heat for the $Mg(OH)_2$ dehydration was supplied through a sheath heater surrounding the reactor's external surface. The chamber was mounted on an electric balance: the reactor's weight changed because of the movement of water vapor from the packed bed to the water reservoir and vice versa during the reactions. Other thermocouples are used to control the temperature of the chamber and piping. Those are controlled by electronic thermostats and solid state relays.

After initial removal of residual gas from chamber and piping using a vacuum pump, the system is driven thermally with no mechanical pump work.

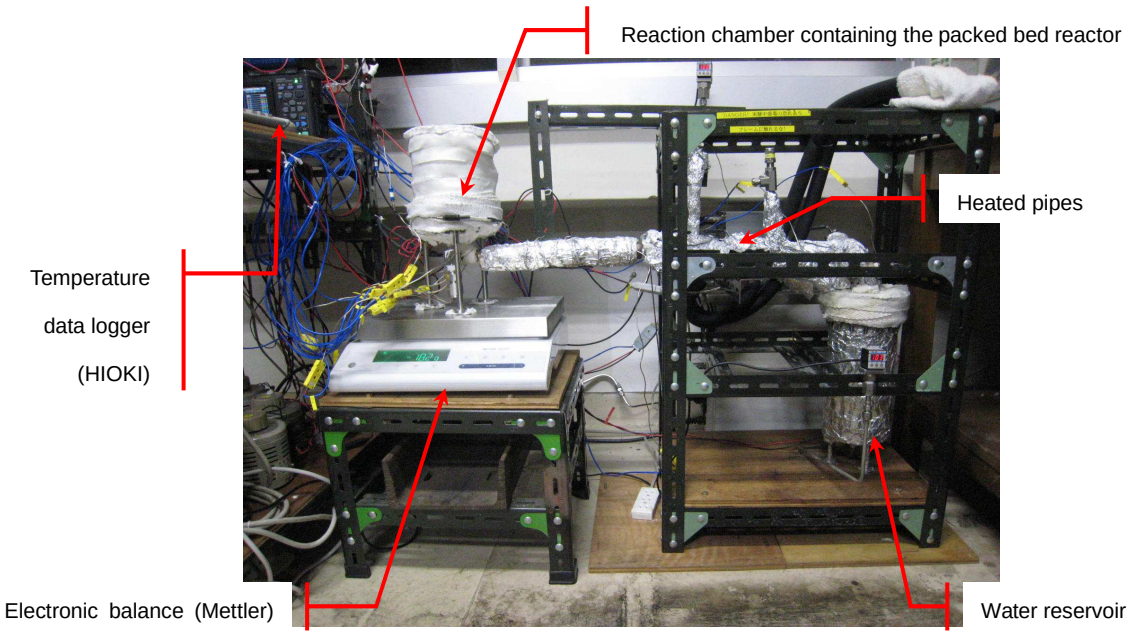

Fig. 2.1 The chemical heat pump apparatus

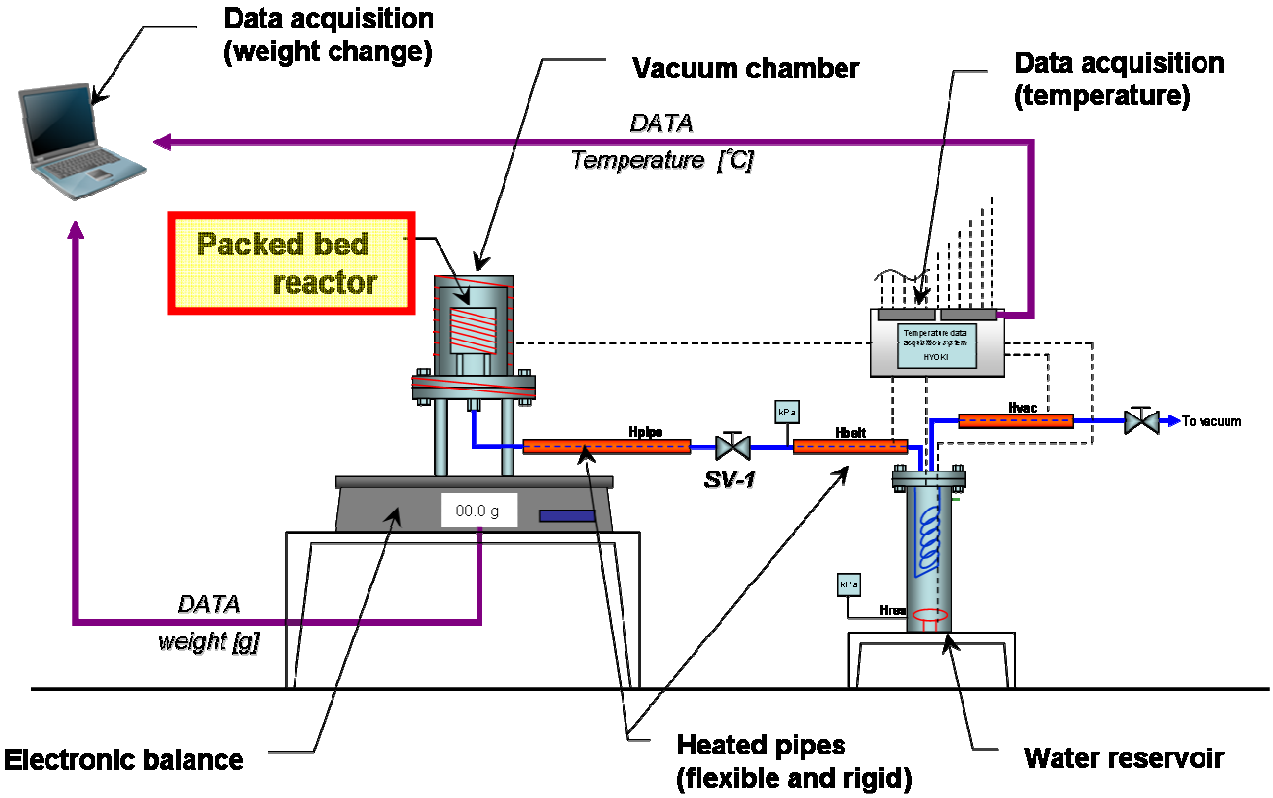

Fig. 2.2 Schematic diagram of experimental apparatus

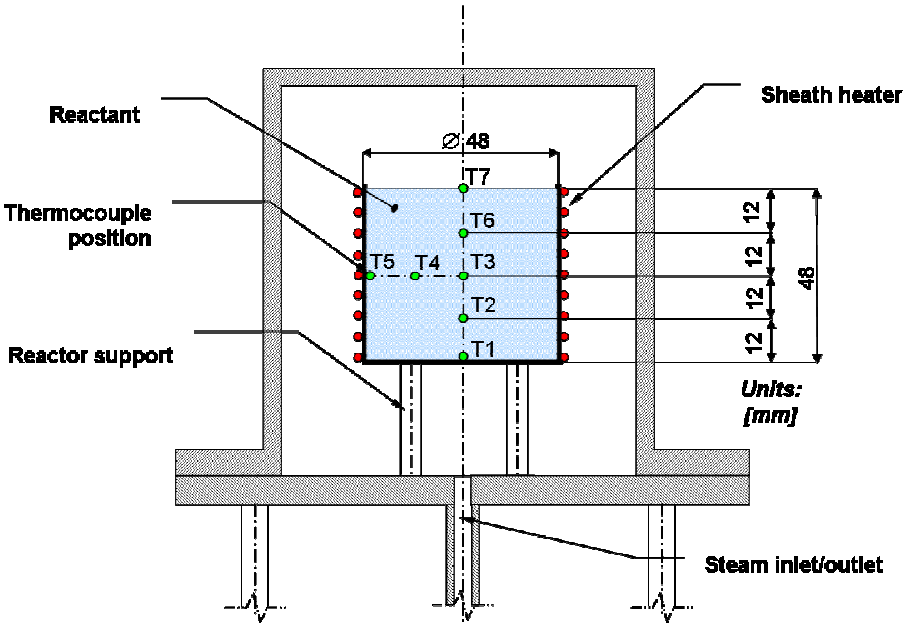

Fig. 2.3 Cross section of reaction chamber containing the packed bed reactor (green points show measurement points of thermocouples.

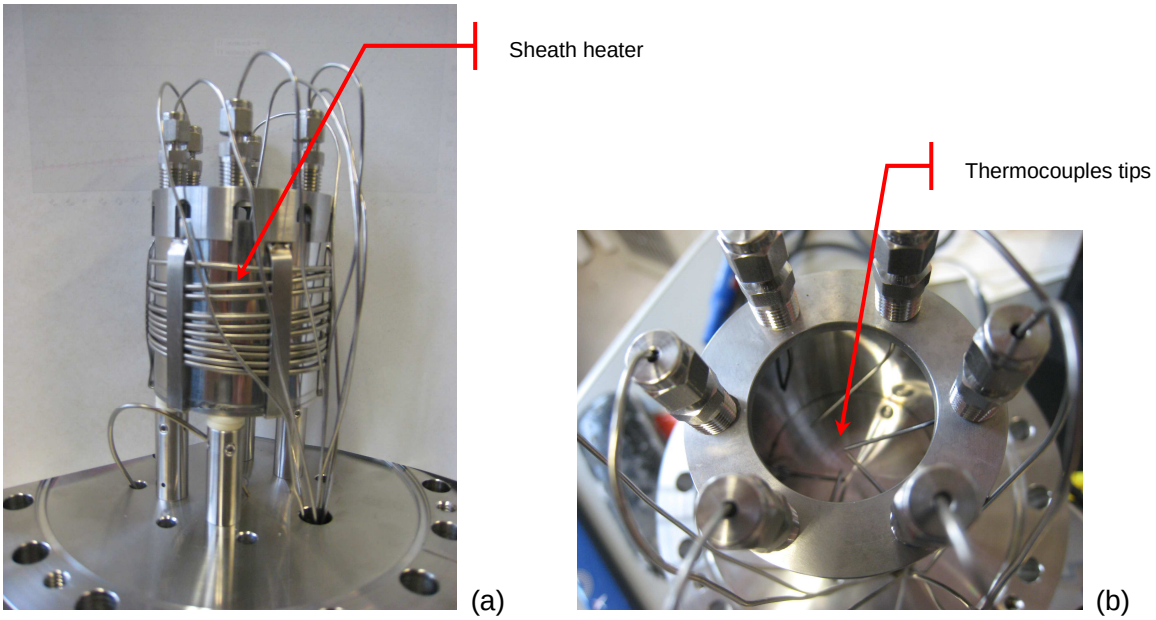

Fig. 2.4 The reactor a) outside view b) top view and thermocouples' positions

2.2.2. Experimental procedure

The experiments consisted of two chemical reactions operated cyclically, starting from dehydration. The hydration experiment started from the dehydrated state. In the dehydration experiment, the reactor's heater was controlled to attain and maintain the inner wall temperature (T_5) at 400°C. The water reservoir was used for condensing the water vapor released from the reaction in the PBR. The condensation temperature was maintained at 20°C using a water chiller. In this manner, the dehydration pressure P_d was fixed at 2.3 kPa. Dehydration was performed until it reached a steady state for each bed temperature and weight change of the PBR. Then, the stop valve (SV-1) was closed, and electricity stopped being supplied to the reactor's heater and chiller. While the PBR cooled down from 400°C, saturated water vapor was prepared in the water reservoir using a Joule heater. When it was observed that the temperature of the packed bed had attained a steady state (all the temperatures in the packed bed were approximately the same), the hydration reaction was started by re-opening stop valve SV-1. The water vapor commenced flowing from the water reservoir to the reaction chamber under a hydration pressure. Four different pressure of hydration P_h were investigated. A different initial temperature of the packed bed reactor was corresponding for each of them. Those information are summarized on Table 2.1

Table 2.1 Water vapor conditions and initial temperature of packed bed in the hydration experiments

Pressure of hydration P_h [kPa]	Vapor saturation Temperature, T_{sat} [°C]	Temperatures of the bed at the beginning of hydration, $T_{1\text{-}7}$ [°C]
47	80	90°C
101	100°C	110°C
198	120°C	130°C
361	140°C	150°C

2.2.3. Evaluation of chemical heat pump performance

The reactor's mass change, Δm [g], was ascribed to the movement of water vapor between the PBR and the reservoir. The reacted fraction, x [-], is calculated using Eq. 2.1:

$$x = 1 + \frac{\Delta m / M_{H_2O}}{m_{Mg(OH)_2} / M_{Mg(OH)_2}} \quad (2.1)$$

where $m_{Mg(OH)2}$ [g] and M [g mol^{-1}] are the initial amount of reactant charged in the bed and molecular weight of the substance, respectively. As observed by Kato *et al.* [1], both the dehydration and hydration were saturated before reaching the ideal completion under reaction conditions. To obtain an objective comparison of the reactivity, we calculated the mole reacted fraction change, Δx, using Eq. 2.2:

$$\Delta x = x - x_{ini} \quad (2.2)$$

where x_{ini} is the initial reacted fraction of the dehydration–hydration reaction cycle. To compare some of the reaction cycles in the following discussion, the value of x_{ini} in each cycle was set to a constant value. The values of Δx were calculated for the dehydration and hydration, denoted respectively as Δx_d and Δx_h.

The heat-storage capacity, q_d [kJ kg$_{Mg(OH)2}^{-1}$], and the gross heat output, q_h [kJ kg$_{Mg(OH)2}^{-1}$], were calculated using Eqs. 2.3 and 2.4, respectively.

$$q_d = \frac{-\Delta H_r^\circ}{M_{Mg(OH)_2}} \cdot \Delta x_d \quad (2.3)$$

$$q_h = \frac{-\Delta H_r^\circ}{M_{Mg(OH)_2}} \cdot \Delta x_h \quad (2.4)$$

They are expressed in terms of the unit mass of $Mg(OH)_2$ in the PBR [kJ kg$_{Mg(OH)2}^{-1}$]. Finally, the mean heat-output rate w_{mean} [W kg $_{Mg(OH)2}^{-1}$] was calculated using Eq. 2.5, where t_h [s] is the time elapsed after the vapor for hydration begins to be supplied.

$$w_{mean} = \frac{q_h}{t_h} \quad (2.5)$$

An analysis of the propagation of uncertainties indicated that the experimental error in the measurements of Δx_d and Δx_h could be less than 3% of the calculated quantity.

These quantities, expressed per unit mass of $Mg(OH)_2$ can be expressed conveniently per unit volume in order to better understand the concept of "energy density". This is required also to have a more practical comparison between materials, characterized by different quantities (and volumes) of EG.

The mass mixing ratio, r_{mix}, used for the preparation of EM is defined as:

$$r_{mix} = \frac{m_{Mg(OH)_2}}{m_{Mg(OH)_2} + m_{EG}} = \frac{m_{Mg(OH)_2}}{m_{bed}} \quad (2.6)$$

where $m_{Mg(OH)2}$ [g] and m_{EG} [g] are respectively the initial amounts of $Mg(OH)_2$ and EG used for the preparation of the packed bed of EM, which mass is m_{bed}.

The density of the packed bed, ρ_{bed} [kg m^{-3}] is defined as the ratio between the mass of the bed, m_{bed} and the volume of the bed, V_{bed}

$$\rho_{bed} = \frac{m_{bed}}{V_{bed}} \tag{2.7}$$

The volumetric heat storage capacity, $q_{d,v}$ [MJ m_{bed}^{-3}], the volumetric gross heat output $q_{h,v}$ [MJ m_{bed}^{-3}] and the volumetric mean heat output rate $w_{mean,v}$ [kW m_{bed}^{-3}] are expressed as follows:

$$q_{d,v} = \frac{-\Delta H_r^\circ}{M_{Mg(OH)_2}} \cdot \Delta x_d \cdot r_{mix} \cdot \rho_{bed} \tag{2.8}$$

$$q_{h,v} = \frac{-\Delta H_r^\circ}{M_{Mg(OH)_2}} \cdot \Delta x_h \cdot r_{mix} \cdot \rho_{bed} \tag{2.9}$$

$$w_{mean} = \frac{q_h}{t_h} \cdot r_{mix} \cdot \rho_{bed} \tag{2.10}$$

2.3. The quick thermal conductivity meter QTM 500

2.3.1. The instrument

The thermal conductivity of the chemical heat storage materials could be measured by using a quick thermal conductivity meter (QTM-500, Kyoto Electronics) shown in Fig. 2.5. It allows measuring the thermal conductivity of a sampled material using an unsteady state hot wire method.

Fig. 2.3 Thermal conductivity meter (QTM-500, Kyoto Electronics)

This instrument is equipped with two different probes, PD-N0S (needle sensor, fig. 2.6 a) and PD-11 (hot wire, fig. 2.6 b). Each of them has a suitable current set point that is required to be specified before beginning the measurement campaign. The current should be enough large to allow an increase of probe temperature in a range from 5 to 20°C while doing the measurement.

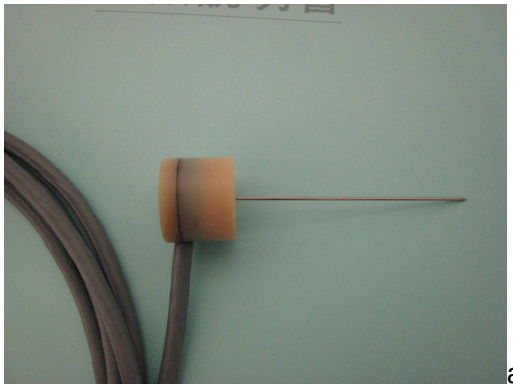
a)
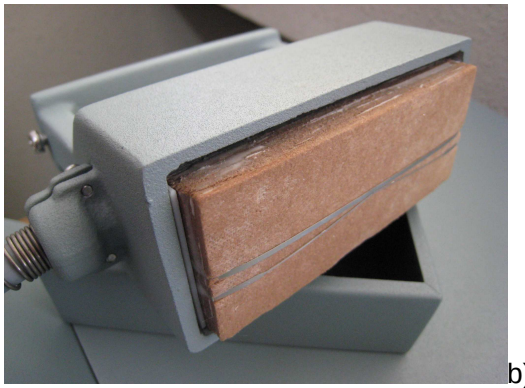
b)

Fig. 2.4 a) PD-N0S needle sensor probe b) PD-11 hot wire on flat plate probe

Here are some probes' specifications:

PD-N0S: needle sensor probe, ∅0.8 mm, length 60 mm. Suitable for measures of thermal conductivity within range of 0.15 ~5.00 W $m^{-1}K^{-1}$ (accuracy of ± 0.01 W $m^{-1}K^{-1}$).

PD-11: hot wire on flat plate probe, length 110 x 50 mm. Suitable for measures of thermal conductivity within range of 0.023 ~11.63 W $m^{-1}K^{-1}$ (accuracy of ± 0.01 W $m^{-1}K^{-1}$).

Wrap film was placed on PD-11 sensor to preserve the hot wire from powders (Fig. 2.7). The thermal resistance of this thin film can be neglected. Another piece was put over so to avoid air drafts eventually present in the experimental room.


(a)
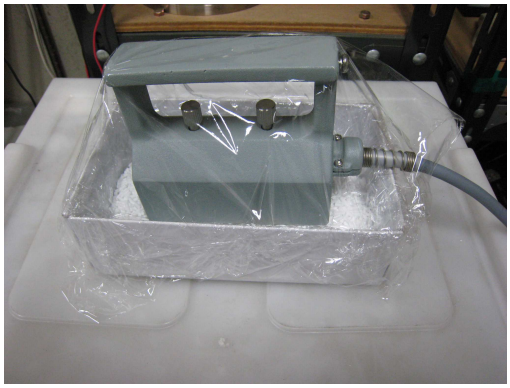
(b)

Fig. 2.5 Protection of the probe with wrap film from material (a) and air drafts (b)

2.3.2. Experimental procedure

2.3.2.1. Measurement on packed beds

Generally speaking, thermal conductivity of packed beds of materials is difficult to be determined. It is also more appropriate to talk about *effective* thermal conductivity, as it depends on the void fraction of the bed and on the fluid present in the interspaces among the bed's particles. Moreover, especially for $Mg(OH)_2$ pellets, the value of thermal conductivity is very small and close to the lower measure scale of the instrument, in other words it is difficult to obtain a precise measure. Finally, thermal resistance

between probe and material is quite high, due to the voids generated by the random particle's arrangements. This is because every time that sample material is loaded in the sample box, the pellets arrangement around the probe changes. The final measure is then affected by the summation of these effects. It is then necessary to repeat many measures and find out an average value. After placing the probe on the sample, it is required to wait about 10 minutes for reaching temperature equilibrium between them. Measure starts automatically. After every measure, the material is shaken in order to change the contact condition with the probe. It takes again about 10 minutes to return to an equilibrium temperature between probe and sample.

Measures are repeated at least 30 times and averaged. The same procedure was followed also for the measurements of thermal conductivity of EM tablets (diameter 7 mm, thickness 3-5 mm).

2.3.2.2. Measurement on slab specimen

In order to measure the thermal conductivity of EM and characterize it more properly, slab specimens have been manufactured. A photo and scheme of the mold are showed on Fig. 2.8. In this way it was possible to characterize the EM composite in function of mixing ratio and density.

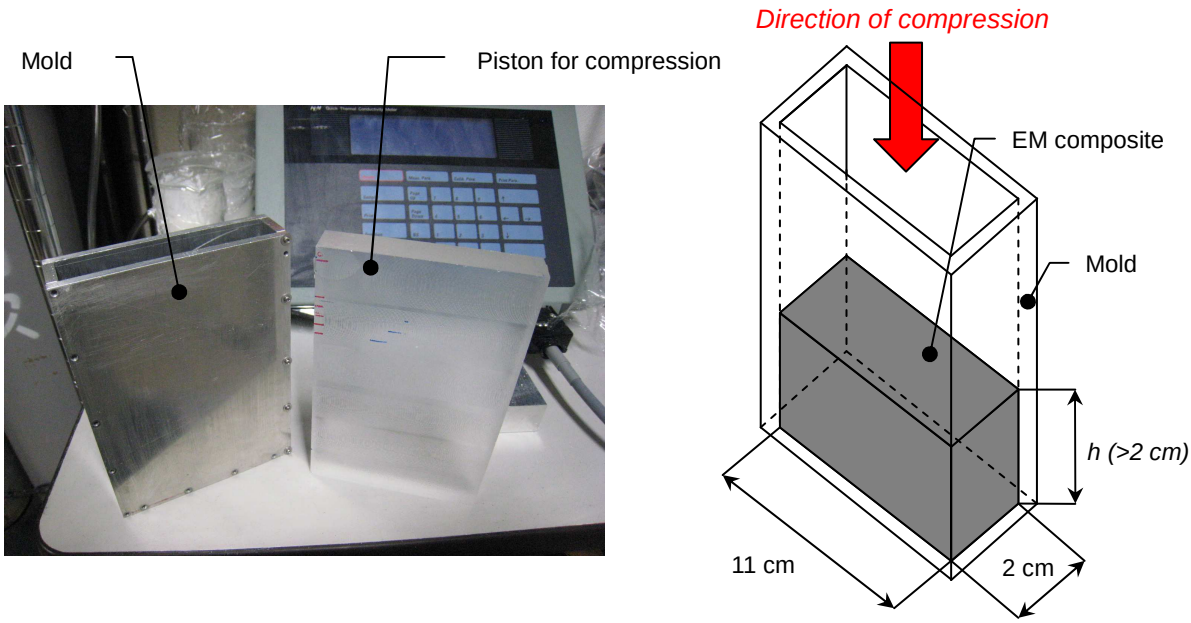

(a) Components of the mold used for preparation of slab samples

(b) Compression of EM into a slab sample of specified density

Fig. 2.6 The mold for preparation of slab samples for thermal conductivity measurements

After having prepared EM, it was loaded in the mold. Then, it was compressed to a pre-established position determined by the thickness *h*. This position was decided in function of the target density of the sample, as the mass of EM and two dimensions of the mold are constant. Plots of thermal conductivity in function of density were prepared for $Mg(OH)_2$ and EM composites having different mass mixing ratio and densities. In particular, it was necessary to measure thermal conductivity in two

directions, as compressed EM shows anisotropic properties. Thermal conductivity was measured in the direction parallel and perpendicular to the direction of compression, as shown on Fig.2.9 a) and b). The measurements were repeated 5 times on every face.

After completion, the specimen was reinserted into the mold and compressed again to a new position $h' < h$. Being the mass of the specimen unchanged and its volume decreased, the density of the specimen could be increased. Then the measurements of thermal conductivity on the 4 faces of the specimens were repeated. The maximum densities of the specimens were achieved for pressures on the block of about 5 MPa.

For some materials, it was also measured the thermal conductivity of the dehydrated sample.

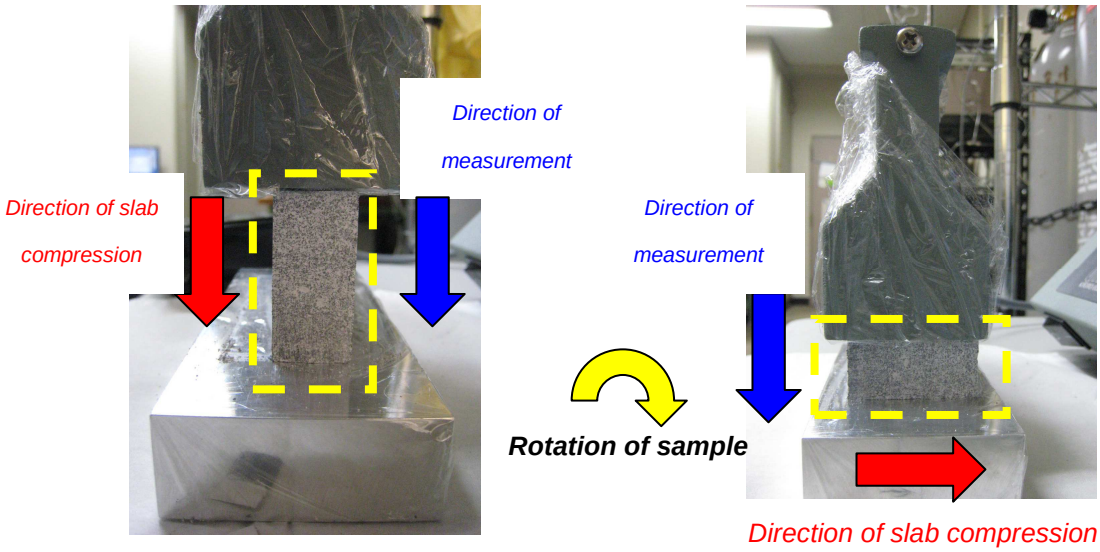

a) Measurement in the direction parallel to the direction of slab compression

b) Measurement in the direction perpendicular to the direction of slab compression

Fig. 2.7 Measurement of thermal conductivity of EM slabs samples

2.4. The differential scanning calorimeter (DSC)

2.4.1. The instrument

Differential scanning calorimetry (DSC) has been used to evaluate the specific heat capacity of $Mg(OH)_2$, MgO and EG. A differential scanning calorimeter (Thermoplus DSC8320, Rigaku) was used. The values of specific heat capacity of materials, expressed in function of temperature, were utilized for the numerical calculations in chapter 5. The specific heat capacity of EM could be obtained by averaging the heat capacities in function of the mass mixing ratio (weight average). This is because it is difficult to achieve a good level of homogeneity of EM samples, being the amount of material charged very small (less than 20 mg) compared to other experiments.

2.4.2. Experimental procedure

The method for obtaining the values of specific heat capacity using a DSC was described by O'Neill [2]. Fig. 2.10 illustrates the principle. It consists in heating two samples contained in the heater of the instrument with a certain rate of temperature increase and measure the heat flux required to keep the prescribed temperature in both samples (Fig. 2.10(b)). In this work, after reaching the temperature of 120°C for 30 minutes, the temperature is increased up to 450°C at a rate of 10°C/min. Three separated measurements are required (Fig. 2.10(a)). At first it is necessary to create the baseline, by placing in the heater of the instrument two empty samples, comprising an aluminum pan and its lid. Then, the preparation of the other samples consists in loading the aluminum pan with a certain amount of material of unknown specific heat capacity and cover with its lid. One of the two samples is loaded with alpha alumina (α-Al_2O_3), which specific heat capacity c_p' is known in function of temperature. Every measure is done keeping one empty pan and one filled with material. By taking the ratio of the heat fluxes *y*' and *y* recorded by the instrument, it is possible to determine the specific heat capacity c_p of the sample material, multiplied the ratio between the mass of the samples *m'* and *m*.

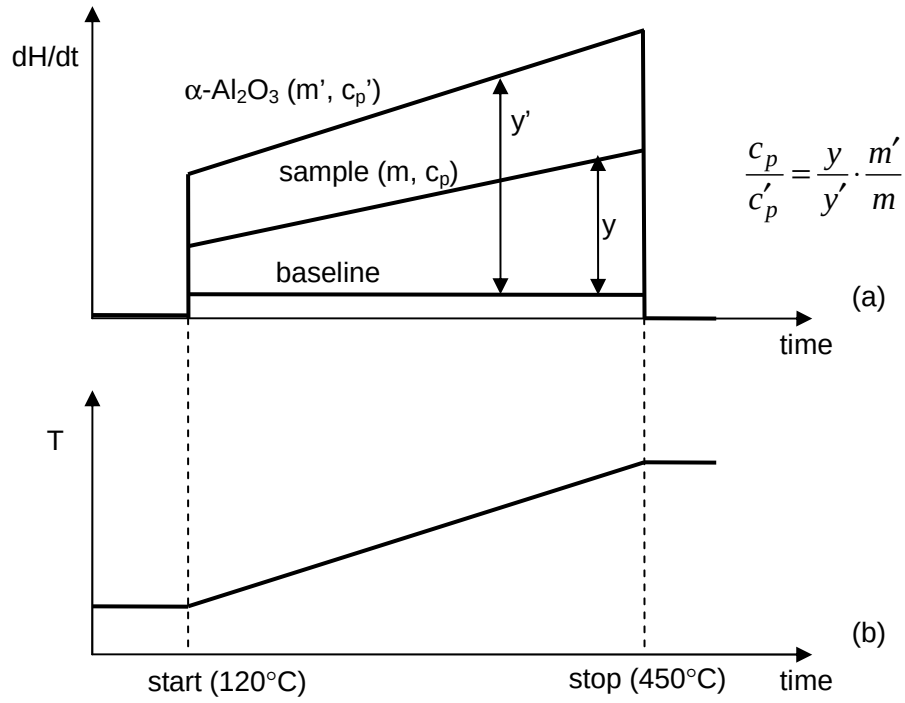

Fig. 2.8 Method of measurement of thermal conductivity of EM slabs samples

(a) dH/dt profile of materials, (b) Measured T profile.

2.5. Thermo-gravimetric experiments (TG)

2.5.1. The apparatus

A chemical kinetic analysis of materials was carried out to measure the reaction rate, reaction conversion, and reacted fraction of materials; the system used for the analysis consisted of a thermobalance (TG-9600, Ulvac-Riko Inc.) and other components (Fig. 2.11).

2.5.2. Experimental procedure

Reaction gases were supplied to the thermobalance via gas lines. Argon (Ar) was used as an inert purge gas for the dehydration of magnesium hydroxide and as a vapor carrier for the hydration of magnesium oxide. Ar was also supplied to an electric-balance chamber in the thermobalance system to prevent vapor invasion from the reactor cell (Kim, 2013) [3]. The dehydration experiments were performed at 270, 330, 370 and 400°C, while hydration was carried out at 110 °C under a vapor pressure of 57.8 kPa.

The determination of reaction rate constant resulted necessary for the numerical analysis, as it will consider the dependency of the reaction rate of dehydration in function of the local temperature in the packed bed. This apparatus was also utilized for verifying the resistance of pellets to repetitive multiple cycle (dehydration at 400°C, hydration at 110°C under a vapor pressure of 57.8 kPa). In general the packed bed experiments operated for about 24 cycles; in case of TG the cycle were repeated 48 times.

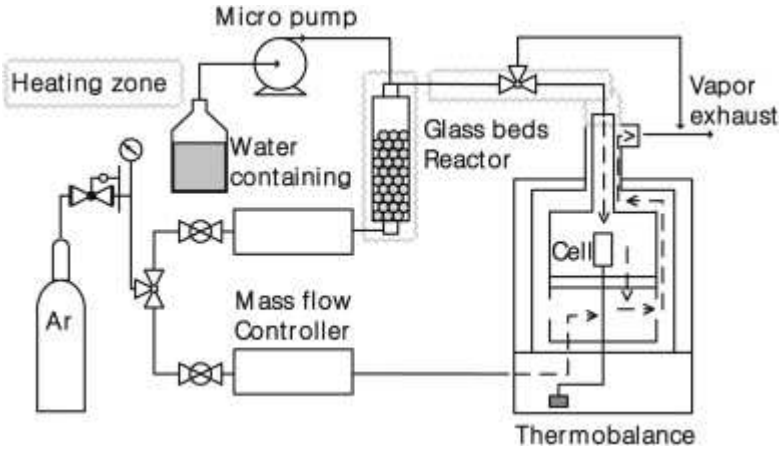

Fig. 2.9 Schematic diagram of thermo-gravimetric analysis system [3]

2.6. References

[1] Y. Kato, N. Yamashita, K. Kobayashi, Y. Yoshizawa, Kinetic study of the hydration of magnesium oxide for a chemical heat pump, Applied Thermal Engineering, 16 (11) (1996), 853-862

[2] M. J. O'Neill, Measurement of specific heat functions by differential scanning calorimetry, Analytical Chemistry, 36 (10)(1966),1331-1336

[3] S. T. Kim, J. Ryu, Y. Kato, Optimization of magnesium hydroxide composite material mixed with expanded graphite and calcium chloride for chemical heat pumps, Applied Thermal Engineering, 50 (1) (2013), 485-490

Massimiliano Zamengo, Y. Kato Laboratory, RLNR, Tokyo Institute of Technology

A Study on Heat Transfer-Enhanced Composites for a Magnesium Oxide/Water Chemical Heat Pump

Chapter 3

Materials and evaluation of their properties

3. MATERIALS AND EVALUATION OF THEIR PROPERTIES

3.1. Introduction

In this Chapter, the chemical heat storage materials used and compared in this work will be explained in detail. In particular, the attention will be focused on the thermal conductivity enhancement achieved by mixing magnesium hydroxide ($Mg(OH)_2$) with expanded graphite (EG). Thermal conductivity was measured on packed bed of particles and on slab samples. Cylindrical tablets of EM had a stable performance for at least 48 cycles in a thermobalance experiment of cyclic dehydration and hydration. Photographs and micrographs taken with optical and scattered electron microscope will be presented for comparison of unused and used materials. The kinetic of dehydration was analyzed in function of dehydration temperature and mass mixing ratio $Mg(OH)_2$ to EG.

3.2. Magnesium Hydroxide ($Mg(OH)_2$):

Magnesium hydroxide ($Mg(OH)_2$ is an environmentally friendly material contained in sea-water and limited hazardousness for human beings. It was successfully employed as reactant for the operation of a chemical heat pump [1]. The durability to repetitive reactions was also investigated [2] and was related with the high purity of the precursor magnesium oxide (MgO). The performance resulted stable for at least 24 cycles. Pellets of pure $Mg(OH)_2$ (MH-V05G, UBE Material Industries, Japan) (diameter of 1.9 mm) are shown on Fig. 3.1. In the experiments, the $Mg(OH)_2$ pellets were employed to form a packed bed reactor.

Fig. 3.1 Magnesium hydroxide pellets

Thermal conductivities were obtained 100 times for the same packed bed of $Mg(OH)_2$ pellet by QTM-500 (Fig.3.2). Fig. 3.2 shows that the average thermal conductivity of such a packed bed of pellets is within 0.15 - 0.16 W m^{-1} K^{-1}. The value is related to the intrinsic low thermal conductivity of $Mg(OH)_2$ and also by the void spaces of the bed. Despite having demonstrated its operability, it is required to enhance thermal conductivity in order to expect better performances and practical utilization.

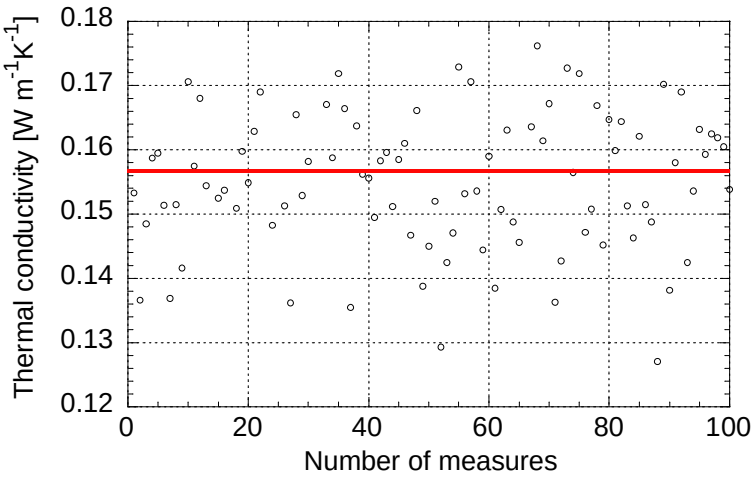

Fig.3.2 Thermal conductivity of $Mg(OH)_2$ pellet packed bed measured by QTM-500 with PD11 probe (hot wire)

3.3. Expanded graphite (EG)

In the research field of chemical heat pumps, it is often observed that reactant have very weak heat transfer properties. Thermal conductivity is particularly important for the purpose of heat transfer; heat conduction mechanism has to be maximized in order to minimize the heat exchanger surfaces. Mold ability is also another feature which allows improving heat transfer between material and heat exchanging devices. It might be possible to shape the material in configurations for which the contact heat transfer resistance is can be decreases. Because having these properties, Expanded Graphite (EG) is a well known binder in the field of chemical heat pumps [4-8]. It is obtained by expansion of expandable graphite flakes (SS-3, Air Water, Inc., Japan). This material is shown in Figs. 3.3. An amount of 1 g of expandable graphite flakes was charged into a 100 ml ceramic crucible and heated in an electrical furnace from a room temperature to 700°C. The rate of temperature increase was 20°C/min. EG was kept at this fixed temperature for 10 minutes, then cooled down to a room temperature. Graphite flakes changed into expanded shape as shown in Figs. 3.4. The length of an expanded graphite “worm” varies almost from 2 to 5 mm.

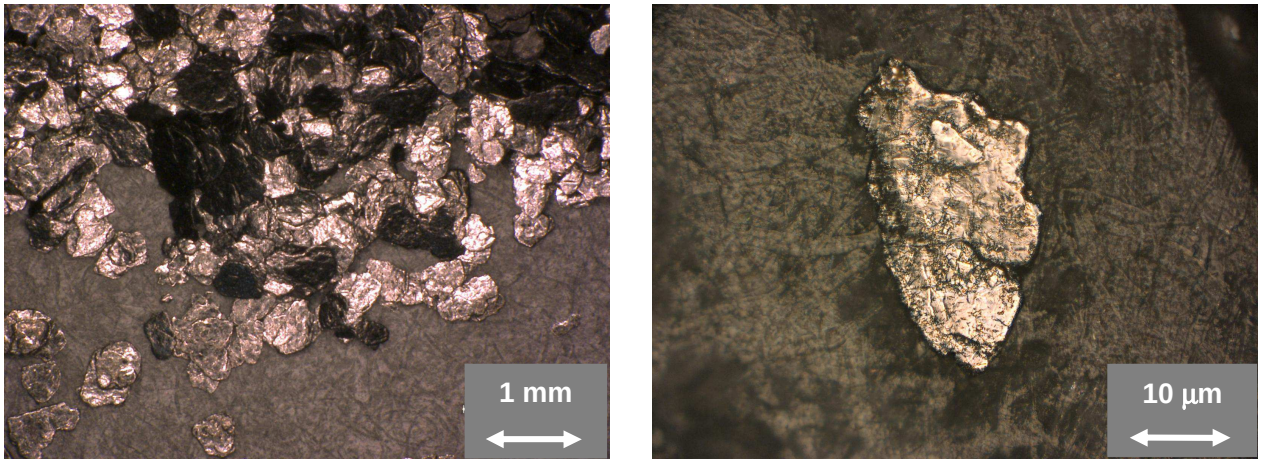

Fig.3.3 Digital microscope image of expandable graphite flakes (a) 50X and (b) 450X

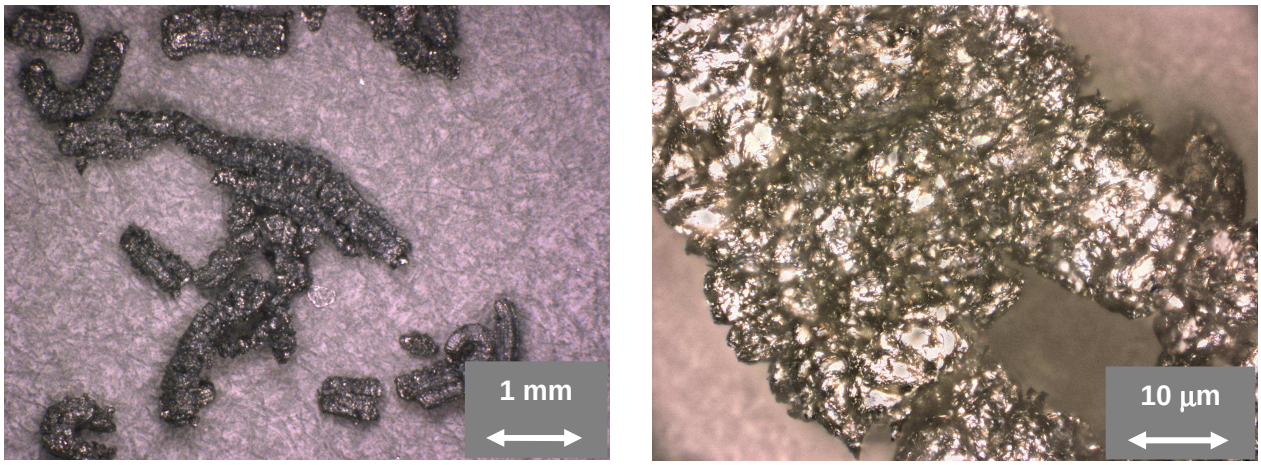

Fig.3.4 Digital microscope image of expanded graphite used in the preparation of EM (a) 50X and (b) 450X

The expansion increases considerably the specific volume of the initially charged material; the final density is quite low, about 0.02 g cm^{-3}.

The advantages of using this material as a binder for the reactant salt are the followings:

- ✓ High thermal conductivity: several studies [9-10] on consolidate graphite composite blocks showed that thermal conductivity was function of density, and increased by pre-compression of block.
- ✓ Mold-ability: when compressed, EG consolidates easily into a stable shape, which varies in function of the mold used. Therefore it is advantageous to provide a shape which fits well with heat exchanger's surfaces and decrease the contact resistance to heat transfer..
- ✓ Chemical stability for water vapor atmosphere: the material is suitable for the reaction's conditions of MgO/water chemical heat pump.
- ✓ It is a non hazardous material, both for human beings and environment.

Thermal conductivity of expanded graphite was measured similarly to $Mg(OH)_2$ but the density of

material could be easily modified by compression. It was observed a dependency between the density and the thermal conductivity of the sample. Measurements under different densities in a sample tube (diameter 2.7 mm and efficient depth 11.5 mm) were obtained using QTM-500 with the needle probe of PD-N0S (Fig. 3.5(a)). Density was changed gradually by compression of the material in the sample tube: measures were repeated 30 times for every density. After several insertions and extractions of the PD-N0S needle, the sample got ruined and material needed to be mixed or replaced in order to preserve a good contact between needle probe and material as shown in Fig 3.5 (b).

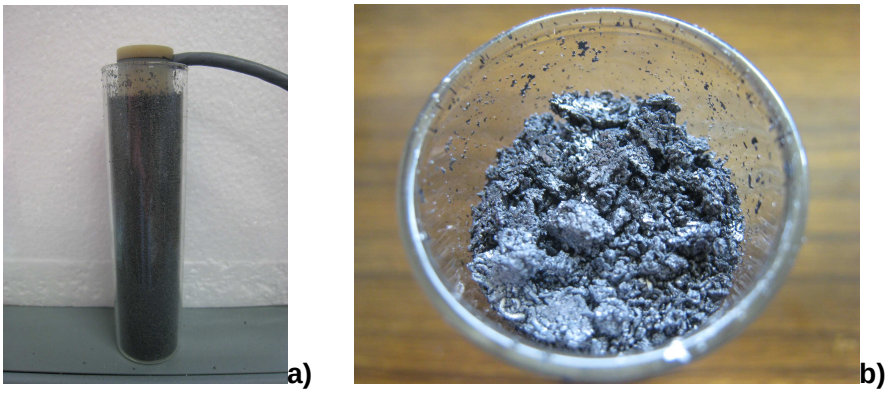

Fig.3.5 (a) Measurement of thermal conductivity of EG by the needle probe (b) surface ruined by needle insertion

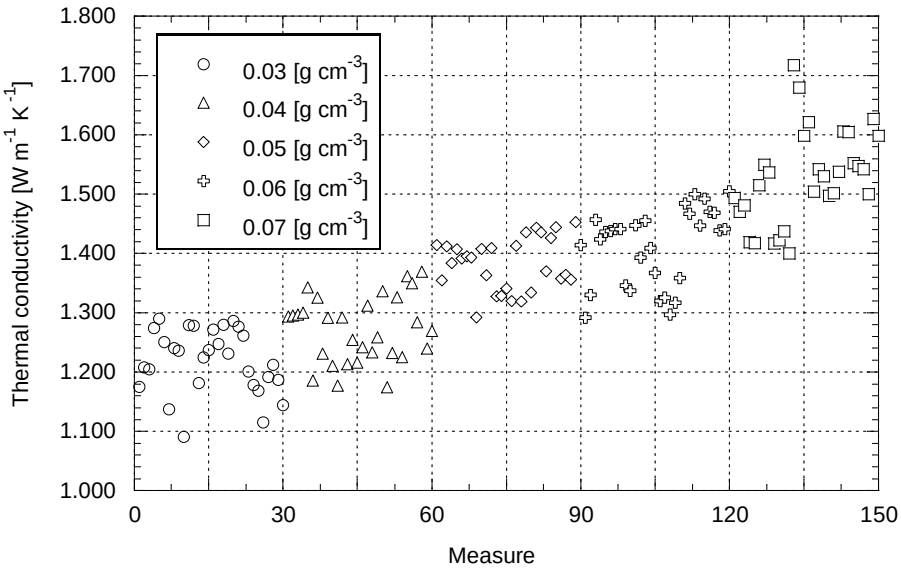

Fig.3.6 the dependency of thermal conductivity of EG in function of sample density

Fig.3.6 shows that thermal conductivity of EG varied from 1.1 to 1.6 $W.m^{-1}.K^{-1}$ in function of the sample's density. Those values are about 10 times higher than the one of a packed bed of $Mg(OH)_2$ pellet (0.15 $W.m^{-1}\ K^{-1}$). Compression of EG had the effect of increasing density and thermal conductivity because of reduction of the number of voids between particle and particle. This is an important aspect to be considered for preparation of a composite material (EG + $Mg(OH)_2$). On the other hand, for a chemical reaction which involves mass transport, the matrix of the composite is

required to be porous: sufficient permeability to the gas phase has to be ensured. Although a strong compression and high density can improve sensibly the heat transfer, it may hamper the gas flow and the reactivity. Then, the density of the composite is another parameter that needs to be optimized.

3.4. Preparation of expanded graphite–magnesium hydroxide composite

$Mg(OH)_2$ pellets were used as the precursors for preparing the EM composite. EG was obtained from graphite flakes after thermal treatment (700°C for 10 min) in an electric muffle furnace under atmospheric conditions. The preparation of EM composite, shown in Figs. 3.7 to 3.14, was as follows:

1. Pure $Mg(OH)_2$ pellets were crushed with a mortar and pestle and sieved (average particle size < 150 μm).
2. Amounts of the sieved were charged on a glass dish; then, purified water was added (approx. 30 ml) to the powder mixture, and the resulting slurry was mixed gently using a spatula. The amounts of $Mg(OH)_2$ powder and EG used for every type of EM are shown on Table 3.1.
3. After obtaining a homogeneous mixture, the glass dish was placed in a furnace for approximately 15 min at 120°C under atmospheric conditions.
4. Because of the different densities of water, EG, and $Mg(OH)_2$, the EG began to float on the upper surface of the mixture. It was necessary to remove the sample from the dryer and remix it using a spatula; then, the sample was again placed in the dryer for 15 min.
5. The glass dish was removed from the furnace, and the materials were mixed again. As some of the water evaporated, the mixture began to agglomerate; finally, a homogeneous mixture of $Mg(OH)_2$ and EG was obtained.
6. The sample was left at 120°C in the furnace until it was completely dry.
7. After removal from the furnace, the EM composite material was cut into small irregular pieces (average dimension < 4 mm) using the spatula.
8. The EM composite was compressed into tablets using a stainless steel mold set (Fig. 3.15). For every tablet, the mold cavity (d = 7.1 mm, h = 30 mm) was completely filled with EM. After applying compression force, the EM tablets had a diameter (ϕ) of 7.1 mm and a thickness (l) of 3.5–4.5 mm.

EM composite pellets with $Mg(OH)_2$ to EG mass mixing ratios (r_{mix}) of 16:1, 8:1, and 4:1 were prepared. These pellets were called EM16, EM8, and EM4, respectively. Fig. 3.16 shows as an example the EM4 tablets used in the packed bed experiments.

Table 3.1 Amounts of materials used for the preparation of EM in the sample dishes

EM type	Mass of $Mg(OH)_2$ in each sample dish [g]	Mass of EG in each sample dish [g]	Mass mixing ratio (r_{mix}) $Mg(OH)_2$:EG
EM16	16.0	1.0	16:1
EM8	8.0	1.0	8:1
EM4	4.0	1.0	4:1

Fig. 3.7 the slurry preparation

Fig. 3.8 the slurry after drying for 15 min

Fig. 3.9 dried slurry homogenization

Fig. 3.10 final look of slurry

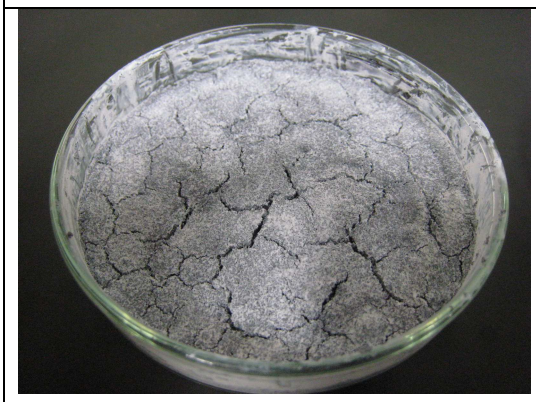

Fig. 3.11 EM after complete drying

Fig. 3.12 breaking rough particles

Fig. 3.13 fine crushing of rough particles

Fig. 3.14 residual $Mg(OH)_2$ on glass

Fig. 3.15 the mold used for pellet preparation

Fig. 3.16 the EM4 pellets used for the packed bed

The hollow cylinder mold is filled will powder all of its height (29 mm), then material is pressed until the punch touches the hollow cylinder top surface. The volume change is then about 1/10 from the initial one. By increasing the amount of graphite, it was observed that from the same initial volume of uncompressed EM, it was possible to obtain tablets with a smaller thickness. This is explainable with the mold ability and plasticity of EG.

3.5. Thermal conductivity measurements

3.5.1 Thermal conductivity measurement of beds of pellets

The values of λ_{bed} were measured using a quick thermal conductivity meter (QTM500, Kyoto Electronics). The measurements were conducted on tablets after the cyclic reactions in the packed bed reactor. The tablets were arranged so that they completely covered the hot wire sensor of the meter. The thickness of the sample bed was 2 cm, which was the same as the thickness of the samples used for calibrating the instrument and the size recommended by the instrument manufacturer. The density of the samples was the same as that in the PBR experiment. Because the contact between the tablets and the hot wire sensor was random and not optimal, a single measurement would not give an accurate result. After the completion of each measurement, the hot wire sensor was lifted from the sample, and the tablets were rearranged to change the contact condition for the following measurement. Measurements were repeated 30 times, and the average of the 30 values was calculated. The averaged apparent thermal conductivities λ_{bed} are plotted in Fig. 3.17. The error bars correspond to +/- one standard deviation from the average. This figure shows that λ_{bed} increased gradually with r_{mix} from 16:1 (EM16) to 4:1 (EM4). Compared with the original $Mg(OH)_2$ pellets, the λ_{bed} of EM4 tablets was two times greater. More precise thermal conductivity measurements of the EM composites are required to consider the anisotropic behavior of the compressed EG and the density of the compressed pellets. Such phenomena were observed by Critoph *et al.* [9], and they will be discussed in the next section. These data however represents the average apparent thermal conductivity of the packed bed which is more close to the thermal conductivity achieved in practical operation of the apparatus. Table 3.1 summarizes the properties of those beds.

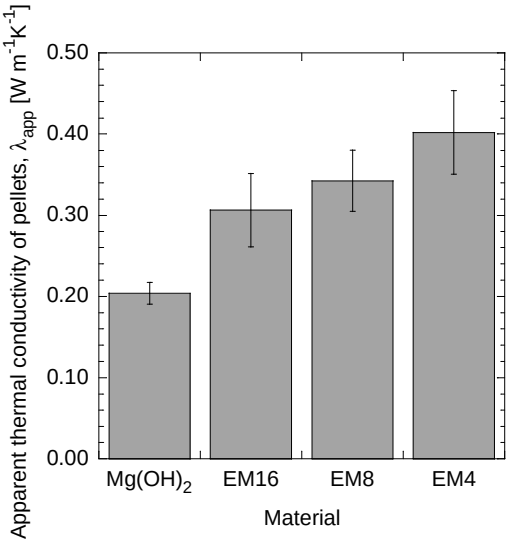

Fig.3.17 Comparison of apparent thermal conductivities, λ_{bed}, of packed beds (average of 30 measurements for each bed after cyclic CHP experiments)

Table 3.1 Properties of packed beds for measurement of apparent thermal conductivity (before the experiments)

Particle type	Particle density [g cm^{-3}]	Bed density [g cm^{-3}]	Void fraction ε [-]
$Mg(OH)_2$	0.966	0.626	0.35
EM16	1.078	0.512	0.53
EM8	1.075	0.504	0.53
EM4	0.976	0.451	0.54

3.5.2 Thermal conductivity measurement of slab specimens

Thermal conductivity of slab specimens was measured. They were prepared as explained in Section 2.3.2. The materials investigated were $Mg(OH)_2$, EM16, EM8 and EM4, respectively. Their thermal conductivity was measured in the direction parallel and perpendicular to the direction of compression. In case of $Mg(OH)_2$, there was no difference between the measurement in the two directions, therefore the $Mg(OH)_2$ slabs had an isotropic behavior. On the other hand, EM composite is characterized by an anisotropic thermal conductivity, as the values in measured in the direction parallel and perpendicular to the direction of compression resulted different. The results are shown in Fig. 3.18.

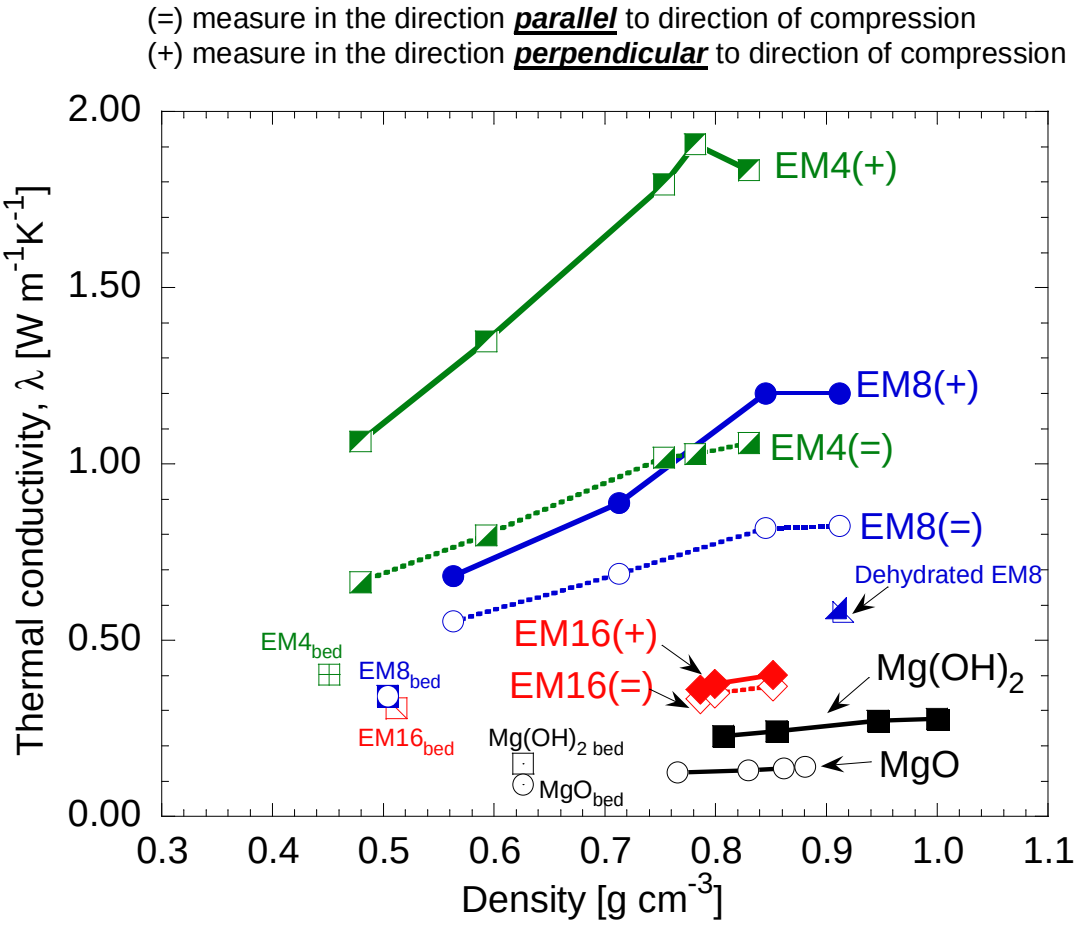

Fig.3.18 Comparison of thermal conductivities, λ, of billet specimens of $Mg(OH)_2$ and EM composites

Thermal conductivity of EM slabs resulted larger in the direction perpendicular to the direction of compression (indicated with (+)). This effect is due to the plastic deformation of EG, which flattens and forms horizontal layers. The results show clearly the enhancement of thermal conductivity related to the presence of EG. The higher the amount, the higher it will be the thermal conductivity. In case of EM4 it reached 1.9 W $m^{-1}K^{-1}$, which is more than 10 times larger than the $Mg(OH)_2$ specimen. With the aim to achieve a high thermal conductivity in the packed bed, EM materials are better than $Mg(OH)_2$, however it can be potentially increased by direct utilization of composite blocks in direct contact with the heat exchanger surface. This kind of block material will be discussed later in the experimental section.

3.5.3 Thermal conductivity measurement on dehydrated materials

The samples of $Mg(OH)_2$ pellets and the EM8 specimen were dehydrated at 400°C for 6 hours in a muffle furnace under atmospheric condition. After measuring mass, it was observed that the reacted fraction of dehydration was 83%. Measures of thermal conductivity were executed with the methods already described. Results are plotted in Fig. 3.19

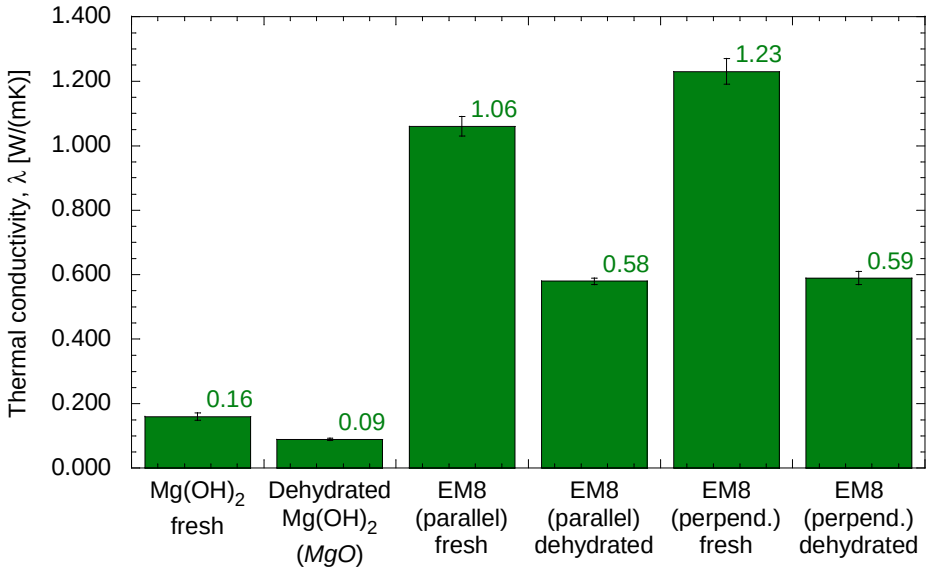

Fig.3.19 Thermal conductivity of materials before and after dehydration

It was observed that, in case of $Mg(OH)_2$ pellets, the value of thermal conductivity of the bed dramatically decreased from 0.16 W $m^{-1}K^{-1}$ to 0.09 W $m^{-1}K^{-1}$. This phenomenon is observed also for EM. The decrease is approximately 50% for both materials. It was not observed any significant shrinkage of bulk pellets or slab, therefore the decrease of thermal conductivity can be related to an increase of porosity caused by water removal at dehydration. The transition from the crystal structure of $Mg(OH)_2$ to the crystal structure of MgO corresponds to a shrinkage of grains and the space among them (porosity) becomes larger. This inevitable issue must be considered when studying heat transfer numerically and, in the future, for the design of new reactors and heat exchangers.

3.6. Stability of EM to repetitive cyclic experiments

3.6.1 Experiments of the packed bed reactor apparatus

In the next Figures from 3.20 to 3.23 it is possible to see the EM4 tablets after operating in the chemical heat pump apparatus. It is important to observe that some amount of material got detached from tablets, but it corresponds to the sharp edges of the tablets and not actually broken tablets. The total amount of detached material accumulated on the bottom of the reactor is very small in comparison with the total amount of material comprised in the bed (Fig.3.21).

Fig.3.20 the EM4 after 23 cycles

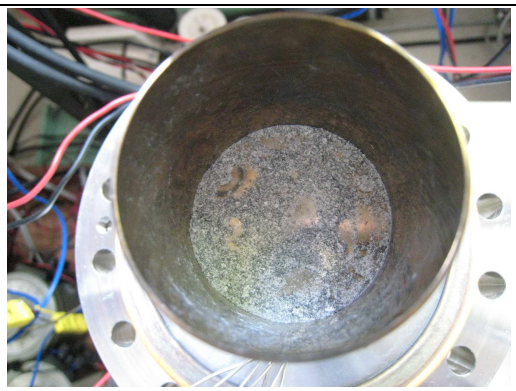

Fig.3.21 material accumulation on the bottom

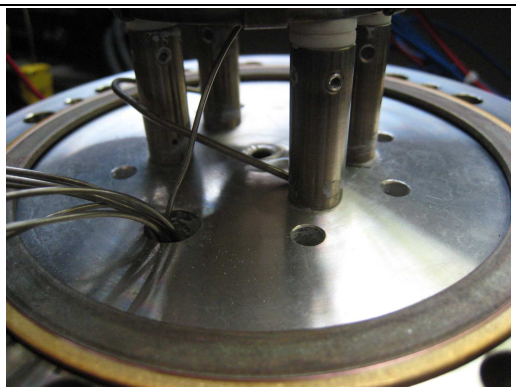

Fig.3.22 chamber's bottom surfaces after dehydration (it was still clean)

Fig.3.23 chamber's internal surfaces after dehydration (it was still clean.)

3.6.2 Experiments on TG

A longer durability test was conducted on thermobalance. In this case 3 tablets of EM8 were investigated. Each of them had diameter (ϕ) of 7.1 mm and a thickness (l) of 4.0 mm, while the average mass 106 mg. The conditions of the chemical reactions were as follows:

- Dehydration at 400°C for 45 minutes
- Hydration at 110°C for 120 minutes, steam pressure 57.8 kPa
- Argon gas was used as purge gas for dehydration or carrier gas for hydration.

Those conditions are exemplified on Fig.3.24. The number of repeated cycles was 48. The results are shown on Fig. 3.24. They show the final reacted fractions of dehydration, $x_{d,max}$, of hydration, $x_{h,max}$, and their difference $\Delta = x_{h,max} - x_{d,max}$.

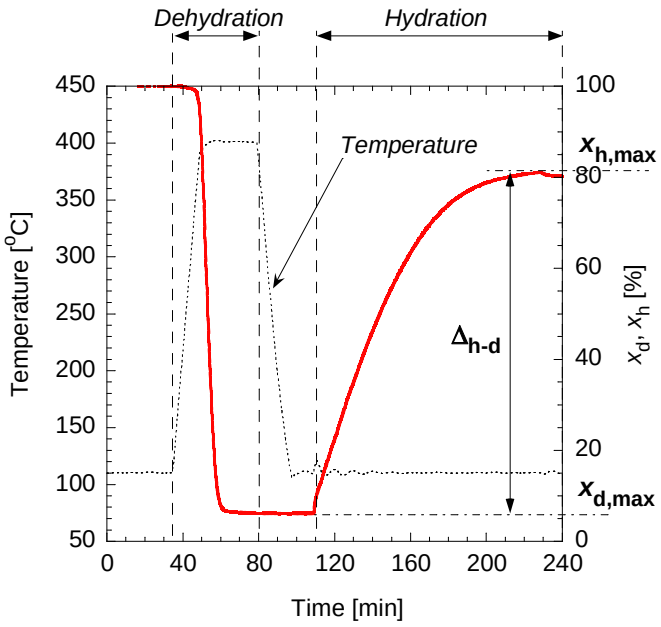

Fig.3.24 Experimental conditions of the typical cycle of dehydration and hydration on TG

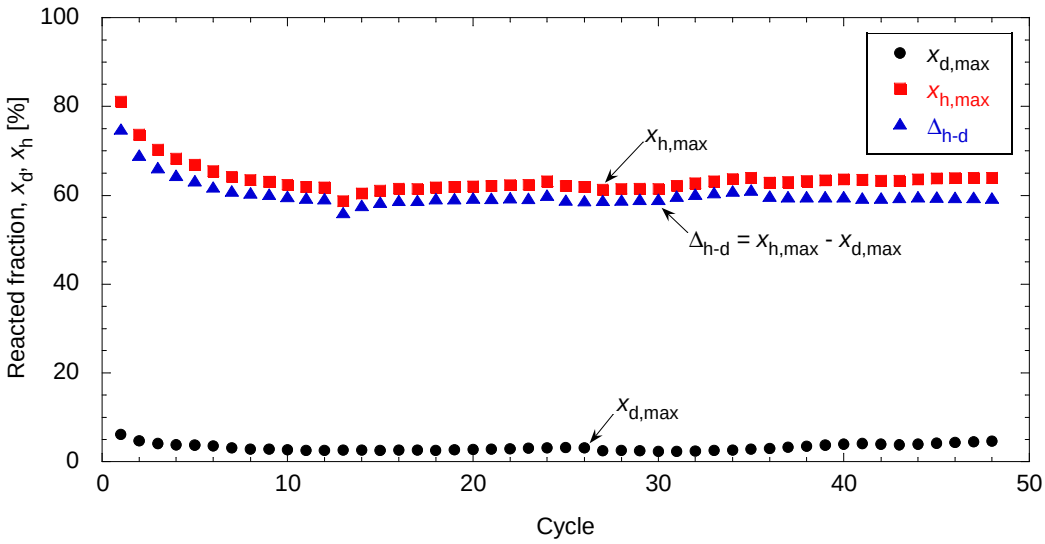

Fig.3.25 Reacted fractions of dehydration, $x_{d,max}$, of hydration, $x_{h,max}$, and their difference $\Delta_{h-d} = x_{h,max} - x_{d,max}$.

The results showed that after an initial decrease of the value of $x_{h,max}$, the value of Δ_{h-d} became constant. The EM tablets demonstrated stability of performance for at least 48 cycles. Micrographs of EM tablet before and after the repetitive cycles are shown on Fig. 3.26 and Fig. 3.27.

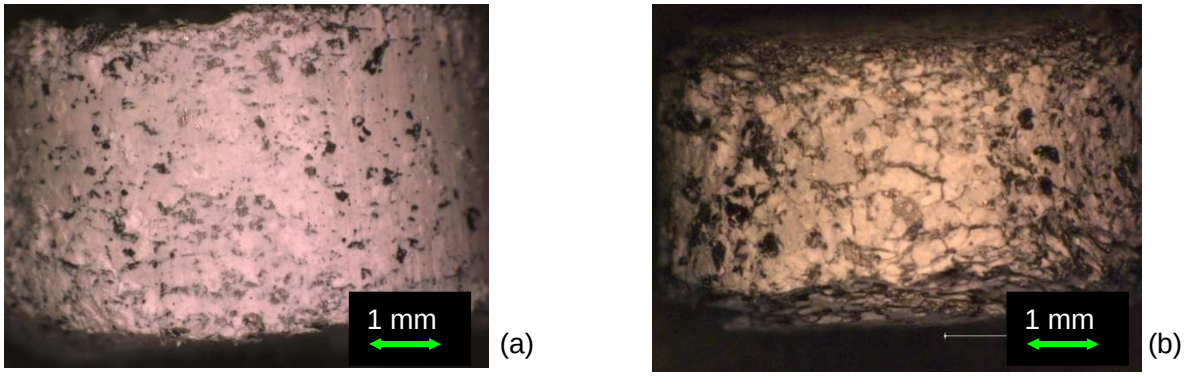

Fig.3.26 Digital microscope images of EM8 tablet (a) outer surface of fresh state and (b) after 48 cyclic experiments of dehydration/hydration

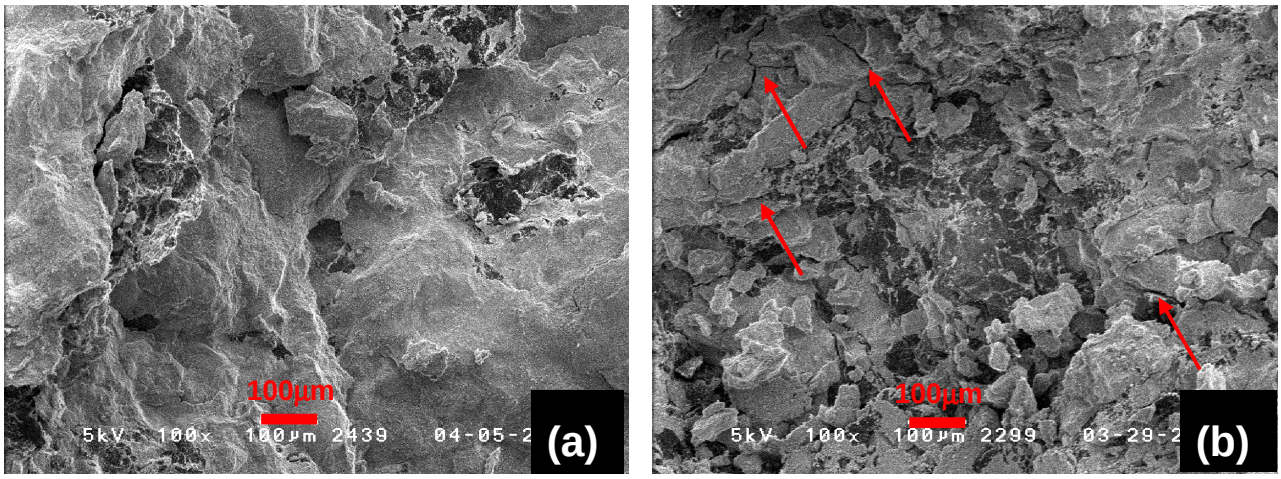

Fig.3.27 SEM images of fresh EM8 pellet (a) and used EM8 pellet (b) taken on a radial cross section

In the fresh pellets the most important thing to observe is the continuous layer of $Mg(OH)_2$ on the EG surface. The original initial particles used for material preparation have a dimension smaller than 150 µm. After the experiments, the "white" $Mg(OH)_2$ surface is interrupted by several cracks and the reactant seems distributed like grains. Actually cracks are generated, because of cyclic crystal modification from $Mg(OH)_2$ and MgO and vice versa. This has a positive feedback, as the porosity of the pellet is increased and water vapor can pass through these passages.

3.7. Kinetic analysis of dehydration

Reaction rate constant has been determined for $Mg(OH)_2$, EM8 and EM4 using TG apparatus. They were obtained by dehydrating sample tablets (ϕ = 7.0 mm, l = 3.5–4.0 mm, m_{tab} = 150 mg) at 300°C, 340°C, 370°C and 400°C. In a the large number of studies involving the dehydration of $Mg(OH)_2$, the kinetics were investigated by a first-order reaction model (Gordon and Kingery [11]). The first-order rate equation is written as follows:

$$-\frac{dx_d}{dt_d} = k_d x \qquad (3.1)$$

where k_d [s^{-1}] and t_d [s] represent the dehydration rate constant and time, respectively. It was assumed that dehydration occurred homogeneously in the particles and $Mg(OH)_2$ dehydration

proceeded as a first-order reaction. Under these assumptions, the rate equation proposed as Eq. (3) has been used. This equation can be integrated by initial condition ($x = x_0$ at $t_d = 0$) as follows:

$$\ln x_d = -k_d \cdot t_d + \ln x_0 \tag{3.2}$$

A dehydration kinetic analysis plots for the EM composite at 300, 340, 370, 400 °C over 30 min based on Eq. (3.2) is shown in Fig. 3.28, where the dot shapes show measured values and solid lines present a linear regression fit of the obtained values. As dehydration is an endothermic chemical reaction, the reaction rate is a function of the temperature. In particular, a higher temperature will produce a higher reaction rate.

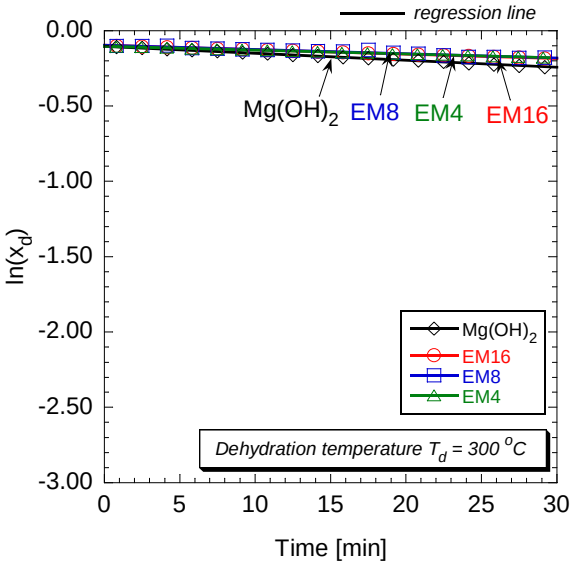

Fig.3.28 (a) Comparison of dehydration rate at 300°C

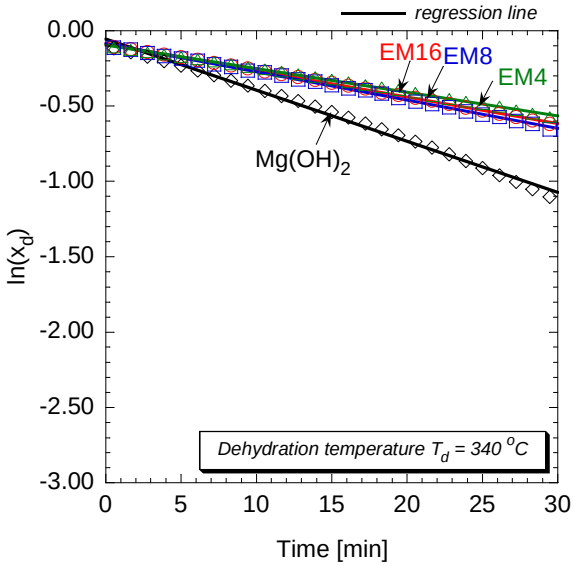

Fig.3.28 (b) Comparison of dehydration rate at 340°C

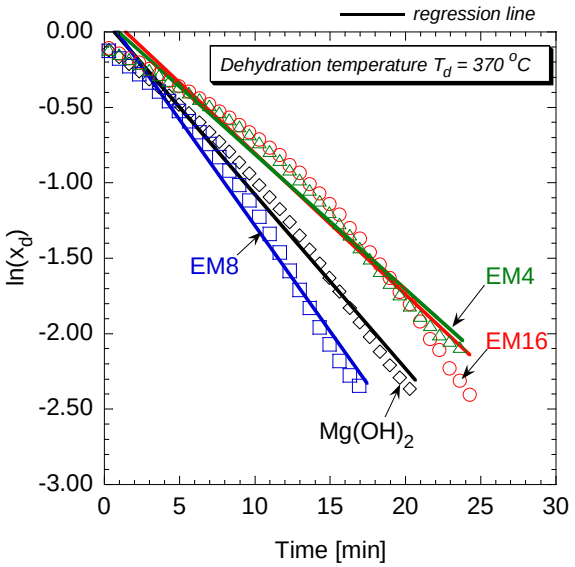

Fig.3.28 (c) Comparison of dehydration rate at 370°C

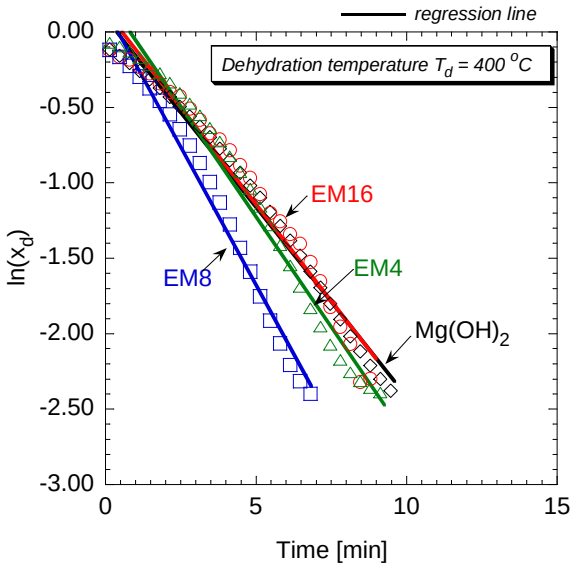

Fig.3.28 (d) Comparison of dehydration rate at 400°C

Fig.3.28 Kinetic analysis of dehydration on $Mg(OH)_2$ pellet and EM tablets (ϕ = 7mm, l = 2.5-4.0 mm, m_{tab} = 150 mg)

Figs. 3.28 a) to d) shows that straight lines resulted at the temperatures studied in a given period. Thus, attempts to fit the data to a first-order rate equation for the EM composite were successful at temperatures between 300 and 340°C. The interpolation of data was conducted for reacted fractions x_d in the range $0.90 \geq x_d \geq 0.09$. Results showed that EM8 could dehydrate earlier than other materials when dehydration was conducted at temperatures higher than 370°C. From the slopes of the lines obtained when $\ln(x_d)$ was plotted against dehydration time, the dehydration rate constant, k_d, was defined as follows:

$$k_d = A\exp\left(-\frac{E_a}{RT_d}\right) \tag{3.3}$$

where E_a [kJ mol^{-1}], A [s^{-1}], R (= 8.314 J mol^{-1} K^{-1}), and T_d [K] are activation energy, pre-experimental factor, gas constant, and dehydration temperature, respectively. Arrhenius plots of ln (k_d) vs. $1/T_d$ for the materials are shown in Fig. 3.29, where plot shapes show measured values and solid lines show a linear regression fit of these values.

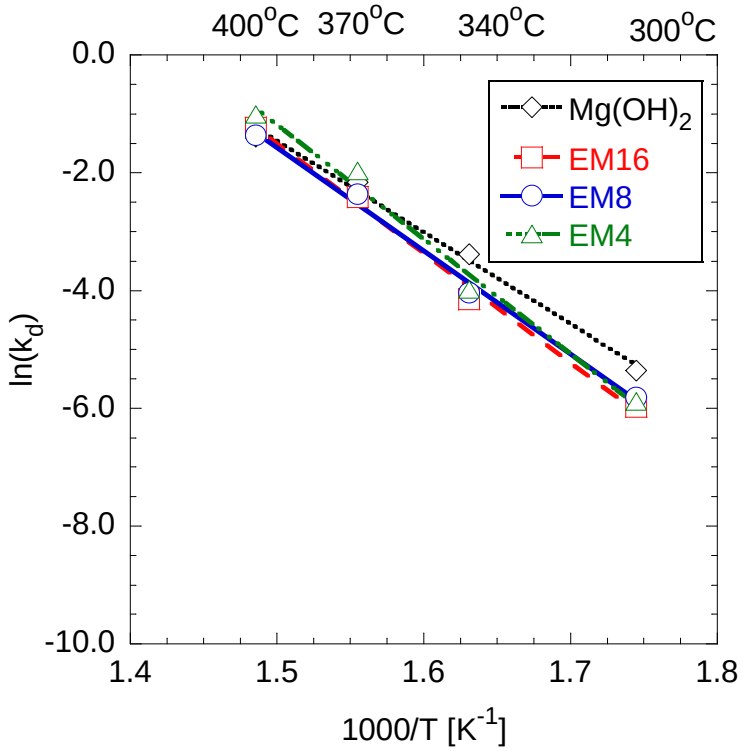

Fig.3.29 Comparison of reaction rate constant k_d for $Mg(OH)_2$, EM16, EM8 and EM4

They show that the lines of the 4 different materials ($Mg(OH)_2$, EM16, EM8 and EM4) almost overlap each other. It was shown that EG had no particular effect on dehydration of $Mg(OH)_2$. The reaction rates calculated in function of temperature will be used in Chapter 5 for the numerical analysis of dehydration in the packed bed reactor experiments. It will be shown in the next chapters that in a larger system comprising a packed bed of tablets, the effect of heat transfer enhancement given by EG is more

effective than in the small scale.

3.8. Further discussion on dehydration kinetics

The first order reaction model applied in the previous section showed a poorer fitting at temperatures over 370°C. Accordingly to other works [12], reaction data can be well fitted by different reaction models, for example the contracting surface model. This is defined as follows:

$$1-(1-\alpha)^{1/2} = k \cdot t \qquad (3.4)$$

where α is defined as $\alpha = 1-x_d$. The analysis has been repeated using Eq. 3.4. The results are shown on Fig. 3.30.

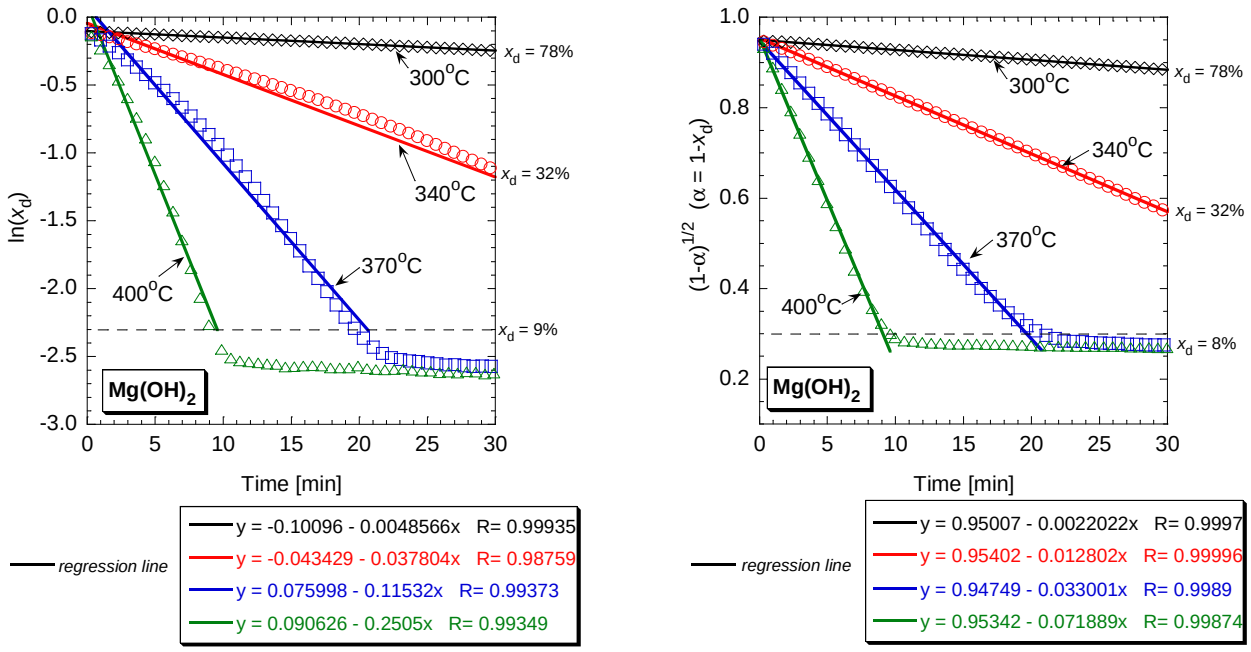

Fig.3.29 Kinetic analysis of dehydration on $Mg(OH)_2$ pellet using (a) first ordered reaction models and (b) contracting surface model. Rates at different temperatures are shown. For easier visual comparison, the y-axis results of contracting surface model have been mirrored with respect of the x-axis.

The results indicate that the contracting surface model can fit better the experimental results, (R^2 = 0.999 and R^2 = 0.990 for contracting surface and first order, respectively). The Arrhenius plot and the activation energy could be recalculated and compared for the two models. The results are shown on Fig 3.29, including $Mg(OH)_2$ pellet and EM8 tablet.

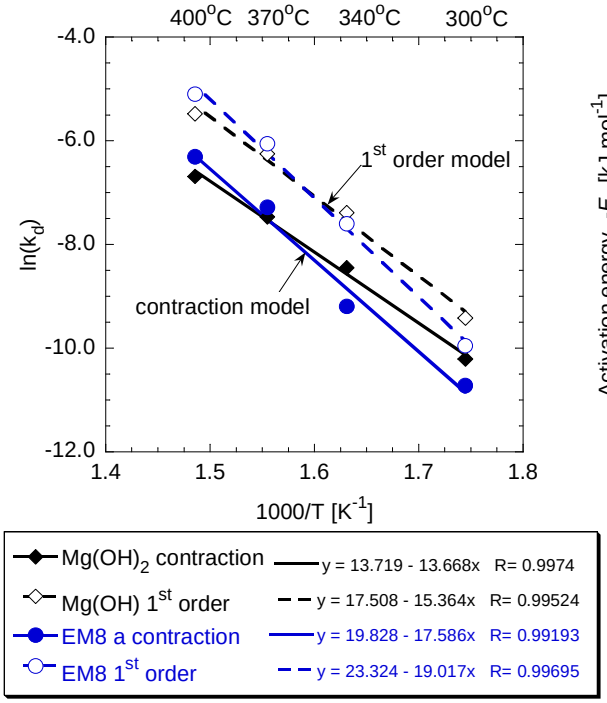

a) Arrhenius plot of reaction rate constants k_d

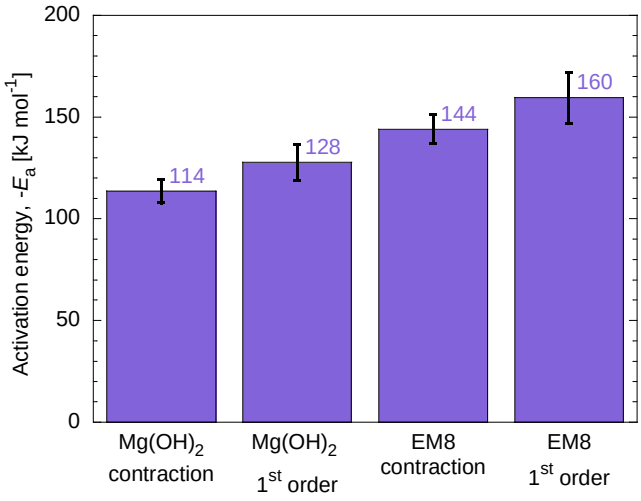

b) Comparison of activation energies evaluated by using different reaction models

Fig.3.30 Comparison of kinetic analysis of dehydration on $Mg(OH)_2$ pellet and EM8 tablet, (a) dehydration rates in function of temperature and (b) activation energies calculated with two chemical reaction models.

Table 3.2 Comparison of activation energies calculated with the two chemical reaction models

Activation energy, $-E_a$ [kJ mol^{-1}]	
$Mg(OH)_2$ contracting surface model	113.6 ± 5.8
$Mg(OH)_2$ 1st order	127.7 ± 8.8
EM8 contracting surface model	144.0 ± 7.0
EM8 1st order	159.6 ± 12.4

From Fig.3.30 Despite the good fitting of both the models ($R^2 > 0.99$), the contracting surface models fits better with a straight line. From the results of calculated activation energy, it is observed a difference of value between the two models. However, such a difference is included within the calculated uncertainty on the results.

It was also observed that the reaction rates are dependent on the density of the sample. Dehydration at different temperature was conducted on EM8 tablet (density 1.1 g cm^{-3}) and EM8 uncompressed powder state (density 0.6 g cm^{-3}). The results are shown on Fig.3.31.

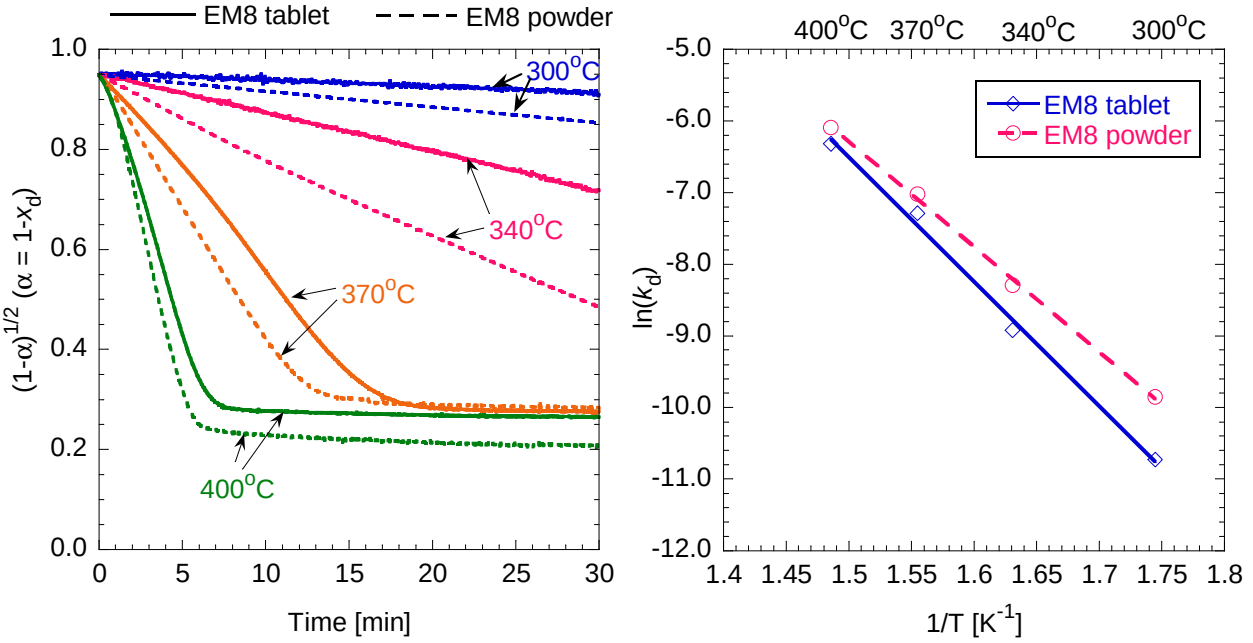

a) Comparison of reaction kinetics for EM8 tablet and uncompressed EM8 powder

b) Arrhenius plot for EM8 tablet and uncompressed EM8 powder

Fig.3.31 Comparison of kinetic analysis of dehydration of EM8 in compressed tablet and powder state, (a) dehydration rates in function of temperature and (b) Arrhenius plot for calculation of activation energies

Table 3.3 Comparison of activation energies calculated with the two chemical reaction models

Activation energy, $-E_a$ [kJ mol^{-1}]	
EM8 uncompressed **powder**	126.0 ± 8.0
EM8 compressed **tablet**	144.0 ± 7.0

The results on Fig. 3.31 (a) indicate that for the same EM8 material, uncompressed material reacts faster than the compressed one. Fig 3.31 (b) shows that the rates are more similar for higher dehydration temperature, while the larger difference is at 300°C. The results of calculated activation energy (table 3.3) give larger values for the tablet. As thermal conductivity would be larger for compressed material, but the rate is smaller, it means that the reaction is controlled by diffusion. It is likely that compression of EM8 do not let water vapor to exit freely from the tablet. This effect is also observed for dehydration and hydration experiments on tablets of compressed $Mg(OH)_2$ powder, therefore it is an effect not related with the presence of EG. Dehydration and hydration experiments on a tablet of $Mg(OH)_2$ compressed powder (3 different increasing density) were conducted. The results are shown on Fig. 3.32. The results indicate that when powder is compressed to reach higher tablet density (the volume is always keep constant, cylinder of diameter 7 mm and thickness 3.5 mm) the rate of reaction of both dehydration and hydration are changed. In particular, the larger the density the slower advanced the reaction.

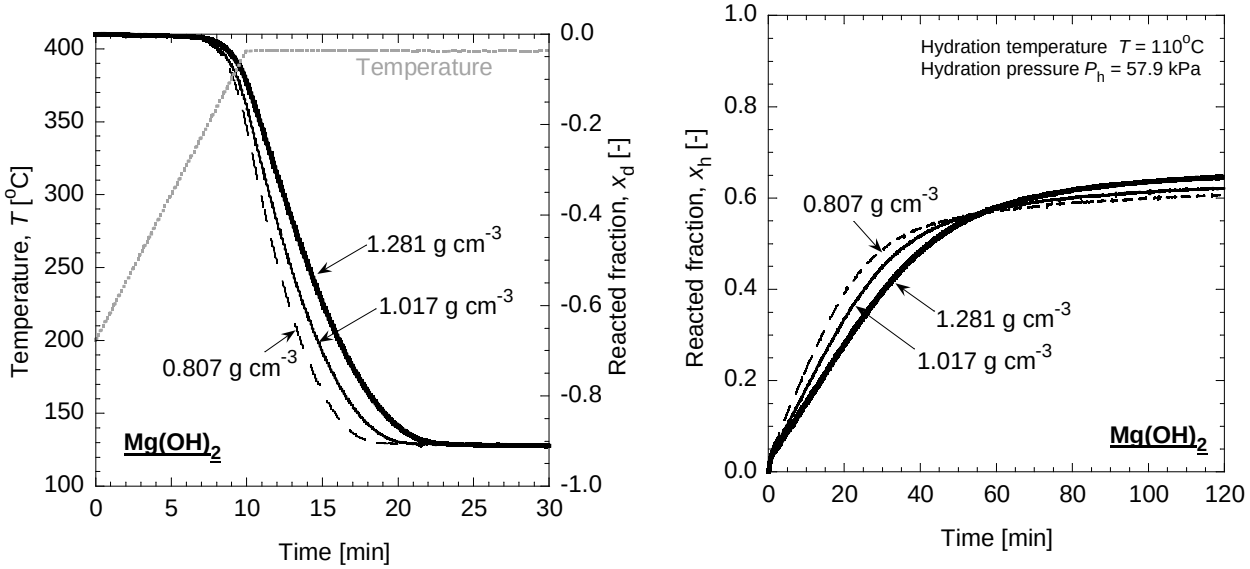

a) Comparison of dehydration reaction on $Mg(OH)_2$ tablet in function of density.

b) Comparison of hydration reaction on $Mg(OH)_2$ tablet in function of density.

Fig.3.32 Comparison of a) dehydration and b) hydration reaction on tablet of compressed $Mg(OH)_2$. Reaction rate changes in function of the density of tablet.

It is understood that density is important for increasing thermal conductivity, but it should be optimized also for diffusion of water vapor. As a concluding figure, the activation energy has been calculated using the contracting surface model for the materials. The Arrhenius plot and the results are shown on Fig. 3.33. In particular it is shown a comparison between $Mg(OH)_2$ pellet and tablet, indicating that the aggregation state of the material (pellets are extruded from slurry and dried, while tablet is compressed powder of crushed pellet) affects the value of activation energy. The activation energies are summarized in the following Table 3.4. It includes also the values of activation energy calculated from Fig.3.29. The first order tends to overestimate the activation energy, however, as observed previously, the materials dehydrated with similar rates of reaction, indicating that for such a small scale experiments, the dominant effect is mass diffusion rather than heat transfer.

Table 3.4 Total comparison of activation energies calculated with the reaction models

Activation energy, $-E_a$ [kJ mol^{-1}]		
Material	*1st order*	*Contracting surface*
$Mg(OH)_2$ pellet	127.7 ± 8.8	113.6 ± 5.8
$Mg(OH)_2$ tablet	143.2 ± 11.4	126.9 ± 10.0
EM16 tablet	157.0 ± 13.5	136.0 ± 4.8
EM8 tablet	159.6 ± 12.4	144.0 ± 7.0
EM4 tablet	165.5 ± 11.4	138.9 ± 1.5

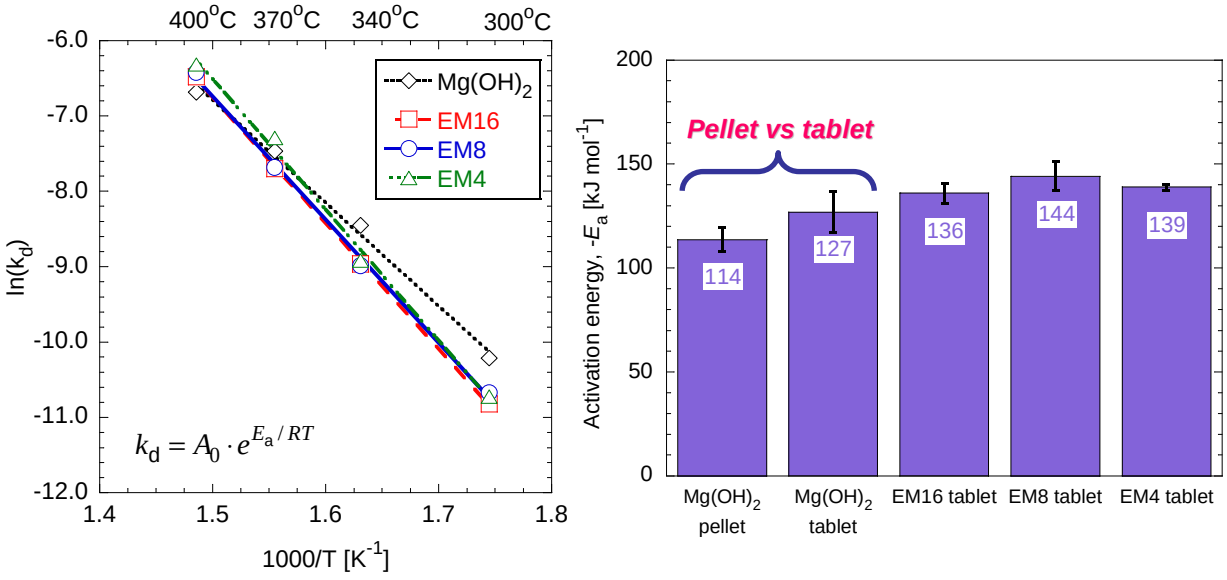

a) Arrhenius plot of reaction rate constants k_d

b) Comparison of activation energy of dehydration.

Fig.3.33 Results of kinetic analysis of dehydration (contracting surface model) of materials ($Mg(OH)_2$ pellets and EM tablets: (a) dehydration rates in function of temperature and (b) activation energies

3.9. Conclusions

The utilization of EG as thermal conductivity enhancer for the MgO – H_2O chemical heat pump was demonstrated by direct measurement of thermal conductivity. It was possible to shape the EM composite in cylindrical tablets or slabs, demonstrating the mold-ability of the EM composite. EM material allowed a stable and proper operation of the chemical heat pump system in thermobalance experiments. Tablets kept their shape without failures or significant exfoliation after 48 cyclic reactions. Several mass mixing ratio $Mg(OH)_2$ to EG were analyzed, demonstrating that the more EG used, the higher it would be the thermal conductivity. The kinetic analysis of dehydration showed that EG behaved as inert in the chemical reaction. It was understood that diffusion of water vapor is a rate controlling mechanism for both dehydration and hydration reactions.

In the next chapters the performances of EM composites with different mixing mass ratios will be compared in a packed bed apparatus in order to understand the role of EG in a larger scale experiments.

3.10. References

[1] Y. Kato, Y. Sasaki, Y. Yoshizawa, Magnesium oxide/water chemical heat pump to enhance energy utilization of a cogeneration system, Energy, 30, 11–12, (2005), 2144-2155

[2] Y. Kato, J. Nakahata, Y. Yoshizawa, Durability characteristics of the hydration of magnesium oxide under repetitive reaction Journal of Material Science, 34 (1999), 475–480

[3] Y. Kato, K. Kobayashi, Y. Yoshizawa, Durability to repetitive reaction of magnesium oxide/water reaction system for a heat pump, Applied Thermal Engineering, Volume 18, 3–4 (1998), 85–92

[4] K. Fujioka, K. Hatanaka, Y. Hirata, Composite reactants of calcium chloride combined with functional carbon materials for chemical heat pumps, Applied Thermal Engineering, 28 (2008), 304-310

[5] M. Bonnissel, L. Luo, D. Tondeur, Compacted exfoliated natural graphite as heat conduction medium, Carbon, 39 (2001), 2151-2161

[6] G. Cacciola, G. Restuccia and L. Mercadante, Composites of activated carbon for refrigeration adsorption machines, Carbon, 33,9 (1995), 1205-1210

[7] S. Mauran, P. Prades, F. L'Haridon, Heat and mass transfer in consolidated reacting beds for thermochemical systems, Heat Recovery Systems & CHP, 13 (4) (1993), 315-319

[8] S. Mauran, H. Lahmidi, V. Goetz, Solar heating and cooling by a thermochemical process. First experiments of a prototype storing 60 kWh by a solid/gas reaction, Solar Energy 82 (2008), 623-636

[9] L.W. Wang, Z. Tamainot-Telto, S.J. Metcalf, R.E. Critoph, R.Z. Wang, Anisotropic thermal conductivity and permeability of compacted expanded natural graphite, Applied Thermal Engineering, 30 (13) (2010), 1805-1811

[10] L.W. Wang, Z. Tamainot-Telto, R. Thorpe, R.E. Critoph, S.J. Metcalf, R.Z. Wang, Study of thermal conductivity, permeability, and adsorption performance of consolidated composite activated carbon adsorbent for refrigeration, Renewable Energy, 36 (8) (2011), 2062-2066

[11] R.S. Gordon, W.D. Kingery, Thermal decomposition of brucite: II, kinetics of decomposition in vacuum, Journal of the American Ceramic Society, 50 (1) (1967), 8-14

[12] P. J. Anderson, R. F. Horlock, Thermal decomposition of Magnesium Hydroxide, Transaction of the Faraday Society., 58 (1962), 1993-2004

Massimiliano Zamengo, Y. Kato Laboratory, RLNR, Tokyo Institute of Technology

A Study on Heat Transfer-Enhanced Composites for a Magnesium Oxide/Water Chemical Heat Pump

Chapter 4

Packed bed reactor experiments

4. PACKED BED REACTOR EXPERIMENTS

4.1. Introduction

In this chapter, the detailed results of packed bed reactor experiments will be presented. In particular, the effects of the higher thermal conductivity in the packed bed on the chemical reactions will be observed. At first, the original $Mg(OH)_2$ pellets will be compared with EM16, EM8 and EM4 tablets. It will be determined an optimal mixing ratio of EM composite for the operation on the packed bed reactor (PBR). Then two solutions for increasing further the heat storage capacity and thermal conductivity will be considered and compared.

4.2. Thermochemical performance parameters

As already explained in Chapter 2, the mass mixing ratio, r_{mix}, used for the preparation of EM is defined as:

$$r_{mix} = \frac{m_{Mg(OH)_2}}{m_{Mg(OH)_2} + m_{EG}} = \frac{m_{Mg(OH)_2}}{m_{bed}} \tag{4.1}$$

where $m_{Mg(OH)2}$ [g] and m_{EG} [g] are respectively the initial amounts of $Mg(OH)_2$ and EG used for the preparation of the packed bed of EM, which mass is m_{bed}.

The reactor's mass change, Δm [g], was ascribed to the movement of water vapor between the PBR and the reservoir. The reacted fraction, x [-], is calculated using Eq. 4.2:

$$x = 1 + \frac{\Delta m / M_{H_2O}}{m_{Mg(OH)_2} / M_{Mg(OH)_2}} \tag{4.2}$$

where $m_{Mg(OH)2}$ [g] and M [g mol^{-1}] are the initial amount of reactant charged in the bed and molecular weight of the substance, respectively. As observed by Kato *et al.* [1], both the dehydration and hydration were saturated before reaching the ideal completion under reaction conditions. To obtain an objective comparison of the reactivity, we calculated the mole reacted fraction change, Δx, using Eq. 4.3:

$$\Delta x = x - x_{ini} \tag{4.3}$$

where x_{ini} is the initial reacted fraction of the dehydration–hydration reaction cycle. To compare some of the reaction cycles in the following discussion, the value of x_{ini} in each cycle was set to a constant value. The values of Δx were calculated for the dehydration and hydration, denoted respectively as Δx_d and Δx_h. The heat-storage capacity, q_d [kJ $kg_{Mg(OH)2}^{-1}$], and the gross heat output, q_h [kJ $kg_{Mg(OH)2}^{-1}$], were calculated using Eqs. 4.4 and 4.5, respectively.

$$q_d = \frac{-\Delta H_r^\circ}{M_{Mg(OH)_2}} \cdot \Delta x_d \tag{4.4}$$

$$q_h = \frac{-\Delta H_r^\circ}{M_{Mg(OH)_2}} \cdot \Delta x_h \tag{4.5}$$

They are expressed in terms of the unit mass of $Mg(OH)_2$ in the PBR [kJ $kg_{Mg(OH)2}^{-1}$]. Finally, the mean heat-output rate w_{mean} [W $kg_{Mg(OH)2}^{-1}$] was calculated using Eq. 4.6, where t_h [s] is the time elapsed after

introduction of the vapor for hydration.

$$w_{\text{mean}} = \frac{q_{\text{h}}}{t_{\text{h}}} \tag{4.6}$$

These quantities, expressed per unit mass of $Mg(OH)_2$ can be expressed conveniently per unit volume in order to better understand the concept of “energy density”. This is required also to have a more practical comparison between materials, characterized by different quantities (and volumes) of EG.

The density of the packed bed, ρ_{bed} [kg m^{-3}] is defined as the ratio between the mass of the bed, m_{bed} and the volume of the bed, V_{bed}

$$\rho_{\text{bed}} = \frac{m_{\text{bed}}}{V_{\text{bed}}} \tag{4.7}$$

The void fraction of the packed bed is expressed as

$$\varepsilon_{\text{bed}} = 1 - \frac{\rho_{\text{particle}}}{\rho_{\text{bed}}} \tag{4.8}$$

where ρ_{particle} [kg m^{-3}] is the average density of the single particle of the packed bed (pellet or tablet).

The volumetric heat storage capacity, $q_{\text{d,v}}$ [MJ m_{bed}^{-3}], the volumetric gross heat output $q_{\text{h,v}}$ [MJ m_{bed}^{-3}] and the volumetric mean heat output rate $w_{\text{mean,v}}$ [kW m_{bed}^{-3}] are expressed as follows:

$$q_{\text{d,v}} = \frac{-\Delta H_{\text{r}}^{\circ}}{M_{\text{Mg(OH)}_2}} \cdot \Delta x_{\text{d}} \cdot r_{\text{mix}} \cdot \rho_{\text{bed}} \tag{4.9}$$

$$q_{\text{h,v}} = \frac{-\Delta H_{r}^{\circ}}{M_{\text{Mg(OH)}_2}} \cdot \Delta x_{\text{h}} \cdot r_{\text{mix}} \cdot \rho_{\text{bed}} \tag{4.10}$$

$$w_{\text{mean,v}} = \frac{q_{\text{h}}}{t_{\text{h}}} \cdot r_{\text{mix}} \cdot \rho_{\text{bed}} \tag{4.11}$$

The properties of the packed beds are given in Table 4.1.

Table 4.1 Properties of materials of packed beds used in experiments

Pellet type	Mass of $Mg(OH)_2$ in packed bed [g]	Mass of EG in packed bed [g]	Mass mixing ratio (r_{mix}) $Mg(OH)_2$:EG	Bed density [g cm^{-3}]	Void fraction ε [-]
Pure $Mg(OH)_2$	43.9	/	n.a.	0.626	0.35
EM16	37.5	2.3	16:1	0.512	0.53
EM8	31.4	4.0	8:1	0.504	0.53
EM4	31.4	8.0	4:1	0.451	0.54

4.3. Dehydration experiments

Dehydration corresponds to the heat storage mode of the chemical heat pump, as already explained in Section 4.2. The packed bed reactor's wall is heated at 400°C until a steady state of temperatures and weight change is reached. In general, the reaction was observed to be completed over 90 minutes at least. The temperatures in the packed bed and the curve of mole reacted fraction change Δx_d was measured. Temperatures in the bed are recorded by 7 thermocouples, which are positioned as in Fig. 4.1. The temporal changes in the temperature distribution (T_1–T_7 [°C]) and the reacted fraction change (Δx_d [-]) for the dehydration of the packed beds of pure $Mg(OH)_2$, EM16, EM8, and EM4 tablets are shown in Figs. 4.2–5, respectively. In particular T_3 and Δx have been highlighted and are assumed representative values for the experimental comparison.

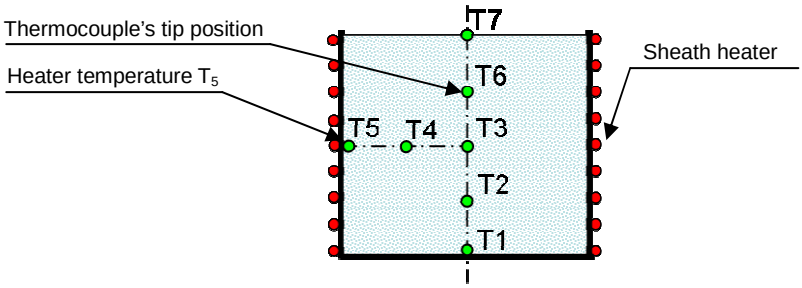

Fig. 4.3 Position of thermocouples inside of the packed bed reactor

The temperatures in the packed beds reached approximately 250°C within 10 min from the start of the experiment (the initial temperature was 120°C). Every thermocouple temperature were recorded periodically Temperatures of T_1–T_7 in the EM beds reached 250°C almost simultaneously about 5 minutes earlier than in the case of pure $Mg(OH)_2$. Because the heat was equally distributed in all portions of the EM-packed beds, the temperatures in those packed beds were more homogeneous than pure $Mg(OH)_2$ pellet bed. Particularly for the EM8- and EM4-packed beds had more uniform temperature distributions than the others. The first saddle of temperature profiles indicated that heat was consumed by the endothermic dehydration, and Δx_d progressively changed during the period. The change in the slope of a temperature profile after dehydration indicated the end of the chemical reaction. Temperatures of T_1–T_7 of EM beds were higher than the ones in the pure $Mg(OH)_2$ pellet bed, and the final value of Δx_d for the former was greater than that of the latter. It was thought that the improvement in the heat-transfer properties and heat diffusion allowed an overall increase of the bed's temperature.

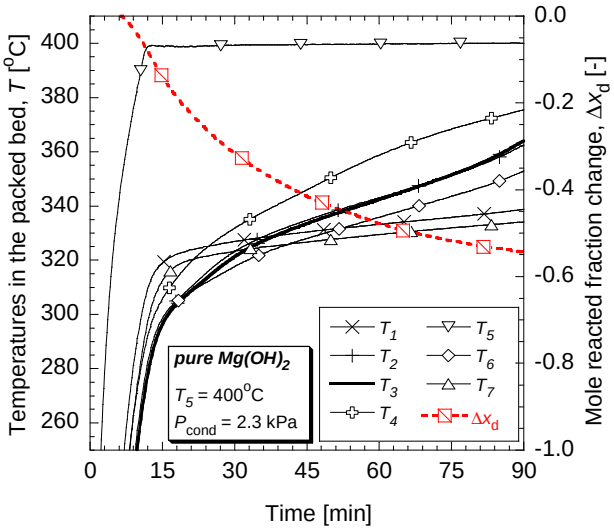

Fig. 4.4: Temperatures of $Mg(OH)_2$-packed bed, *T*, and mole reacted fraction, Δx_d, during dehydration reaction (T_5 = 400°C, P_{cond} = 2.3 kPa, T_{cond} = 20°C)

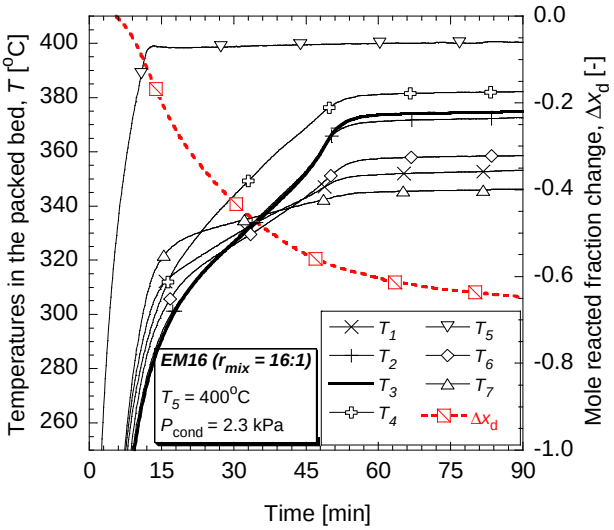

Fig.4.3: Temperatures of EM16-packed bed, *T*, and mole reacted fraction, Δx_d, during dehydration reaction (T_5 = 400°C, P_{cond} = 2.3 kPa, T_{cond} = 20°C)

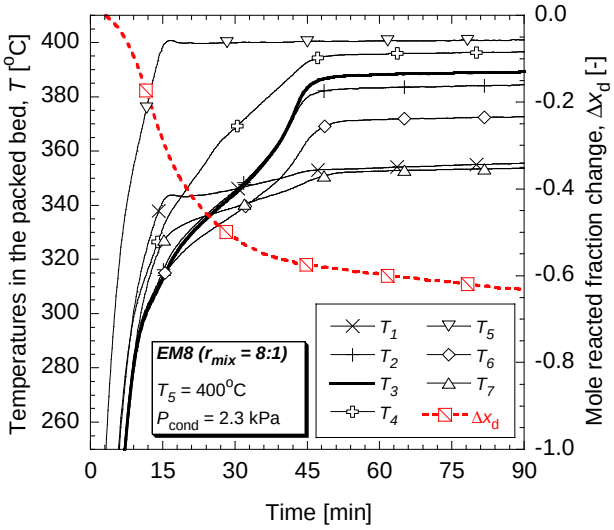

Fig. 4.4: Temperatures of EM8-packed bed, *T*, and mole reacted fraction, Δx_d, during dehydration reaction (T_5 = 400°C, P_{cond} = 2.3 kPa, T_{cond} = 20°C)

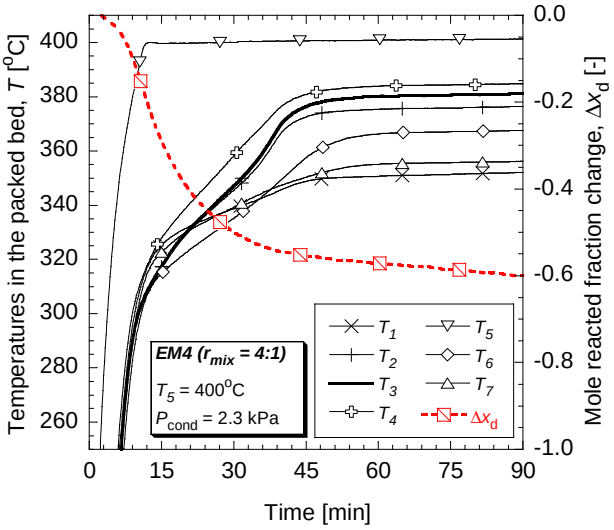

Fig. 4.5: Temperatures of EM4-packed bed, *T*, and mole reacted fraction, Δx_d, during dehydration reaction (T_5 = 400°C, P_{cond} = 2.3 kPa, T_{cond} = 20°C)

In Fig. 4.6 a comparison of the temperatures measured at the center of the packed beds (T_3) is shown for every material. Even though the heater's set temperature was the same for every packed bed experiment, it was observed that T_3 increased at different rates and reached different final values. In particular, the slopes increased gradually from EM16 to EM4. Fig. 4.7 shows a comparison of the packed beds in terms of Δx_d. It was observed that the steepness of the Δx_d curves, which correspond to the dehydration rates, was higher for the EM-packed beds. The reaction completion times in the case of the EM beds decreased progressively for the mixing ratios of 16:1, 8:1, and 4:1, in the same order. The dehydration reaction times were the shortest for EM8 and EM4. As dehydration is an endothermic

1st order chemical reaction [2], the reaction rate is a function of the temperature. In particular, a higher temperature will produce a higher reaction rate. This is because the enhancement of the heat conduction in the PBR provided by EG made it possible to reach higher temperatures with a uniform distribution. Thus, the rate of the endothermic reaction was increased, allowing a faster and more efficient completion of the dehydration. Previous work by Spinner et al. [3] on an EG composite material for CHP indicated that the optimal performance could be achieved using mass mixing ratios of 8:1 to 4:1. This explains why, despite the fact that EM4 contained more EG than EM8, their performances did not differ significantly.

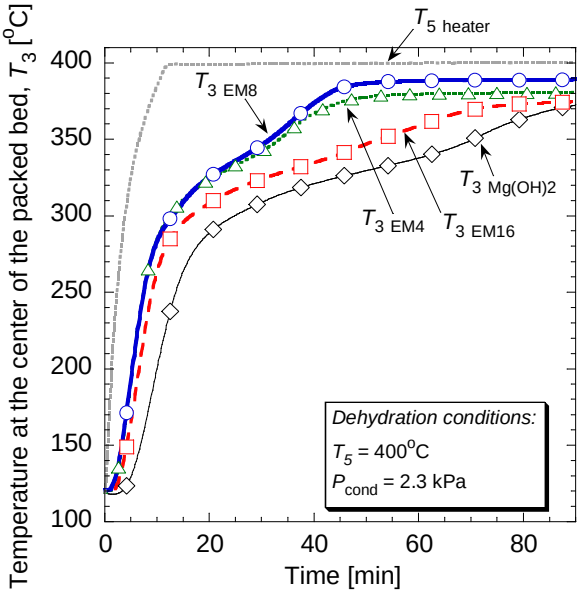

Fig. 4.6: Comparison of temperatures at packed bed center, T_3, during dehydration reaction (T_5 = 400°C, P_{cond} = 2.3 kPa, T_{cond} = 20°C)

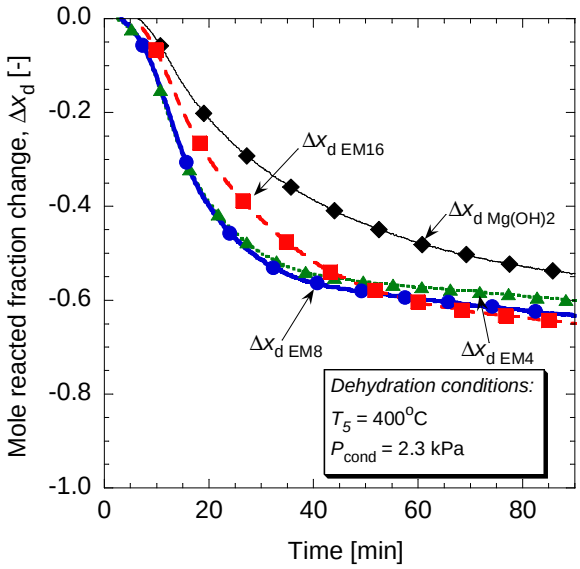

Fig. 4.7: Comparison of mole reacted fractions, Δx_d, during dehydration reaction (T_5 = 400°C, P_{cond} = 2.3 kPa, T_{cond} = 20°C)

The calculated heat-storage capacities, q_d, defined in Eq. 4.4 are shown in Fig. 4.8. It can be seen that the EM composite tablets could store heat at a quicker rate than could pure $Mg(OH)_2$ pellets. Among the EM composites, the accumulation rates of EM8 and EM4 were relatively higher. After 90 min of dehydration, the EM beds accumulated more heat per unit mass of $Mg(OH)_2$ in the PBR; in particular, $q_{d\ EM16}$ = 902 kJ $kg_{Mg(OH)2}^{-1}$, $q_{d\ EM8}$ = 881 kJ $kg_{Mg(OH)2}^{-1}$, and $q_{d\ EM4}$ = 834 kJ $kg_{Mg(OH)2}^{-1}$. However, for pure $Mg(OH)_2$, $q_{d\ Mg(OH)2}$ = 755 kJ $kg_{Mg(OH)2}^{-1}$. In the packed-bed experiments, the EM composite tablets could approach the maximum heat-storage capacity corresponding to the theoretical enthalpy change $\Delta H°_r$ = 1,390 kJ $kg_{Mg(OH)2}^{-1}$ in a better manner than the pure $Mg(OH)_2$.

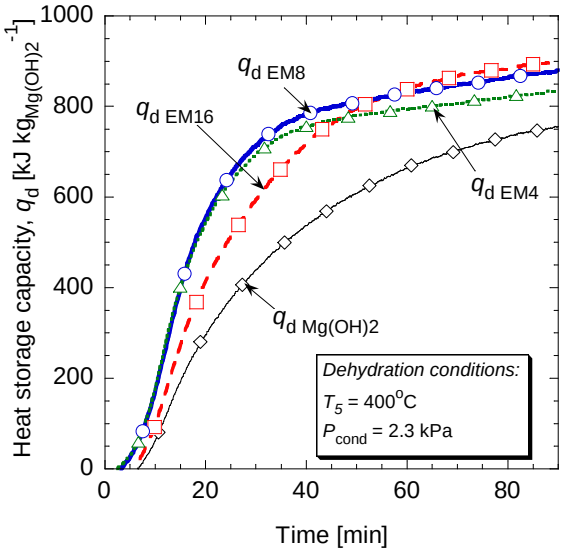

Fig. 4.8: Heat-storage capacity expressed per unit mass of $Mg(OH)_2$ in pellets (T_5 = 400°C, P_{cond} = 2.3 kPa, T_{cond} = 20°C)

4.4. Hydration experiments

This section presents the results of MgO hydration conducted under P_h = 101 kPa. As shown in Figs. 4.9–4.12, the temperatures of the seven thermocouples and the mole-reacted fraction change in hydration (Δx_h [-]) were measured for pure $Mg(OH)_2$ pellets, EM16, EM8, and EM4 tablets. It was observed that a gap existed between the temperatures measured in the core region of the bed (T_2, T_3, T_4, and T_6) and those measured at the surface boundary regions (T_1, T_5, and T_7), where heat was dissipated by conduction, convection, and radiation. The gap between these regions shrunk progressively when shifting from a mixing ratio of 16:1 to 8:1 and then from 8:1 to 4:1. This means that when the amount of graphite in the bed was larger, the temperatures in the packed bed became more uniform during hydration.

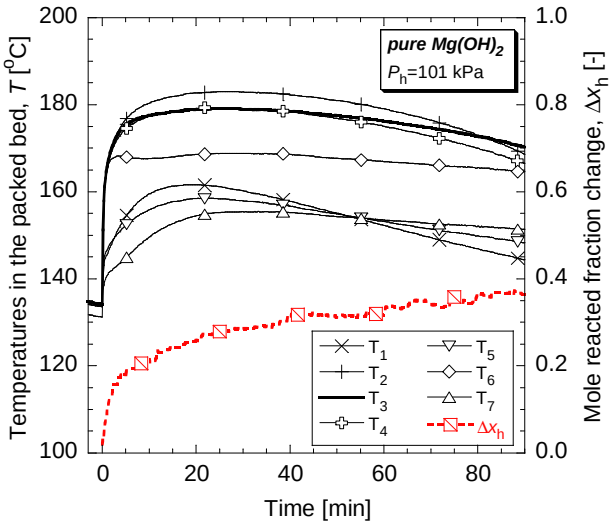

Fig.4.9: Temperatures in $Mg(OH)_2$ pellet-packed bed, *T*, and mole reacted fraction, Δx_h, during hydration reaction (P_h = 101 kPa)

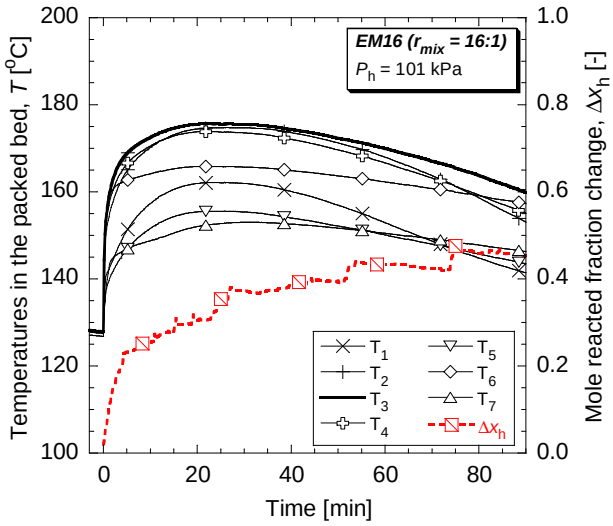

Fig.4.10: Temperatures in EM16-packed bed, *T*, and mole reacted fraction, Δx_h, during hydration reaction (P_h = 101 kPa)

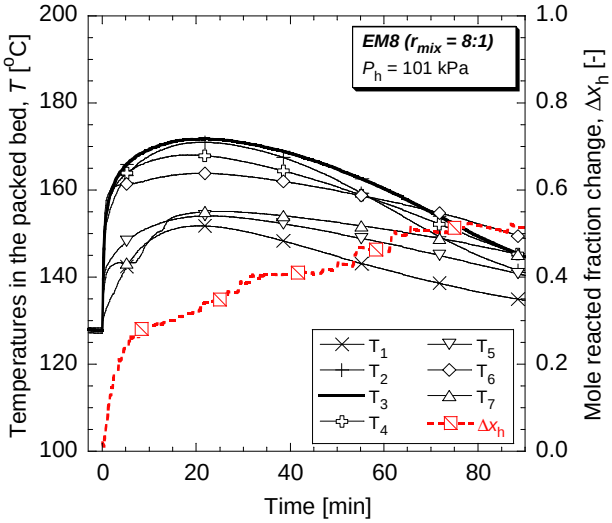

Fig.4.11: Temperatures in EM8-packed bed, *T*, and mole reacted fraction, Δx_h, during hydration reaction (P_h = 101 kPa)

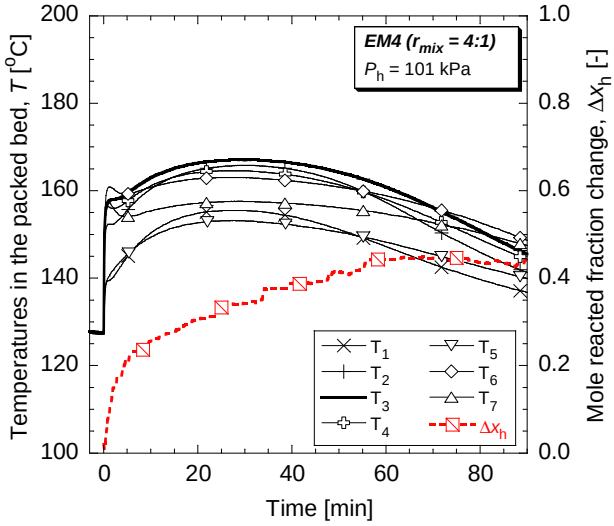

Fig.4.12: Temperatures in EM4-packed bed, *T*, and mole reacted fraction, Δx_h, during hydration reaction (P_h = 101 kPa)

Fig. 4.13 compares the temporal changes in temperature at the centers of all the packed beds (T_3). The highest value of T_3 in the EM beds was always lower than the T_3 value for the pure $Mg(OH)_2$. In particular, EM8 and EM4 showed lower T_3 peaks in comparison with EM16 and pure $Mg(OH)_2$. These temperature results demonstrated that EG was more efficient at dissipating the heat of hydration. Fig. 4.14 shows a comparison of the Δx_h values observed during hydration. The rapid initial increase in Δx_h in the first 2 min is ascribed to the physical adsorption of water on the MgO, in the form of $MgO \cdot H_2O$, as described in a previous study [1]. The initial hydration enthalpy releases were similar for all the materials in the packed bed. Then, the conversion of $MgO \cdot H_2O$ into $Mg(OH)_2$ proceeded as the reaction rate control step.

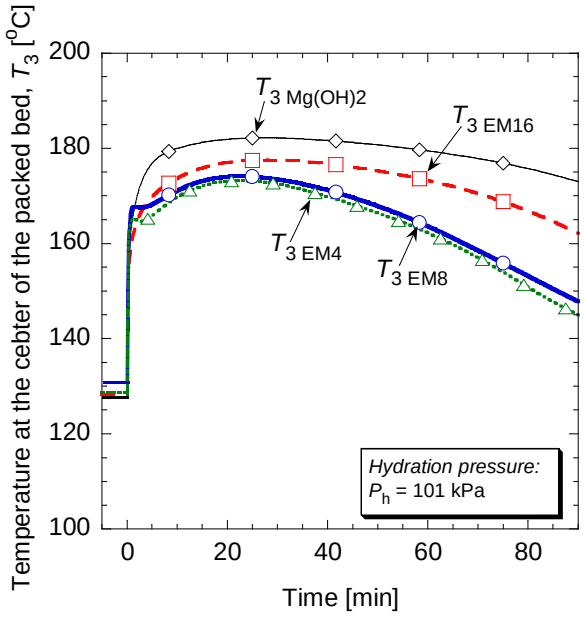

Fig. 4.13: Comparison of temperatures at packed bed center, T_3, during hydration reaction (P_h = 101 kPa)

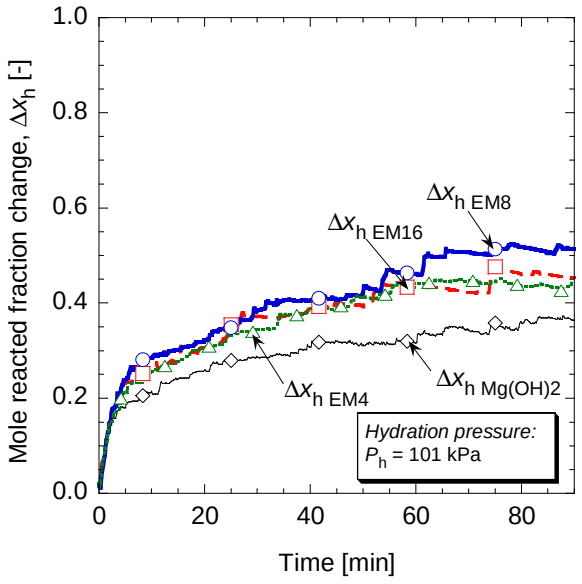

Fig. 4.14: Comparison of mole reacted fraction changes, Δx_h, during hydration reaction (P_h = 101 kPa)

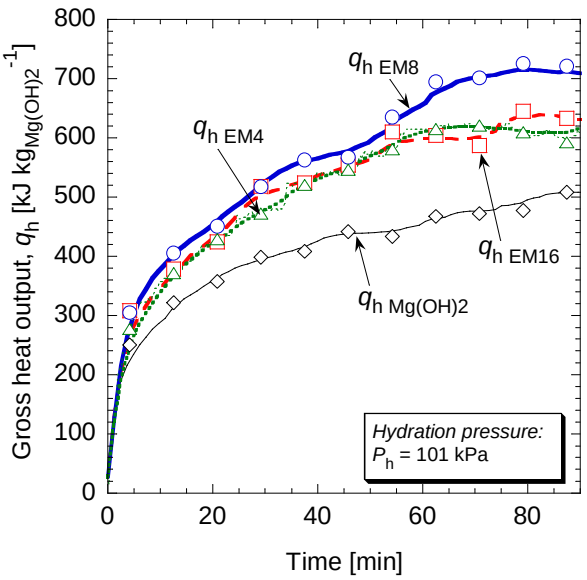

Fig. 4.15: Gross heat output expressed per unit mass of $Mg(OH)_2$ in pellets (P_h = 101 kPa)

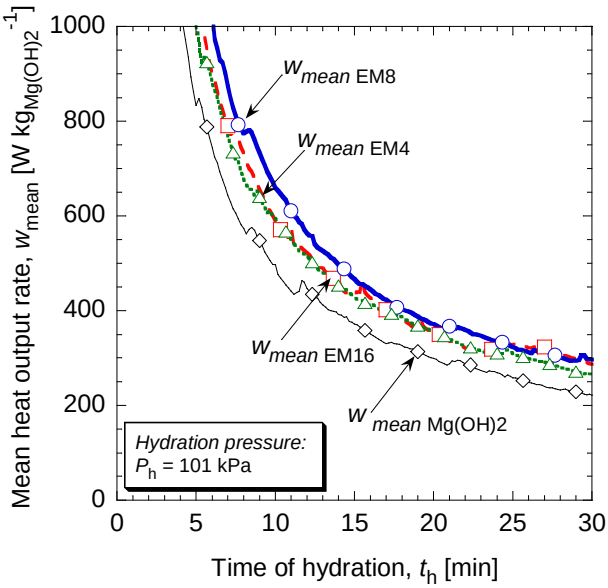

Fig. 4.16: Mean heat-output rate of hydration (P_h = 101 kPa) expressed per unit mass of $Mg(OH)_2$ in pellets

Fig. 4.15 shows the gross heat output, q_h [kJ $kg_{Mg(OH)2}^{-1}$], calculated using Eq. 4.10. Because all the EM composites showed higher Δx_h values than the pure $Mg(OH)_2$, the q_h values of the EM composites were greater than those of pure $Mg(OH)_2$. The mean heat-output rates of the hydration reaction, w_{mean} [W $kg_{Mg(OH)2}^{-1}$], calculated using Eq. 4.11, are shown in Fig. 4.16. It is clear from this figure that the EG in the packed beds contributed to the increase in w_{mean}. In the results, EM8 showed the largest mean heat-output rate in the first 30 min of hydration. Compared with pure $Mg(OH)_2$, the EM composites were found to be more capable of following rapid changes in heat demand from the demand side

because of their larger w_{mean} values.

4.5. The optimized mass mixing ratio of EM

From the results of the experiments conducted using several EM beds, it was possible to understand how their thermochemical performances could be changed as a function of the mass mixing ratio r_{mix}. The thermal conductivity and rate of reaction could be increased gradually by introducing EG with $Mg(OH)_2$; however, over a certain limit, the EG addition was disadvantageous in terms of the thermochemical performance *per unit volume*. In fact, if r_{mix} was greater than 4:1, the volume of the reactor would be filled with a greater quantity of EG than $Mg(OH)_2$. To understand this aspect, the volumetric heat-storage capacity, $q_{d,v}$ [MJ m_{bed}^{-3}], was calculated using Eq. 4.9, which considers the mass mixing ratio and density of the packed bed. The results for $q_{d,v}$ are plotted in Fig. 4.17.

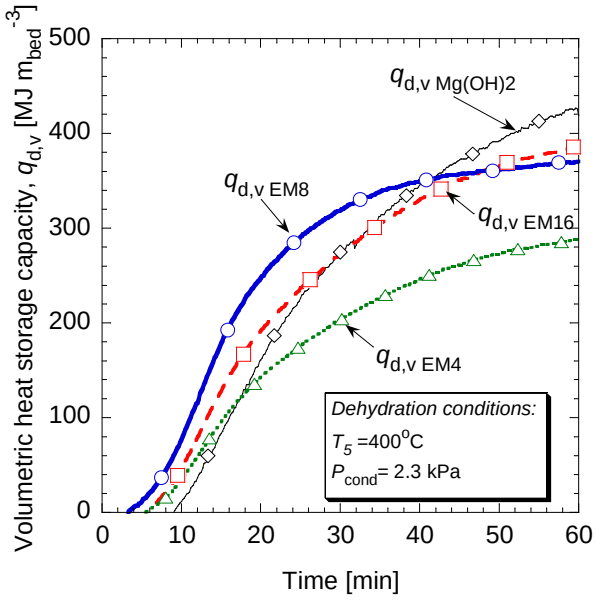

Fig. 4.17 Comparison of calculated volumetric heat-storage capacities, $q_{d,v}$ of packed beds

It was observed that in 1 h of dehydration, $Mg(OH)_2$ could store a larger amount of thermal energy per unit volume than the EM composites. However, within the first 40–50 min, EM8 and EM16 had larger $q_{d,v}$ values than the pure $Mg(OH)_2$. Although EM4 had the highest thermal conductivity, its amount of heat per unit volume was not comparable to the other materials. EM8 showed superior performance compared with the other materials within 40 min of dehydration, because its $q_{d,v}$ was the largest for this time range. The EM-packed beds were characterized by a larger ε_{bed} than the pure $Mg(OH)_2$ bed (as reported on Table 4.1, section 4.2). This imposed a limitation on the experimentally obtained values of $q_{d,v}$ for the EM composite tablets because only about 50% of the bed was occupied by them as compared to 68% in the case of the $Mg(OH)_2$ bed. In addition, a large void fraction reduces the thermal conductivity in a packed bed because of the interspaces between pellets and the poor inter-pellet contact. However, the apparent thermal conductivity and thermochemical performance of the EM beds were higher and better, respectively, than those of the pure $Mg(OH)_2$ bed. This means that by decreasing the

void fraction of packed beds of EM tablets (in other words, increase the packed bed's density), it might be possible to further enhance the thermal performance of the system, in terms of both the thermal conductivity and heat-storage capacity per unit volume.

4.6. The increase of heat storage capacity

4.6.1. Decreasing the packed bed's void fraction

Following the previous discussion on optimization of EM, it was prepared a new packed bed of EM8 tablets in which the void fraction was reduced by packing the tablets more tightly. This was possible by changing the size and arrangement of tablets in the packed bed reactor, as shown in Fig. 4.18. The previous EM8 tablets having a diameter ϕ_{EM8} = 7.1 mm, thickness $l_{EM\text{-}a}$ = 3.5-4.5 mm will be referred as EM8 tablets while larger size pellets having diameter $\phi_{EM8\text{-}b}$ = 10.1 mm, thickness $l_{EM8\text{-}b}$ = 6.1 mm will be referred as EM8-b tablets. The corresponding beds of tables will be indicated respectively EM8 bed and EM8-b bed , respectively. EM8 tablets were charged directly into the reactor, assuming a random orientation, as shown on Fig. 4.18 (b). On the other hand, the EM8-b tablets were arranged in piles inside of the reactor, as shown on Fig. 4.18 (c). This tight packing of the EM8-b tablets allowed charging a larger amount of EM8 inside of the reactor. Even if the densities of EM8 tablets were similar (ρ_{EM8} = 1.07 g cm^{-3}, $\rho_{EM8\text{-}b}$ = 1.06 g cm^{-3}) the density of the packed bed of EM8-b tablets arranged in piles, ρ_{bed} = 0.714 g cm^{-3}) resulted larger. The properties of the packed beds are summarized in Table 4.2. In case of EM8-b bed, the same amount of $Mg(OH)_2$ as in the pure $Mg(OH)_2$ bed experiment (44 g, Fig.4.18 (a)) could be loaded in the reactor.

a) pure $Mg(OH)_2$ bed **b) EM8 bed** **c) EM8-b bed**

Fig.4.18 The packed beds used in this work, (a) pure $Mg(OH)_2$, (b) EM-a small tablets in random arrangement and (c) EM-b big tablets arranged in piles for increasing the density of the bed.

Table 4.2: The properties of the packed beds

Bed material	Mass of bed m_{bed} [g]	Mass of $Mg(OH)_2$ in bed $m_{Mg(OH)2}$[g]	Particle size ϕ x l [mm]	Density of particle $\rho_{particle}$ [g cm^{-3}]	Density of bed ρ_{bed} [g cm^{-3}]	Void fraction of bed ε [-]
$Mg(OH)_2$ bed, pellets randomly arranged	43.9	43.9	Pellet ϕ 2 x 10	0.966	0.626	0.35
EM8 bed, tablets randomly arranged	39.4	32.0	Tablet ϕ 7 x 4	1.07	0.504	0.53
EM8-b bed, tablets arranged in piles	49.1	43.6	Tablet ϕ 10 x 6	1.056	0.714	0.32

4.6.2. Evaluation of thermal conductivity of EM8-b

The particular arrangement of the EM8-b tablets has an advantage: because of the anisotropic thermal conductivity of EM, the direction of larger thermal conductivity in the tablets (radial) is the same direction of heat supply from the wall of the reactor. The thermal conductivities of piles of EM8-b tablets were measured after cyclic experiments. They were arranged over the thermal conductivity meter's hot wire sensor as showed on Fig. 4.19. Such an arrangement can be representative of the EM8-b bed, as material was loaded similarly in the packed bed reactor (Fig. 4.18(c)). The averages of 30 measurements are summarized on Table 4.3.

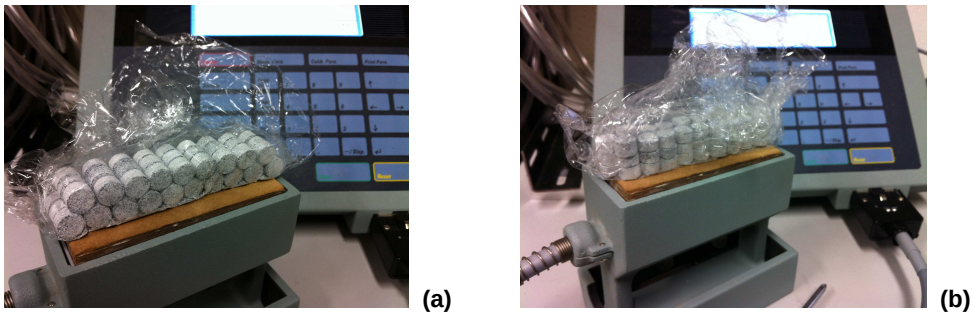

(a) **(b)**

Fig. 4.19 Measurements of thermal conductivity on two different directions for used EM tablets

Table 4.3 Results of thermal conductivity measures on used EM8-b bed of tablets arranged in piles

	Thermal conductivity [W $m^{-1}K^{-1}$]
EM8-b λ_{bed} measured **perpendicular** to direction of compression (Fig. 3.19 (a))	0.55
EM8-b λ_{bed} measured **parallel** to direction of compression, (Fig. 3.19 (b))	0.45

Fig 4.20 shows a comparison between the thermal conductivities of EM8 bed (small tablets randomly arranged in the reactor) and the results on table 4.3, representative of the EM8-b bed (big tablets

arranged in piles in the reactor). The thermal conductivity of the EM8-b bed resulted higher than the one of EM8 bed. The pile arrangement showed the following advantages:

- increase the thermal conductivity of the bed because of smaller void fraction
- in the radial direction, which is the direction of heat supply from the wall or the reactor, the value of thermal conductivity could be maximized.
- The tidy packing allowed to increase the amount of $Mg(OH)_2$ contained in the bed.

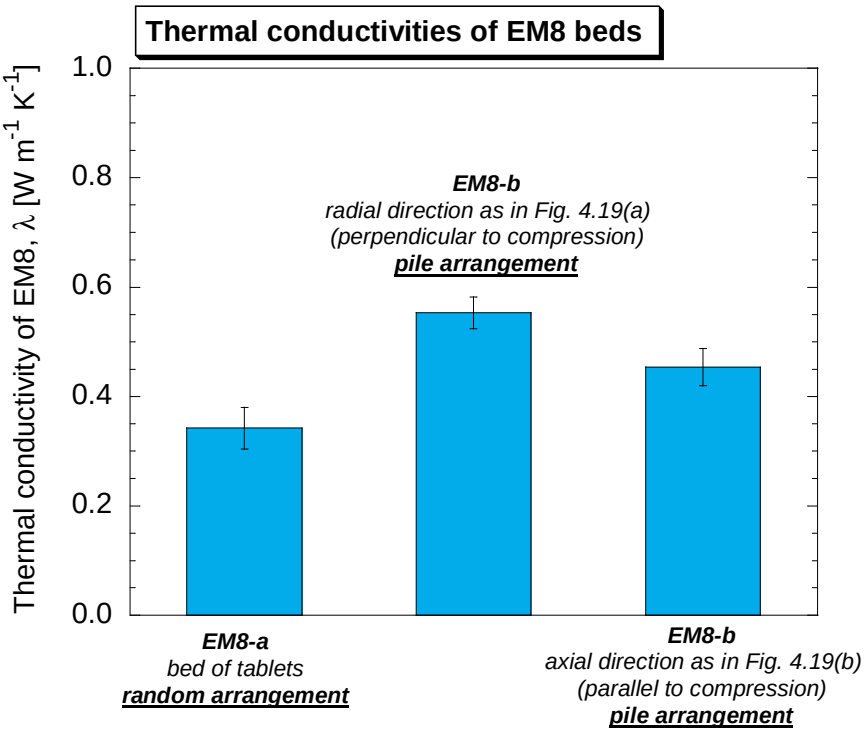

Fig. 4.20 Comparison between measurements of thermal conductivities of beds having different size and arrangements of EM8 tablets

4.6.3. Dehydration experiments

In this section, the results of dehydration experiments on the beds on Fig. 4.18 will be presented. Fig. 4.21 shows the temperature at the center of the packed bed reactor, T_3, and the mole reacted fraction change, Δx_d, in function of time during dehydration. The temperature set of the heater, controlled by T_5 = 400 °C, was the same for all the experiments. The comparison of dehydration results in Fig. 4.21 shows that EM8 and EM8-b were characterized by a similar temperature increase of T_3, despite EM8-b contained a larger amount of mass to be heated. The slopes of curves of their mole reacted fraction change, Δx_d, were also similar. From these Δx_d, the volumetric heat storage capacity, $q_{d,v}$ was calculated with Eq. 4.9. The results are shown on Fig. 4.22. It was already observed in Fig. 4.17 that, after about 40 minutes, EM8 bed of tablets was saturated, while in $Mg(OH)_2$ bed the dehydration was still going on. However, the EM8-b bed of tablets contained the same amount of $Mg(OH)_2$ of the pure $Mg(OH)_2$ bed of pellets. It was calculated that in 40 minutes the EM8-b bed stored

$q_{d,v}$ = 442 MJ m_{bed}^{-3} while $Mg(OH)_2$ and EM8 beds stored respectively 342 and 349 MJ m_{bed}^{-3}. The tight packing of the EM8-b bed allowed storing about +29% of energy in the same time in comparison with the other beds. After 90 minutes, a maximum of 482 MJ m_{bed}^{-3} was achieved by $Mg(OH)_2$ bed. The same value was achieved by EM8-b bed in 77 minutes.

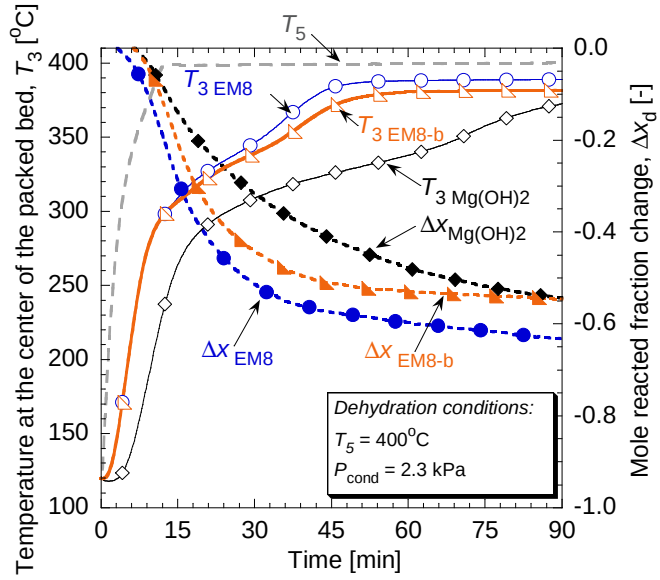

Fig. 4.21 Comparison of results for dehydration of the packed beds (T_5 = 400°C, P_{cond} = 2.3 kPa, T_{cond} = 20°C)

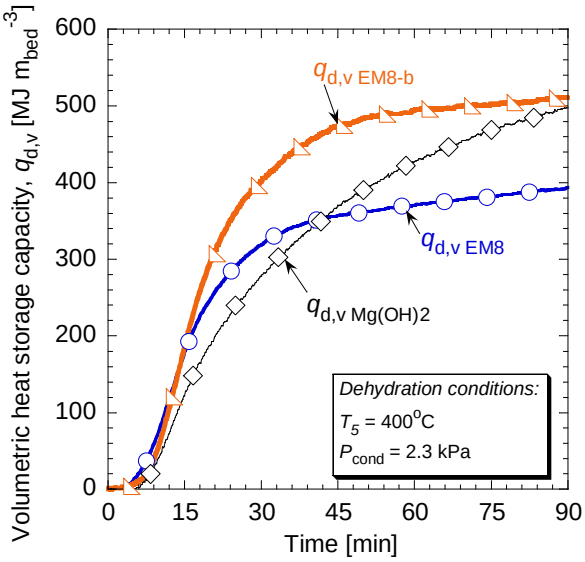

Fig. 4.22 Comparison of calculated volumetric heat-storage capacities, $q_{d,v}$ of packed beds (T_5 = 400°C, P_{cond} = 2.3 kPa, T_{cond} = 20°C)

4.6.4. Hydration experiments

In this section, the results refer to hydration conducted by supplying saturated water vapor at 47 kPa (T_{sat} = 80°C). This pressure was lower than the previous at 101 kPa. Other researchers [4] observed poor performance at low gas pressure, determined by scarce diffusion of the gas phase into their consolidated block of $MnCl_2$ and expanded graphite. Therefore, it was made an attempt to verify if the rate of reaction could be affected by diffusion resistance in tablets having a larger shape.

Fig. 4.23 shows the results of the hydration experiments, including the temperature at the center of the bed T_3 and the mole reacted fraction change Δx_h. It indicates that Δx_h resulted slightly better for EM8 bed than EM8-b bed, however the Δx_h EM8-b bed was still much larger than the $Mg(OH)_2$ pellets. Fig. 4.24 shows the results of volumetric gross heat output q_h [MJ m_{bed}^{-3}] calculated with Eq. 4.10. It interesting to observe that EG enhanced the chemical reaction, as EM8 and $Mg(OH)_2$ beds had a similar curve profile of $q_{h,v}$ [MJ m_{bed}^{-3}], despite EM-a bed contained a smaller amount of reactant. The highest volumetric gross heat output was achieved by EM8-b bed because it had the same amount of reactant as in the $Mg(OH)_2$ bed and a Δx_h profile similar to EM8 bed. Moreover, despite EM8-b bed had higher heat output, it had a temperature T_3 lower than in case of $Mg(OH)_2$ bed, suggesting again that EG helped the dissipation of hydration heat from the packed bed to the surroundings.

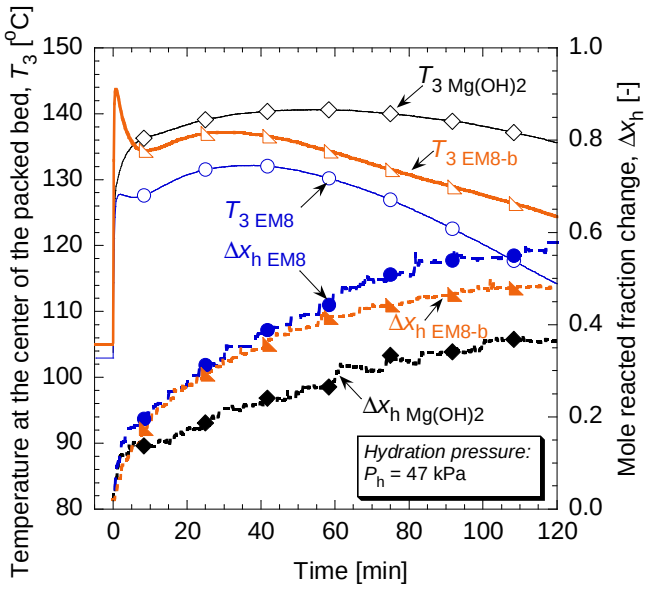

Fig. 4.23 Comparison of results for hydration of the packed beds (P_h = 47 kPa, T_{evap} = 80°C)

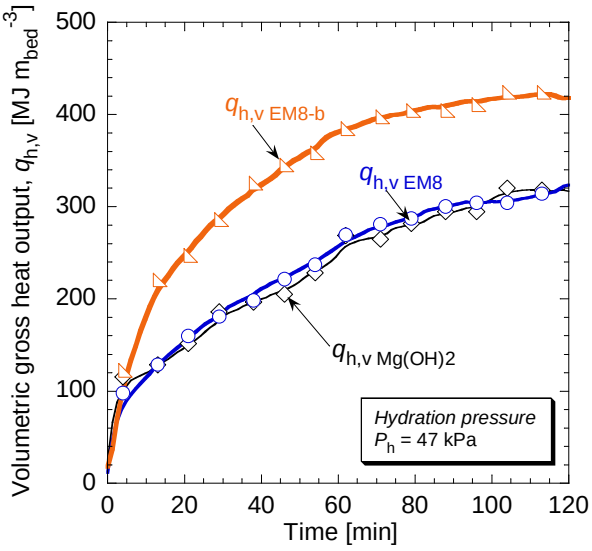

Fig. 4.24 Comparison of calculated volumetric gross heat output, $q_{h,v}$ of packed beds (P_h = 47 kPa, T_{evap} = 80°C)

4.7. Reactive block of EM

4.7.1. Preparation of the reactive block of EM8

It has been just demonstrated that the EM8-b bed of tablets showed better performances of the pure $Mg(OH)_2$ bed of pellets. However, in the experiments with EM8-b bed, tablets arranged in piles were utilized, therefore thermal conductivity was still than the bulk slab of EM8s already measured in Chapter 3 (in the direction perpendicular to compression, thermal conductivity of EM8 slab was double than EM8-b bed of tablets). Moreover the contact between packed material and reactor's inner heated surface is poor. EM8 bed has still margin for improving thermal conductivity and thermal performance. It was therefore required to manufacture a reactive block of EM8. The preparation is showed from Fig. 4.25 (a) to (e). It was also tried a new preparation method of EM, in order to avoid the manual crushing of $Mg(OH)_2$ precursor pellets and the sieving operations. In this time, EM8 was prepared as follows:

- $Mg(OH)_2$ pellets (64.83 g) were crushed by rotating in a mill for 24 hours. Water was added in order to obtain slurry (approx. 500 ml).
- To help the milling and stirring process, a small pestle was introduced in the bottle. It resulted that all the pellets resulted crushed after the milling time.
- An amount of 8.09 grams of expanded graphite was added in the bottle containing the slurry.
- To homogenize the composite, the bottle rotated at very low speed in the mill for 3 minutes.
- The homogeneous EM slurry was then introduced inside of a Pyrex beaker and dried into an electric oven, at 95°C for 2 days.
- After compression of the block (diameter 47 mm, height 40 mm), a hole for thermocouple insertion was prepared with a screwdriver.

From the initial 72.92 g of EM8, the final amount was 70.93g. About 2 g of EM8 were lost in the

preparation method (attached to glass, on mold surface, physical water). Considering the mass mixing ratio 8:1, the amount of $Mg(OH)_2$ in the block is 63.05 g. This mass is 63 / 44 = 1.43 times larger than in the packed beds of the pure $Mg(OH)_2$ pellets and EM8-b tablets. It is expected that the amount of heat stored per unit volume of packed bed would be larger in case of the EM8 block. Experiments were conducted as usual, completing 24 cycles of dehydration at 400°C and hydration at different pressures. The EM8 block has been compared with the original pure $Mg(OH)_2$ bed of pellets and the EM8-b bed of tablets. Table 4.4 shows the properties of the packed beds. The density of the EM8 block is very close to the density of the single tablet used for the EM8-b and EM-a beds.

Table 4.4: Properties of the packed beds object of comparison

Material	Charged mass of $Mg(OH)_2$ [g]	Mass of packed bed[g]	Density of particle [g cm^{-3}]	Density of bed [g cm^{-3}]
$Mg(OH)_2$ bed, pellets randomly arranged	43.9	43.9	0.966	0.626
EM8 bed, tablets randomly arranged	43.6	49.1	1.056	0.714
EM8 block, fitting with reactor's inner wall	63.1	70.9	1.022	1.022

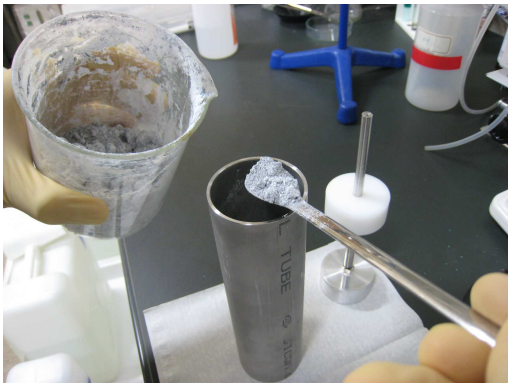

Fig.4.25 a) Raw EM8 is loaded in the mold

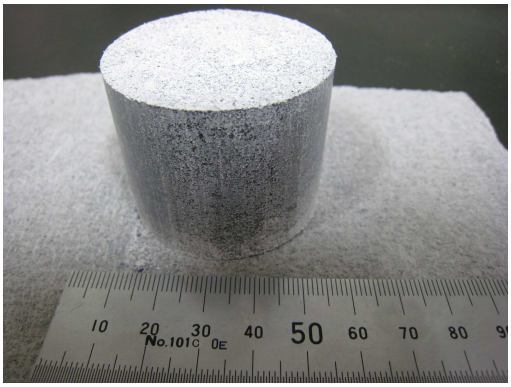

Fig.4.25 b) The EM8 block after compression

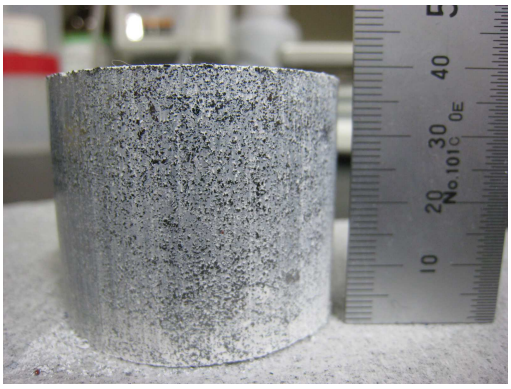

Fig.4.25 c) Side surface of the EM8 block

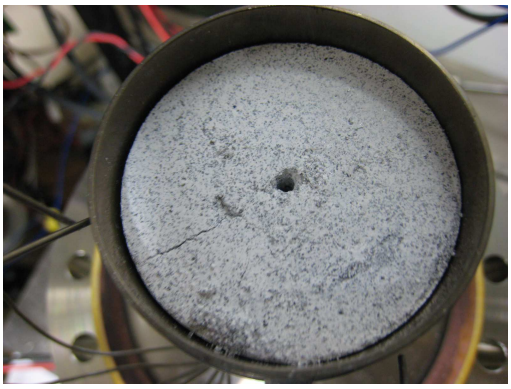

Fig.4.25 d) EM8 block loaded in the reactor

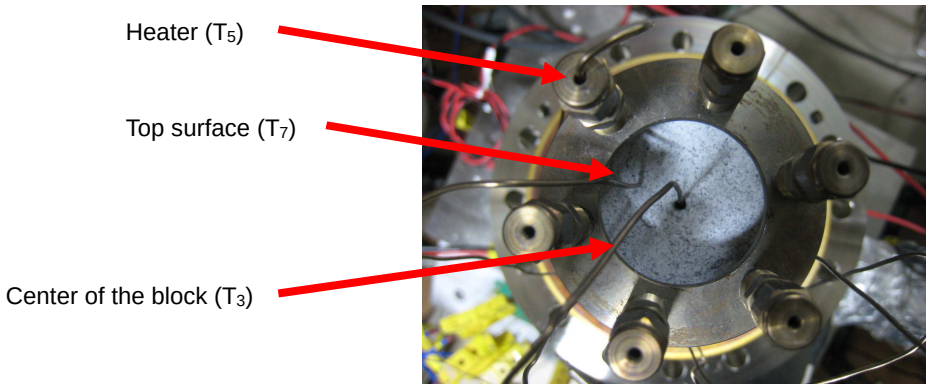

Fig.4.25 e) Positions of the thermocouples (3 in total)

Fig. 4.25 Preparation procedure of EM block packed bed experiment

4.7.2. Dehydration experiments

In Fig. 4.26 we can see the comparison of dehydration results (temperature at center T_3 and mole reacted fraction change Δx_d). The results show that for the EM8 block the reaction seems to proceed more slowly than EM8-b bed, but still faster than the $Mg(OH)_2$ one. This is because of the larger mass of the EM8 block. However, when calculating the heat storage capacity we obtain the plot on Fig. 4.27. It shows that the EM8 block is the solution which has the largest volumetric heat storage capacity. EM8 block stored heat as fast as EM8 pellets in the early 20 minutes, but it could store 750 MJ m^{-3} rather than 500 MJ m^{-3} after 120 minutes of reaction.

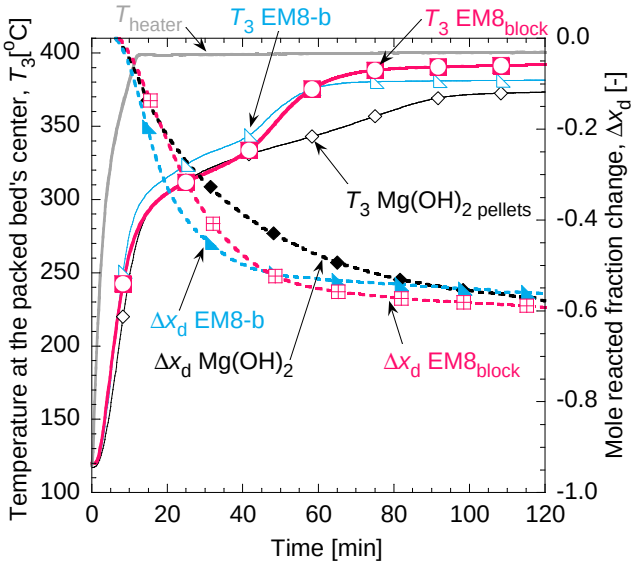

Fig. 4.26 Comparison of results for dehydration of the packed beds (T_5 = 400°C, P_{cond} = 2.3 kPa, T_{cond} = 20°C)

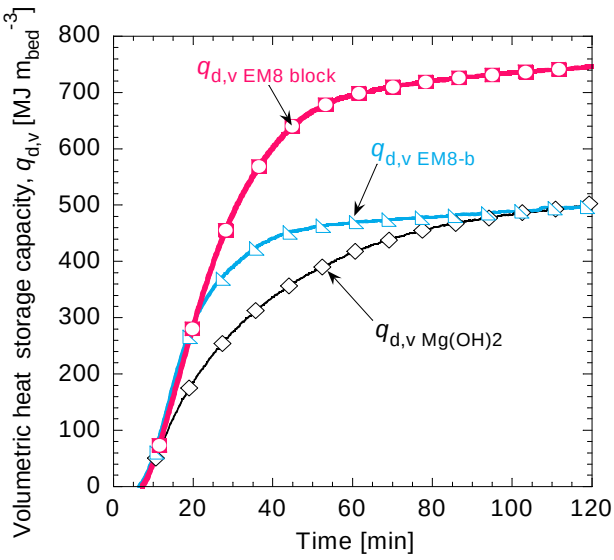

Fig. 4.27 Comparison of calculated volumetric heat-storage capacities, $q_{d,v}$ of packed beds (T_5 = 400°C, P_{cond} = 2.3 kPa, T_{cond} = 20°C)

4.7.3. Hydration experiments

The results of hydration at 47 and 361 kPa are shown in Figs. 4.28-29. They include the temperature at the center of the bed T_3, the mole reacted fraction change Δx_h and the volumetric gross heat output $q_{h,v}$. It was observed that the reactivity of the EM8 block is not as good as the tablets in the EM8-b bed at pressure of 47 kPa. The shape of the Δx_h curve of EM8 block is completely different from the others of EM8-b bed and $Mg(OH)_2$ bed, suggesting that the reaction mechanism might be controlled by diffusion of water vapor. Wishing to utilize the EM8 block at low hydration pressures, gas diffusion has to be improved, for example by creating vertical channels parallel to the axis of the block. Despite this, Fig. 4.29 shows that the volumetric gross heat output of the EM8 block is still larger than the one of $Mg(OH)_2$ bed of pellets.

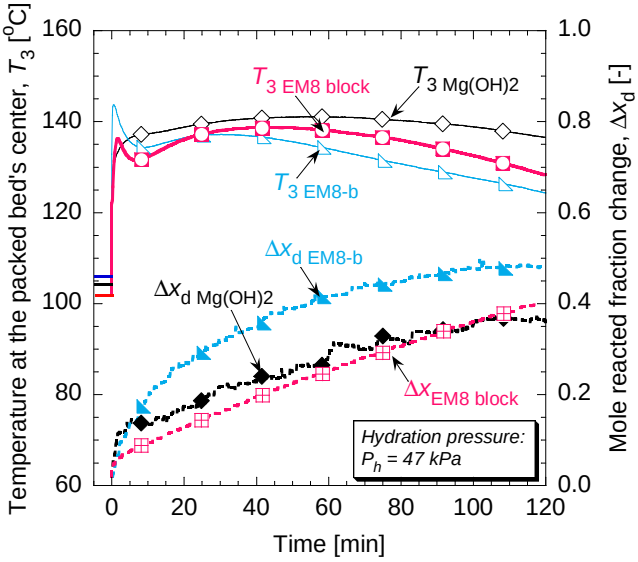

Fig. 4.28 Comparison of results for hydration of the packed beds (P_h = 47 kPa, T_{evap} = 80°C)

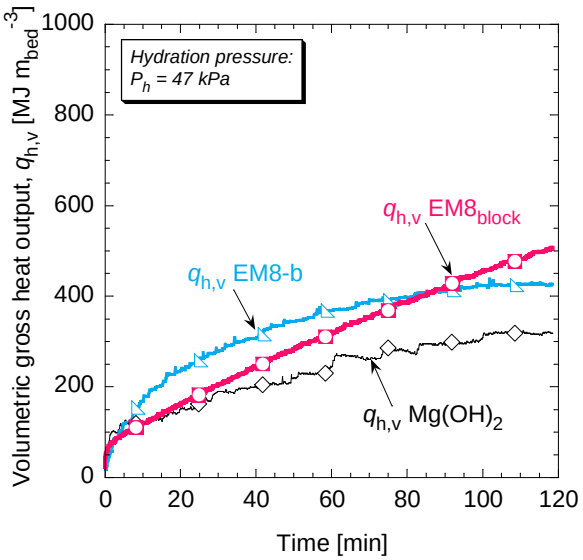

Fig. 4.29 Comparison of calculated volumetric gross heat output, $q_{h,v}$ of packed beds (P_h = 47 kPa, T_{evap} = 80°C)

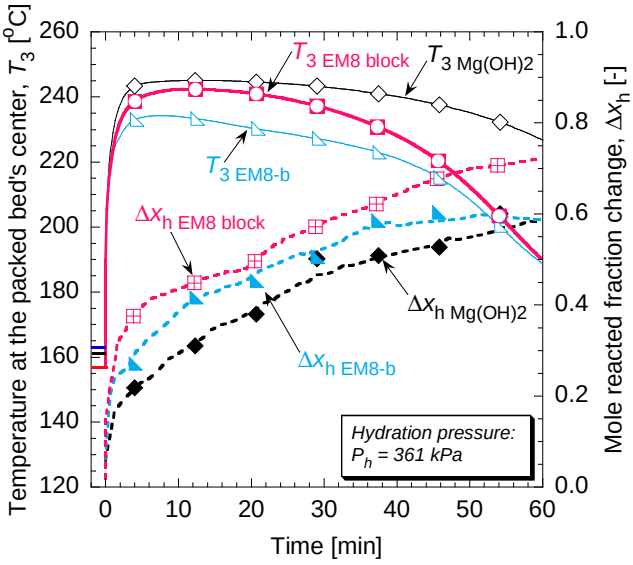

Fig. 4.30 Comparison of results for hydration of the packed beds (P_h = 361 kPa, T_{evap} = 140°C)

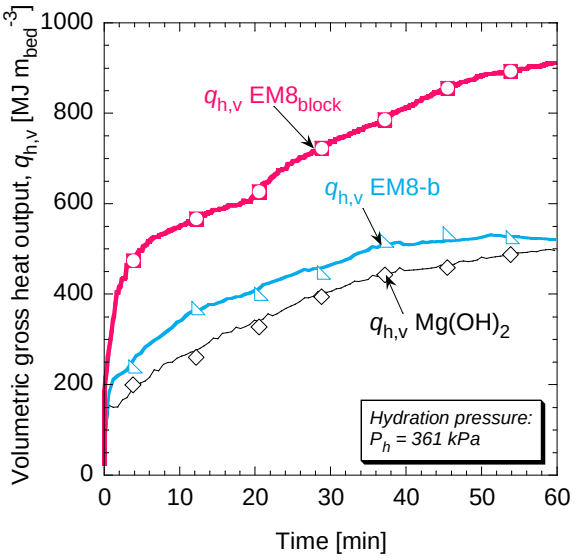

Fig. 4.31 Comparison of calculated volumetric gross heat output, $q_{h,v}$ of packed beds (P_h = 361 kPa, T_{evap} = 140°C)

For the experiments at hydration pressure of 361 kPa, Fig.4.28 shows that the EM8 block had the highest rate of increase of Δx_h. For what concerns the temperature at the center of the EM8 block, it resulted closer to the temperature measured in the EM8-b bed than to the one in the $Mg(OH)_2$ bed. Fig. 4.31 indicates also that the EM8 block exhibited the largest gross heat output. These aspects demonstrate that the high thermal conductivity in the EM8 block and the improved contact with the reactor's wall helped the dissipation of heat of hydration: as the temperature resulted lower, the rate of hydration was enhanced in comparison with the other materials. Especially for hydration at 361 kPa, it is possible to recover heat at higher temperature (approximately 220°C-230°C). The reaction rate of hydration is strongly influenced by the hydration pressure. It was observed that at P_h = 47 kPa, the

reaction was saturated after about 120 min or mode. In case of P_h = 361 kPa, hydration was saturated in about 60 minutes. Hydration at high pressure allows releasing heat more promptly and at higher temperature. This feature is crucial for reutilization of heat in industrial applications. Reactivity enhancement at low pressures is not discussed in this work, however detailed studies were provided by Ishitobi *et al.* [5], Kim *et al.* [6]. and Myagmarjav *et al.* [7]

Finally, the volumetric mean heat output rate $w_{mean,v}$ was calculated with Eq.4.11 for the hydration of materials at 47 kPa and 361 kPa. The results are showed respectively in Fig. 4.32 and 4.33 for P_h = 47 kPa and in Fig. 4.34 and 4.35 for P_h =361 kPa.

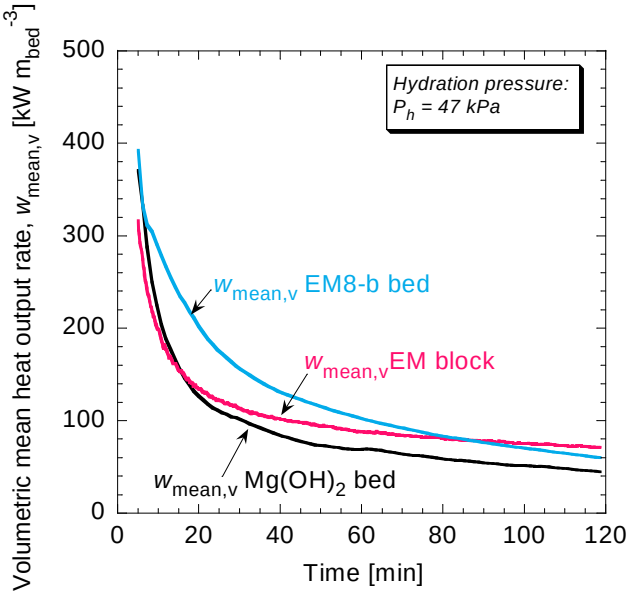

Fig.4.32 Volumetric mean heat-output rate of hydration $w_{mean,v}$ (P_h = 47 kPa)

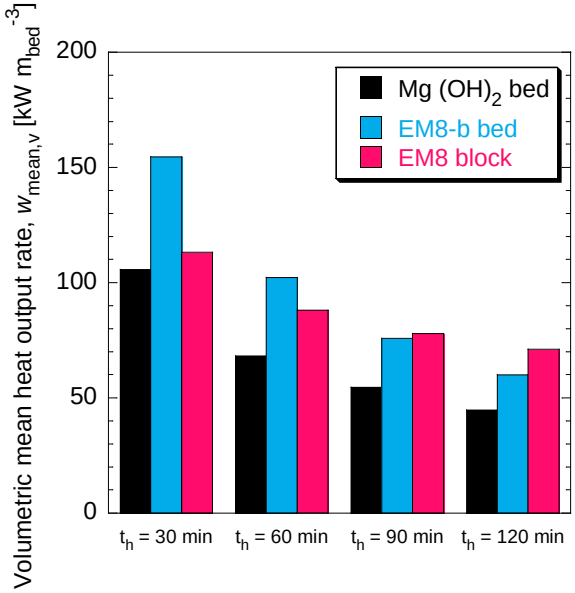

Fig.4.33 Volumetric mean heat output $w_{mean,v}$ for hydration times of 30, 60 and 90 min (P_h = 47 kPa)

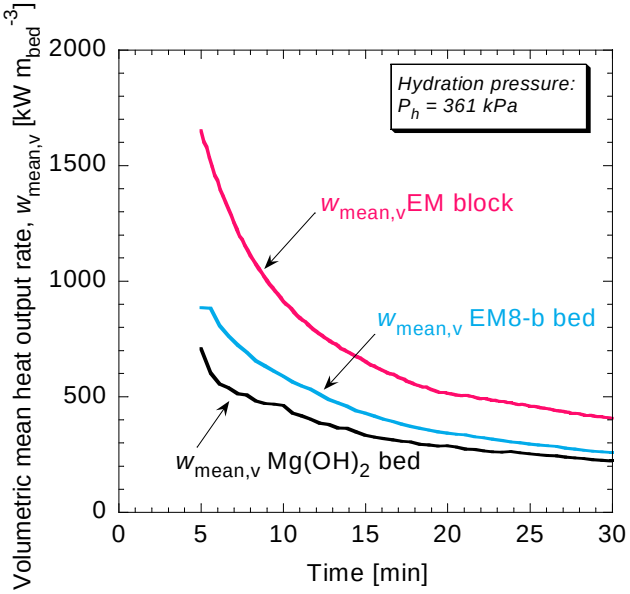

Fig.4.34 Volumetric mean heat-output rate of hydration $w_{mean,v}$ (P_h = 361 kPa)

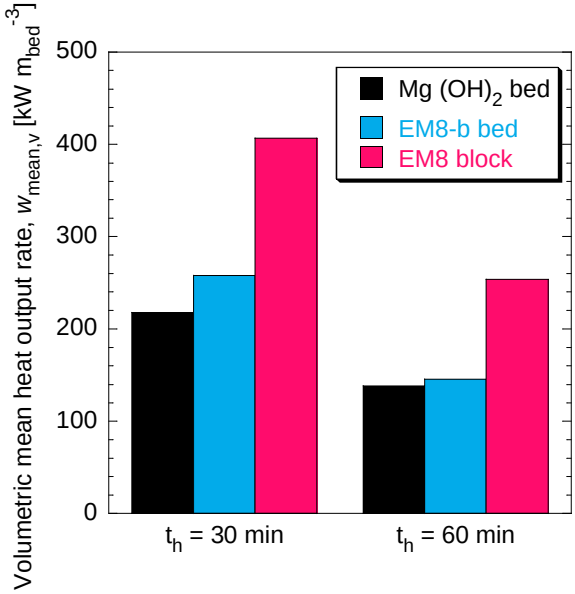

Fig.4.35 Volumetric mean heat output $w_{mean,v}$ for hydration times of 30 min and 60 min (P_h = 361 kPa)

When P_h = 47 kPa Fig. (4.32 and 4.33), for t_h < 90 min the highest $w_{mean,v}$ was recorded by the EM8-b bed. The EM8 block had lower $w_{mean,v}$ than $Mg(OH)_2$ bed for t_h < 15 min but higher than EM8-b bed for t_h > 90 min. The utilization of EM8 block at P_h = 47 kPa is advantageous only in particular conditions, in which the demand from the user lasts more than 90 with and can be satisfied with a $w_{mean,v}$ of 70 kW m_{bed}^{-3}. When the demand of heat lasts from 30 to 60 minutes, EM8-b can satisfy the demand with a $w_{mean,v}$ of 100-150 kW m_{bed}^{-3}.

When P_h = 361 kPa (Fig. 4.34 and 4.35), the highest $w_{mean,v}$ was recorded by the EM8 block. The EM8 block showed a $w_{mean,v}$ in 30 minutes of hydration at 361 kPa of 407 kW m_{bed}^{-3}, which is almost two times larger than the 258 and 218 kW m_{bed}^{-3} obtained respectively from EM8-b bed of tablets and $Mg(OH)_2$ bed of pellets. The EM8 block is therefore the solution which releases more heat in a shorter time in comparison with the EM8-b and $Mg(OH)_2$ beds. It would respond more quickly to sudden demand of heat from users. As the temperature of heat release with P_h = 361 kPa is 220°C-230°C, while with P_h = 47 kPa is 130°C-140°C, and heat is stored at 350°C-400°C, the operation at P_h = 361 kPa or larger would be more efficient from the exergetic point of view, as it allows to recover heat at higher temperature.

To enable a fair comparison of the rate of hydration as a function of pressure, the mean rate of hydration, $\Delta\bar{x}_h$ [s^{-1}], for a certain time of hydration, Δt_h [s], can be expressed by:

$$\Delta\bar{x}_h = \Delta x_h / \Delta t_h \qquad (4.12)$$

The values of achieved after Δt_h = 30 min of hydration, [s^{-1}], obtained at different hydration pressures of 47, 101, 191, and 361 kPa, were compared in a logarithm plot (Fig. 4.36). In this plot, P_0 was assumed to be the atmospheric pressure (P_0 = 101.325 kPa). The range for the evaluation of was selected as Δt_h = 30 min: within this time, hydration was advancing steadily in all the experiments at different hydration pressure (P_h) in both the packed beds. The relation between the mean rate of hydration $\Delta\bar{x}_h$ and the rate constant of hydration k_h [s^{-1}] is expressed by:

$$\Delta\bar{x}_h = k_h \cdot (P / P_0)^n \qquad (4.13)$$

by taking the natural logarithms of Eq.4.13, we obtain:

$$\ln(\Delta\bar{x}_h) = \ln(k_h) + n \cdot \ln(P_h / P_0) \qquad (4.14)$$

By using the values of $\Delta\bar{x}_{h,\,30\,min}$ in Eq.4.14, the values of ln (k_h) and n when Δt_h = 30 min could be determined from the logarithm plot for both the hydration experiments on the bed of $Mg(OH)_2$ pellets and the EM8 block. The value of ln(k_h) was similar for both cases (approximately ln(k_h) = -8.7) , while the coefficient n for the EM8 block was 1.8 times larger than the n calculated for the bed of $Mg(OH)_2$ pellets. This indicated that $\Delta\bar{x}_h$ of the EM8 block is more sensitive to hydration pressure (P_h) than the $\Delta\bar{x}_h$ of the bed of $Mg(OH)_2$ pellets. In particular, for P_h < 101 kPa, the $\Delta\bar{x}_h$ of EM8 block is lower than that of the bed of $Mg(OH)_2$ pellets, while for P_h > 101 kPa, an opposite trend is observed. As the reaction conditions are identical, it was concluded that the rate of hydration is controlled by mass transfer for P_h <

101 kPa (poor water vapor diffusion in the EM8 block), while it is controlled by heat transfer for P_h > 101 kPa (higher thermal conductivity of EM8 enhanced the removal of the heat of hydration from the packed bed reactor).×

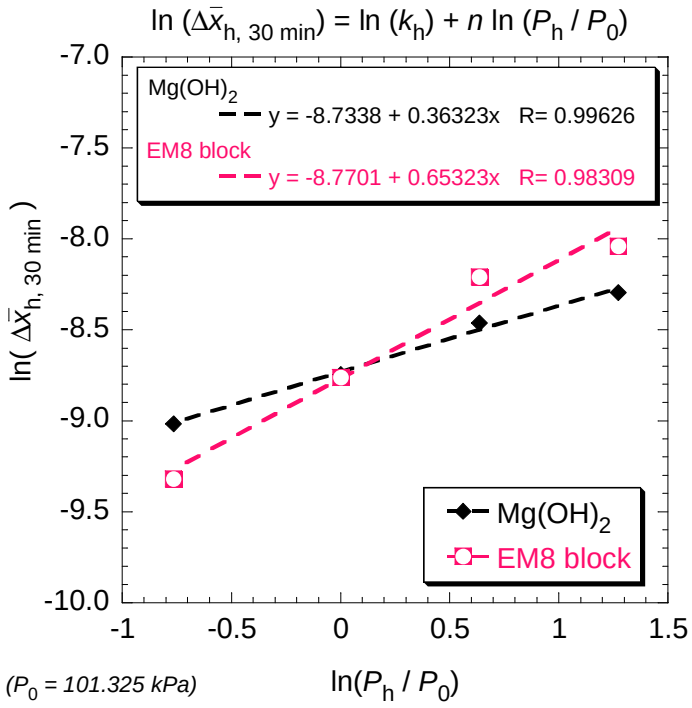

Fig. 4.36 Logarithm plot showing the relation between hydration pressure (P_h / P_0) and mole reacted fraction change after 30 min of hydration, $\Delta\bar{x}_{h,\ 30\ min}$ for the packed bed of $Mg(OH)_2$ pellets and EM8 block.

4.8. Conclusions

EG was successfully incorporated into EM to enhance the thermal conductivity of the packed bed reactor of a MgO/H_2O chemical heat pump. Under identical dehydration conditions, the higher thermal conductivities of packed beds comprising EM tablets made it possible to reach higher and more homogeneous temperatures, leading to an enhancement of the reaction rate. Compared with pure $Mg(OH)_2$ bed of pellets, the dehydration reaction in the EM packed beds was completed in a shorter time. The heat-storage capacity, q_d, per unit mass of $Mg(OH)_2$ was higher for the EM beds in the chemical heat pump experiments. The use of EG as a thermal conductivity enhancer also proved advantageous for the hydration reaction; the EM beds showed a larger change in the mole reacted fraction than did the pure $Mg(OH)_2$ bed. The temperature observed during hydration indicated that the removal of reaction heat progressively improved with the addition of EG. Additionally, the calculated gross heat output, q_h, and mean heat-output rate, w_{mean}, of the EM beds were greater than the corresponding values for pure $Mg(OH)_2$ bed. EM8, which corresponds to a mass ratio r_{mix} = 8:1, performed better than EM16 and EM4. EM8 dehydrated as fast as EM4, but the power output from hydration of the former was larger than the latter. EM8 was then utilized for other experiments, in which the volumetric heat storage capacity was increased by decreasing the void fraction of the bed. In the EM8-b bed, for which the

tablets were tidily arranged in piles, it was possible to load a larger amount of $Mg(OH)_2$ in the reactor than in EM8 bed, for which the orientation of tablets was random. The volumetric heat storage capacity and the volumetric gross heat output of the EM8-b bed were larger than the ones achievable with EM8 bed. Finally, the reactor was filled completely with an EM8 block, which ensured an improved contact with the heater's surface. The EM8 block had a mean heat output rate in 30 minutes of hydration at 361 kPa of 407 kW m_{bed}^{-3}, which is almost two times larger than the 258 and 218 kW m_{bed}^{-3} obtained respectively from EM8-b bed of tablets and $Mg(OH)_2$ bed of pellets. EM8 block demonstrated to be the optimal solution as chemical heat storage material and heat output at temperatures of 230-240°C. In case of hydration at low pressure (47 kPa) EM8 block has still better performance than $Mg(OH)_2$, but it is necessary to improve the diffusion of water vapor, similarly to the EM8-b bed, in order to let the hydration to be conducted with higher rates of reaction. For the EM8 block, in particular, it was understood that the rate of hydration is controlled by mass transfer when operating at $P_h < 101$ kPa, while it is controlled by heat transfer for $P_h > 101$ kPa.

4.9. References

[1] Y. Kato, N. Yamashita, K. Kobayashi, Y. Yoshizawa, Kinetic study of the hydration of magnesium oxide for a chemical heat pump, Applied Thermal Engineering, 16 (11) (1996), 853-862

[2] R.S. Gordon, W.D. Kingery, Thermal decomposition of brucite: II, kinetics of decomposition in vacuum, Journal of the American Ceramic Society, 50 (1) (1967), 8-14

[3] M. Balat, B. Spinner, Optimization of a chemical heat pump: energetic density and power, Heat Recovery Systems & CHP, 13 (3) (1993), 277-285

[4] H.B. Lu, N. Mazet and B. Spinner, Modelling of gas-solid reaction--coupling of heat and mass transfer with chemical reaction, Chemical Engineering Science, 51, 15 (1996), 3829-3845

[5] H. Ishitobi, K. Uruma, M. Takeuchi, J. Ryu, Y. Kato, Dehydration and hydration behavior of metal-salt-modified materials for chemical heat pumps, Applied Thermal Engineering, 50 (2),(2013), 1639-1644

[6] S. T. Kim, J. Ryu, Y. Kato, Reactivity enhancement of chemical materials used in packed bed reactor of chemical heat pump, Progress in Nuclear Energy, 53 (7), (2011), 1027-1033

[7] O. Myagmarjav, J. Ryu, Y. Kato, Lithium bromide-mediated reaction performance enhancement of a chemical heat-storage material for magnesium oxide/water chemical heat pumps, Applied Thermal Engineering, 63(1), (2014), 170-176

Massimiliano Zamengo, Y. Kato Laboratory, RLNR, Tokyo Institute of Technology

A Study on Heat Transfer-Enhanced Composites for a Magnesium Oxide/Water Chemical Heat Pump

Chapter 5

Numerical analysis of packed bed reactor

5. NUMERICAL ANALYSIS OF PACKED BED REACTOR

5.1. Introduction

In this Chapter, a numerical analysis of heat transfer combined with chemical reaction (dehydration) has been proposed for a better understating of the importance of higher thermal conductivity in the packed bed reactor. The thermal conductivity, heat capacity and rate of reactions of the materials were already measured in Chapter 3. Those results have been used for the calculations. Object of this Chapter is to predict temporal changes of the temperature in some representative positions of the packed bed and the reacted fraction by solving heat transfer equations combined with heat storage from the chemical reaction. Two materials was considered: $Mg(OH)_2$ pellets and the EM8-b (diameter ϕ = 10.1, thickness l = 6.1 mm) arranged in piles. As showed on Chapter 4, each of these beds contained 44 g of $Mg(OH)_2$, therefore the amount of heat stored per unit volume could be the same after 90 minutes of reaction. However, EM8-b could store heat in a shorter time. The numerical analysis was useful for understanding this phenomenon more in detail.

5.2. Definition of the numerical model

5.2.1. Control volumes and general equations

The temporal changes of temperatures and reacted fraction in the packed bed reactor during the dehydration have been calculated by solving the heat transfer equations and considered also the heat stored by the endothermic dehydration. A two-dimensional cylindrical heat transfer domain, shown on Fig. 5.1, represents a cross section of the experimental reactor bed. It has been divided into nodes using Δr and Δz as mesh sizes in the radial and axial direction, respectively. With exclusion of the nodes on the axis (j = 1), which have a cylindrical shape, the general node at radius (r_j) of the bed has a annular shape with volume $V_{i,j}$ [m^3], while $A_{r\text{-}in}$ [m^2] and $A_{r\text{-}out}$ [m^2] are the side areas and A_z [m^2] is the area of the top and bottom bases of the node. Every node is characterized by a local value of density, $\rho_{i,j}$ [kg m^{-3}], specific heat capacity $c_{i,j}$ [J kg^{-1} K^{-1}], and effective thermal conductivities λ_r and λ_z [W m^{-1} K^{-1}], respectively in the radial and axial directions. Those properties are function of the local reacted fraction, $x_{i,j}$ [-] and local temperature, $T_{i,j}$ [K].

For every node, the heat balance equations were expressed accordingly to the finite difference scheme. Implicit method was utilized, therefore the equation for temperature $T_{i,j}$ at time τ+$\Delta\tau$ [s] of the generic node is given by:

$$\frac{\lambda_{r\,i,j} A_{r-out\,i,j}}{\Delta r}\cdot(T_{i,j+1}-T_{i,j})+\frac{\lambda_{r\,i,j} A_{r-in\,i,j}}{\Delta r}\cdot(T_{i,j-1}-T_{i,j})+$$
$$+\frac{\lambda_{z\,i,j} A_{z\,i,j}}{\Delta z}\cdot(T_{i-1,j}-T_{i,j})+\frac{\lambda_{z\,i,j} A_{z\,i,j}}{\Delta z}\cdot(T_{i+1,j}-T_{i,j})=S_{i,j}+\sum E_{bound}+\frac{\rho_{i,j}\cdot c_{i,j}}{\Delta\tau}\cdot V_{i,j}\cdot(T_{i,j}-T^{\circ}_{i,j}) \quad (5.1)$$

where $\Delta\tau$ [s] is the time step of the calculations, $T^{\circ}_{i,j}$ is the temperature at time τ [s], $S_{i,j}$ [W] is the heat storage term, which corresponds to the heat consumed by the endothermic dehydration in the time $\Delta\tau$.

The terms $S_{i,j}$, E_{bound}, and the properties of materials $\rho_{i,j}$ (density) and $c_{i,j}$ (specific heat capacity) will be discussed separately later in this Chapter.

The results of simulations will be compared with the experimental results on the first cycle of dehydration, for which is precisely known the amount of initial $Mg(OH)_2$ in the packed bed.

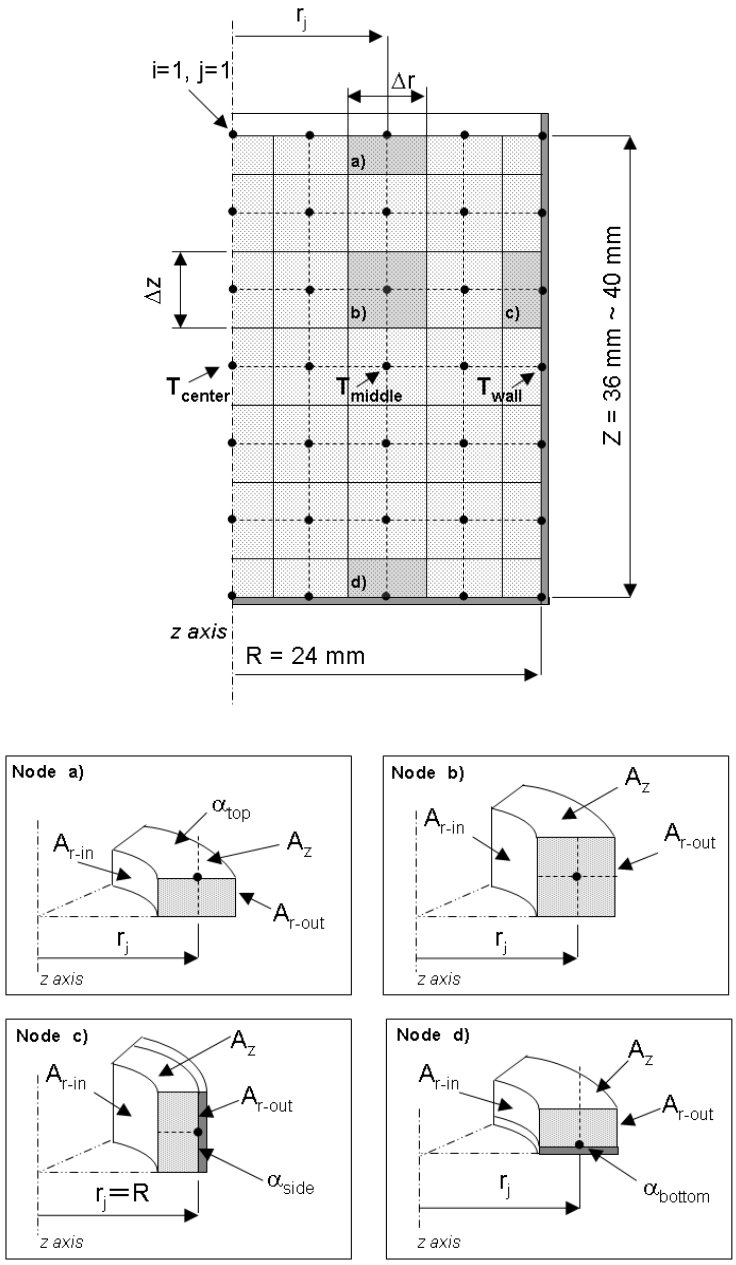

Fig. 5.5 Model of packed bed reactor used for the numerical simulations and boundary conditions.

5.2.2. Boundary conditions

For a generic node of the packed bed (node b in Fig. 5.1), Eq.1 can be used straightforward. On the boundaries of the reactor (top, side and bottom, respectively node a),c) and d)), the Eq. (5.1) was modified on its left hand side to include the boundary conditions. On the vertical side surface of the reactor, heat is supplied by the sheath heater. Its temperature T_{side} is described by a function which

was determined from experiments. For the nodes in contact with the wall (node c)), on the left hand side of Equation (5.1) the term:

$$E_{\text{side}} = \alpha_{\text{side}} \cdot A_{\text{r-out}\,i,j} \cdot \left(T_{i,j} - T_{\text{heater}}\right) \quad (5.2)$$

has been added, where the coefficient α_{side} [W m^{-2} K^{-1}] represents the thermal conductance between reactor's wall and packed bed materials. Similarly, for the nodes on the bottom side of the reactor (node d)), the term

$$E_{\text{bottom}} = \alpha_{\text{bottom}} \cdot A_{\text{z}\,i,j} \cdot \left(T_{i,j} - T_{\text{bottom}}\right) \quad (5.3)$$

has been added. Because the bottom of the reactor is not directly heated, the value of T_{bottom} was lower than T_{heater}. It was determined experimentally that $T_{bottom} \approx 0.82\ T_{heater}$.

The last boundary condition, corresponding to the top, was considered by adding the following term on the left hand side of Equation (5.2)

$$E_{\text{top}} = \alpha_{\text{top}} \cdot A_{\text{z}\,i,j} \cdot \left(T_{i,j} - T_{\text{top}}\right) \quad (5.4)$$

where T_{top} is the temperature of the chamber (120°C) which is constant during the experiments and the coefficient α_{top} represents a global heat transfer coefficient. The values of α_{top}, α_{bottom} and α_{side} [W m^{-2} K^{-1}] have been assumed as constants. Their values are given on Table 5.1, while the properties of the beds are given on Table 5.2.

Table 5.1 Heat transfer coefficients used at the boundaries

Material in the bed	α_{side} [W m^{-2}K^{-1}]	α_{bottom} [W m^{-2}K^{-1}]	α_{top} [W m^{-2} K^{-1}]
$Mg(OH)_2$ (pellets randomly arranged)	60	60	1
EM8-b (EM8 tablets arranged in piles)	25	70	5

Table 5.2: Properties of the packed beds object of comparison

Bed ID	Mass of $Mg(OH)_2$ [g]	Mass of packed bed[g]	Density of particles [g cm^{-3}]	Density of bed [g cm^{-3}]	Thermal conductivity [W m^{-1} K^{-1}]
$Mg(OH)_2$	43.9	43.9	0.966	0.626	0.16
EM8-b	43.6	49.1	1.056	0.714	0.55 radial 0.45 axial

5.2.3. Reaction rates and heat storage term

The dehydration is a first order endothermic reaction. The reaction rate constant, already determined on Chapter 3), depends on temperature accordingly to the following Arrhenius equation:

$$k_{i,j} = A_0 \cdot e^{-E/RT_{i,j}} \quad (5.5)$$

where A_0 is the frequency factor, E the activation energy and R the universal constant of gas.

The reacted fraction $x_{i,j}$ of the generic node can be calculated from the following Equation:

$$\ln x_{i,j} = k_{i,j} \cdot \tau + \ln x_0 \quad (5.6)$$

It is considered that $k_{i,j}$ does not change during the interval of calculations, $\Delta\tau$, but its value is recalculated at the new calculation time $\tau+\Delta\tau$ in function of the temperature of the node. Therefore, at

time $\tau+\Delta\tau$ the equation can be rewritten as:

$$\ln x'_{i,j} = k_{i,j} \cdot (\tau + \Delta\tau) + \ln x_0 \quad (5.7)$$

where $x'_{i,j}$ is the reacted fraction at time $\tau+\Delta\tau$

Subtracting Equation (5.6) to Equation (5.7) it is obtained:

$$\ln x'_{i,j} - \ln x_{i,j} = k_{i,j} \cdot \Delta\tau \quad (5.8)$$

Or

$$\ln \frac{x'_{i,j}}{x_{i,j}} = k_{i,j} \cdot \Delta\tau \quad (5.8')$$

Therefore $x'_{i,j}$ can be expressed as

$$x'_{i,j} = x_{i,j} \cdot e^{k_{i,j} \cdot \Delta\tau} \quad (5.9)$$

The heat stored per every time step $\Delta\tau$ is calculated in function of the difference

$$S_{i,j} = \frac{-\Delta H^{\circ}}{\Delta\tau} \cdot \rho_{ini} \cdot \Delta x_{i,j} \cdot V_{i,j} \quad (5.10)$$

where

$$\Delta x_{i,j} = x'_{i,j} - x_{i,j} \quad (5.11)$$

In case of packed bed of EM, the mixing ratio ψ [–], defined as the ratio between the mass of $Mg(OH)_2$ in the bed and the total mass of the bed of EM, has to be also accounted:

$$S_{i,j} = \frac{-\Delta H^{\circ}}{\Delta\tau} \cdot \rho_{ini} \cdot \Delta x_{i,j} \cdot V_{i,j} \cdot \frac{\psi}{\psi+1} \quad (5.12)$$

5.2.4. Thermal properties of materials

For what concerns the thermal properties of materials in the packed beds, their thermal conductivity was measured before and after dehydration (λ_{ini} and λ_{end}, respectively), as already explained in Chapter 3). It is assumed that thermal conductivity changes linearly with mole reacted fraction, as expressed in the following equation. In particular, at $\tau = 0$, $x_{i,j} = 0$

$$\lambda_{i,j} = (1 - x_{i,j}) \cdot \lambda_{ini} + x_{i,j} \cdot \lambda_{end} \quad (5.13)$$

Specific heat capacity of $Mg(OH)_2$ and MgO has been measured with DSC. It was calculated for every node at every time step in function of temperature and reacted fraction by using the following equation:

$$c_{i,j} = (1 - x_{i,j}) \cdot c_{Mg(OH)_2}(T_{i,j}) + x_{i,j} \cdot c_{MgO}(T_{i,j}) \quad (5.14)$$

To take into account of the heat capacity of expanded graphite, Equation (14) is modified as follows:

$$c_{i,j} = \left[(1 - x_{i,j}) \cdot c_{Mg(OH)_2}(T_{i,j}) + x_{i,j} \cdot c_{MgO}(T_{i,j})\right] \cdot \frac{\psi}{\psi+1} + c_{EG}(T_{i,j}) \cdot \frac{1}{\psi+1} \quad (5.14')$$

For what concerns density, it was calculated as the ratio between the mass of the node and the volume of the node.

$$\rho_{i,j} = \frac{(1 - x_{i,j}) \cdot m_{\mathrm{Mg(OH)_2}\,i,j} + x_{i,j} \cdot m_{\mathrm{MgO}\,i,j}}{V_{i,j}} \qquad (5.15)$$

or

$$\rho_{i,j} = \frac{(1 - x_{i,j}) \cdot m_{\mathrm{Mg(OH)_2}\,i,j} + x_{i,j} \cdot m_{\mathrm{MgO}\;\,i,j} + m_{\mathrm{EG}\,i,j}}{V_{i,j}} \qquad (5.15')$$

in the case of packed beds of EM tablets.

These properties were updated at every time step in function of the new values of temperature and reacted fraction

.

5.3. Results of simulations and comparison with experiments

Finite difference implicit method was used and the algebraic system of equations was solved at every time step using the Gauss-Seidel iteration method. Over-relaxation technique was utilized to accelerate the calculations (the time required to get data for 90 minutes of dehydration ranges between 1 and 2 minutes with a mesh size of Δr x Δz of 2 mm x 2 mm.

Fig. 5.2 shows the comparison between experimental data and simulation of dehydrations in a packed bed of $Mg(OH)_2$ pellets and EM8-b bed, respectively. The temperatures across the radius at height $Z/2$ have been considered. Those are T_{center}, T_{middle}, and T_{wall}, which are respectively, the temperature at the center of the bed (previously called T_3), at the position $R/2$ (T_4) and at the position in contact with the wall of the reactor (T_5). The properties of the bed are summarized on Table 3.

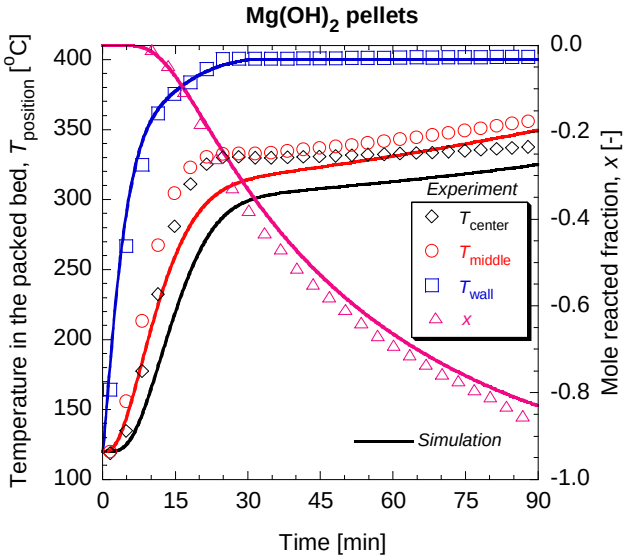

Fig. 5.2.a) comparison between simulations and experimental results in a packed bed of $Mg(OH)_2$ pellets (T_{wall} = 400°C, P_{cond} = 2.3 kPa)

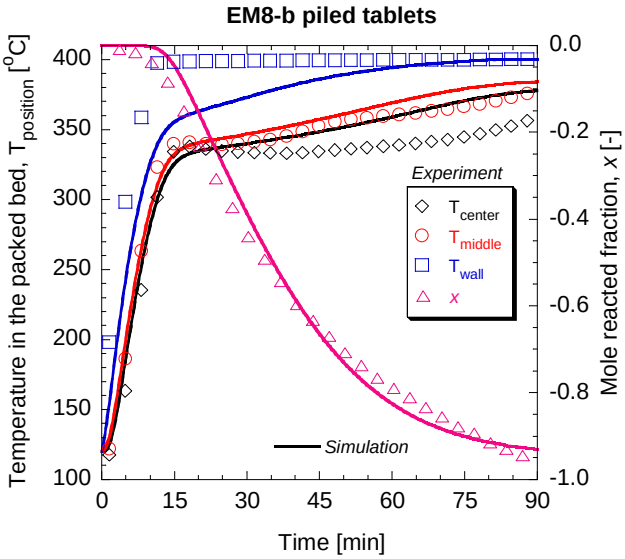

Fig. 5.2.b) comparison between simulations and experimental results in a packed bed piled EM8-b blets (T_{wall} = 400°C, P_{cond} = 2.3 kPa)

Fig. 5.6 Comparison between experimental data and numerical simulations for dehydration

The results show a substantial agreement between experimental results and calculated data. The discrepancies are likely related to the experimental errors of the measures and simplified assumption. Especially, beds were considered as homogeneous, however this is not, especially for the EM8-b bed, in which the tablets are tidily arranged. The numerical analysis allows getting local information, for example the local mole reacted fraction in a certain position of the packed bed. This information cannot be obtained by the experiments, which consider only a total mass change. In the next Fig. 5.3 the local concentrations of $Mg(OH)_2$, $\xi_{position}$ [%], are shown for three positions of the packed bed, respectively, on the wall, on the position *R*/2 (middle point of the reactor's radius) and at the center of the bed.

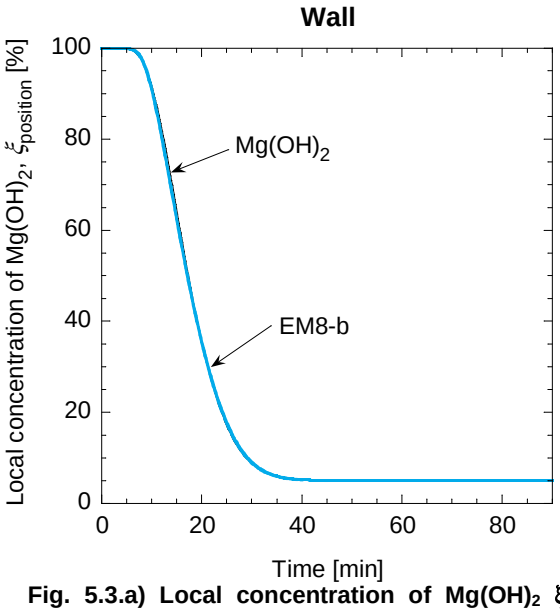

Fig. 5.3.a) Local concentration of $Mg(OH)_2$ ξ_{wall} near the reactor's wall (heater)

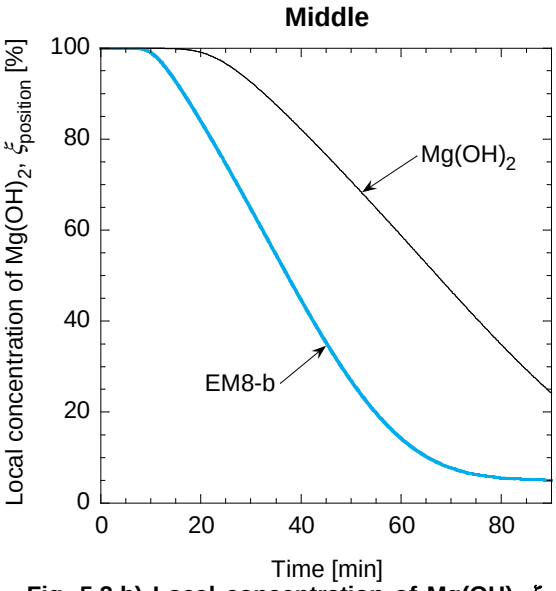

Fig. 5.3.b) Local concentration of $Mg(OH)_2$ ξ_{middle} at position (*R*/2, *Z*/2)

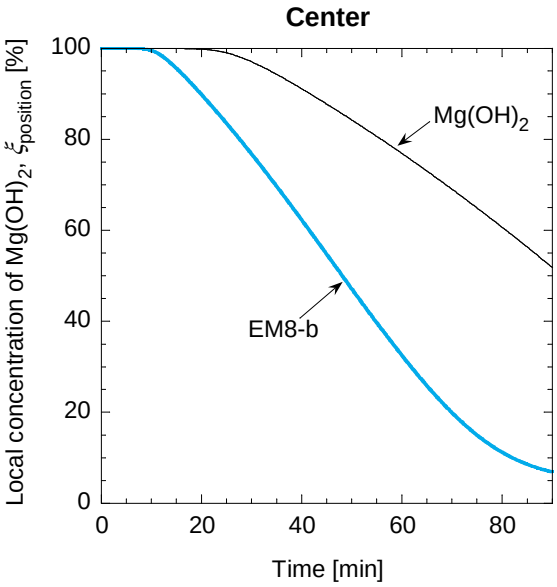

Fig. 5.3.c) Local concentration of $Mg(OH)_2$ ξ_{center} at the center of the packed bed

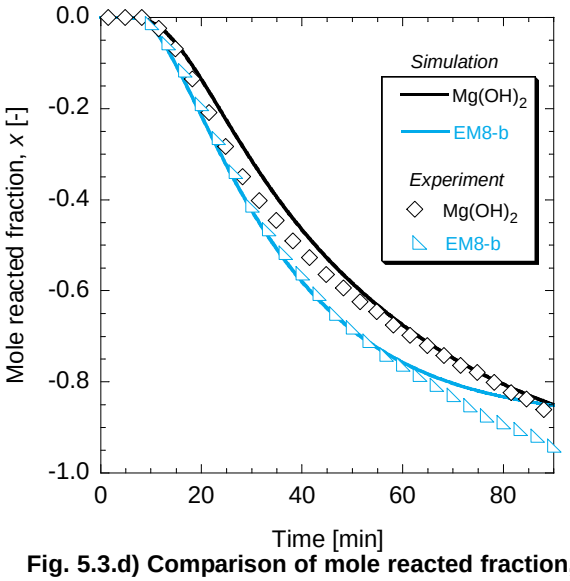

Fig. 5.3.d) Comparison of mole reacted fraction, *x* between simulation and experiments (first cycle of the experiments)

Fig. 5.7 Comparison of local and total reacted fractions for beds of $Mg(OH)_2$ pellets and EM8-b tablets

On the position close to the wall, there is no substantial difference between the results of ξ_{wall}. On the other hand, for the middle and center positions, it looks clear that the reaction advanced much faster in the packed beds of EM8-b tablets. The reaction in the bed of $Mg(OH)_2$ pellets could not be completed after 90 minutes. It was thought that EM8-b bed reached higher temperatures due to the large thermal conductivity of EM8, and allowed achieving higher rate of reaction also in the positions far from the reactor wall. This was the effect and advantage given by the larger thermal conductivity of the packed bed of EM8-b tablets. Then, for the three positions (center middle and wall) it was calculated the quantity *s* [kJ s^{-1} m^{-3}], corresponding to the heat stored per unit volume per unit time [s]. Those

were calculated with equations (5.16) for the $Mg(OH)_2$ bed of pellets and (5.16') for the EM8-b bed of tablets.

$$s_{i,j} = \frac{-\Delta H^0}{\Delta \tau} \cdot \rho_{ini} \cdot \Delta x_{i,j} \cdot V_{i,j} = \frac{S_{i,j}}{V_{i,j}} \qquad (5.16)$$

$$s_{i,j} = \frac{-\Delta H^0}{\Delta \tau} \cdot \rho_{ini} \cdot \Delta x_{i,j} \cdot V_{i,j} \cdot \frac{\psi}{\psi + 1} = \frac{S_{i,j}}{V_{i,j}} \qquad (5.16')$$

The results are shown in Fig. 5.4 a) - c).

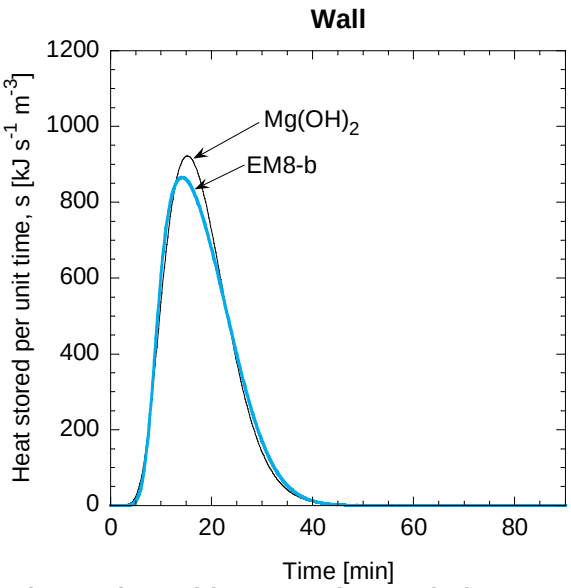

Fig. 5.4.a) Local heat stored per unit time, s_{wall} , near the reactor's wall (heater)

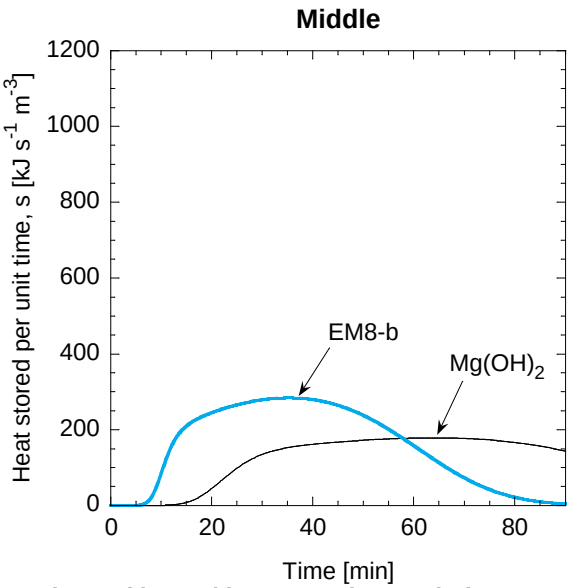

Fig. 5.4.b) Local heat stored per unit time s_{middle} at position (R/2, Z/2)

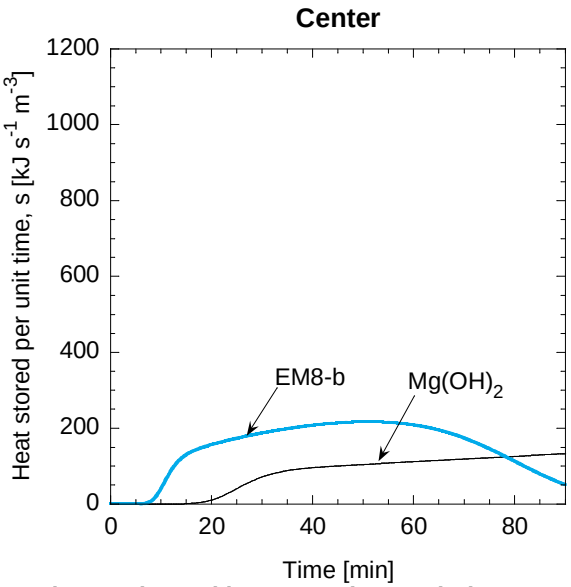

Fig. 5.4.c) Local heat stored per unit time s_{center} at the center of the packed bed

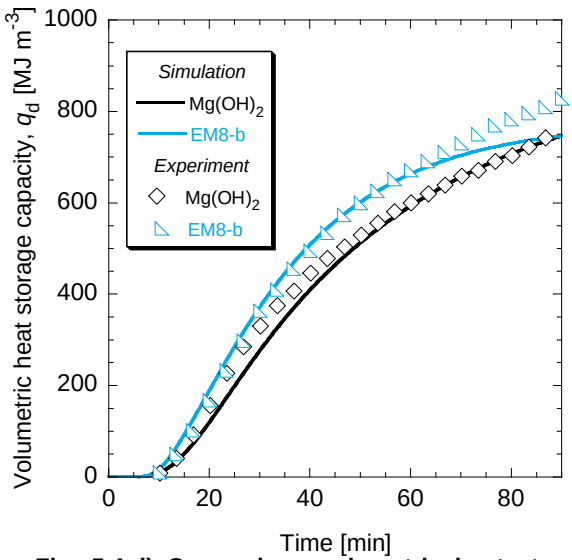

Fig. 5.4.d) Comparison volumetric heat storage capacity, $q_{d,v}$ between simulation and experiments (first cycle of experiments)

Fig. 5.8 Comparison of local and total heat storage performances of $Mg(OH)_2$ pellets and EM8-b tablets

As previously observed, in proximity of the heater (wall), there was no substantial difference between the beds. A maximum was reached between 15 and 20 minutes after starting heating the packed bed from the initial temperature of 120°C. When observing the results on the middle position (Fig 5.4 (b)), it appears clear that heat is stored in the EM-b bed after 7 minutes, but in the same position it took 15 minutes for the $Mg(OH)_2$ bed.

This demonstrates that in case of $Mg(OH)_2$ bed of pellets, heat can be store stored effectively just near the hot wall, but it will take more than 90 minutes to store it in the middle and center positions. This issue has been solved in the EM8-b bed of tablets, which allowed a more rapid temperature increase in the bed, therefore enhanced the completion of the dehydration even in the positions far from the wall heater.

5.4. Discussion on water vapor flow

The numerical analysis In terms of mass balance and energy balance, it has been assumed that the mass of water vapor “disappears” gradually with the reaction advancement. In order to consider the heat exchange between water vapor going upward and the materials in the bed before exiting from the reactor, it is useful to calculate the Peclet number. The Peclet number is a non dimensional parameter which expresses the ratio between heat transport by convection and heat transport by conduction. It is defined as the product between the Reynolds number and the Prandtl number (Pe = RePr). It has been determined using the method in [1].

From the experiments, the average mass flow coming out from the packed bed is very small. When the mole reacted fraction change Δx_d, changes from -0.2 to -0.3, the corresponding mass change is 1.4 g. It took 570 s for this. Therefore the average mass flow is $m_{vap} = 0.0025$ g s^{-1}. Considering water vapor at pressure of 2.3 kPa and $T_{vap} = 350$°C, we can summarize its properties on the following Table 5.3:

Table 5.3: Properties of water vapor assumed for the evaluation of non dimensional parameters

Temperature, T_{vap}	350°C
Pressure, P_{vap}	2.3 kPa
Density, ρ_{vap}	0.0079 kg m^{-3}
Thermal conductivity, λ_{vap}	0.049 W $m^{-1}K^{-1}$
Dynamic viscosity, μ_{vap}	$2.24 \cdot 10^{-5}$ Pa·s
Prandtl number, Pr	0.93

For the given density of water vapor, ρ_{vap}, the volumetric flow is $w_{vap} = 3.02 \cdot 10^{-4}$ m^3 s^{-1}. Considering the cross section of the reactor (diameter of 48 mm, S = $1.81 \cdot 10^{-3}$ m^2), we can estimate the superficial velocity v_0 [m s^{-1}] with the following equation:

$$v_0 = \frac{w_{vap}}{S} = 0.167 \qquad [m\ s^{-1}] \qquad (5.17)$$

The superficial mass flux, G_0 [kg $s^{-1}m^{-2}$] is defined as

$$G_0 = \rho v_0 = 1.36 \cdot 10^{-3} \qquad [kg\ s^{-1}\ m^{-2}] \qquad (5.18)$$

The Reynolds number is given by

$$\mathrm{Re} = \frac{6G_0}{a\mu\gamma} \qquad (5.19)$$

where *a* is used to determine the equivalent diameter for water vapor flow, m is the dynamic viscosity Where γ is a particle shape factor (γ = 0.92 for cylinders). We define a as the wetted surface, defined from the specific surface av, corresponding to the ratio between the surface and the volume of the single $Mg(OH)_2$ pellet. For $Mg(OH)_2$ pellets, the diameter is 2.0 mm and the average length is 10 mm. Therefore a_v = 2,020 m^{-1}. To obtain a, it is given that:

$$a_v = \frac{a}{1-\varepsilon} \qquad (5.20)$$

where ε = 0.35 is the void fraction of the packed bed of $Mg(OH)_2$ pellets. It is obtained a = 1,313 m^{-1}. After introducing all the numerical values into equation (3), it results that Re = 0.307. For the given steam conditions, Pr = 0.930, hence the Peclet number Pe = Re·Pr = 0.280. The Peclet number expresses the ratio between heat transport by convection and heat transport by conduction. Therefore, when Peclet number is zero (Pe = 0), the heat transfer by conduction is the dominating factor. In practical packed beds (for instance reactor columns with catalysts or, in general, when is present a flow of reagents or products), Pe number is very high (Pe >> 1) and heat transfer is dominated by convection. In case of EM8-b (piled tablets of EM8), Re and Pr resulted higher because of the channeling and the higher rate of dehydration. In EM8-b bed, Re = 0.698 and Pe = 0.650. The Pe number is increased, meaning that convection heat transfer contribution became larger than the case of the $Mg(OH)_2$ packed bed of pellets. Accordingly to these considerations, the numerical model would better consider the contribution of convection given by the water vapor; however this contribution would be very small in this work. On a larger scale, different geometry or other reaction conditions its effects might not be negligible.

5.5. Considerations on numerical analysis for hydration

In this work hydration was not studied numerically because of several reasons. The most important is that there are only empirical chemical reaction models for hydration [2]. The model would require further assumptions concerning diffusion of water vapor and fluid dynamics, because the water vapor supplied for the reaction at an established condition of temperature and pressure, would be heated from the heat of reaction before reaching the bed (Fig. 5.9). Water vapor participates both to chemical reaction and heat transfer more actively than in hydration reaction. This makes difficult to analyze the

chemical reaction because new assumptions are required. Measurements of gas permeability in the materials are also necessary in order to prepare a model for calculating the vapor diffusion coefficients.

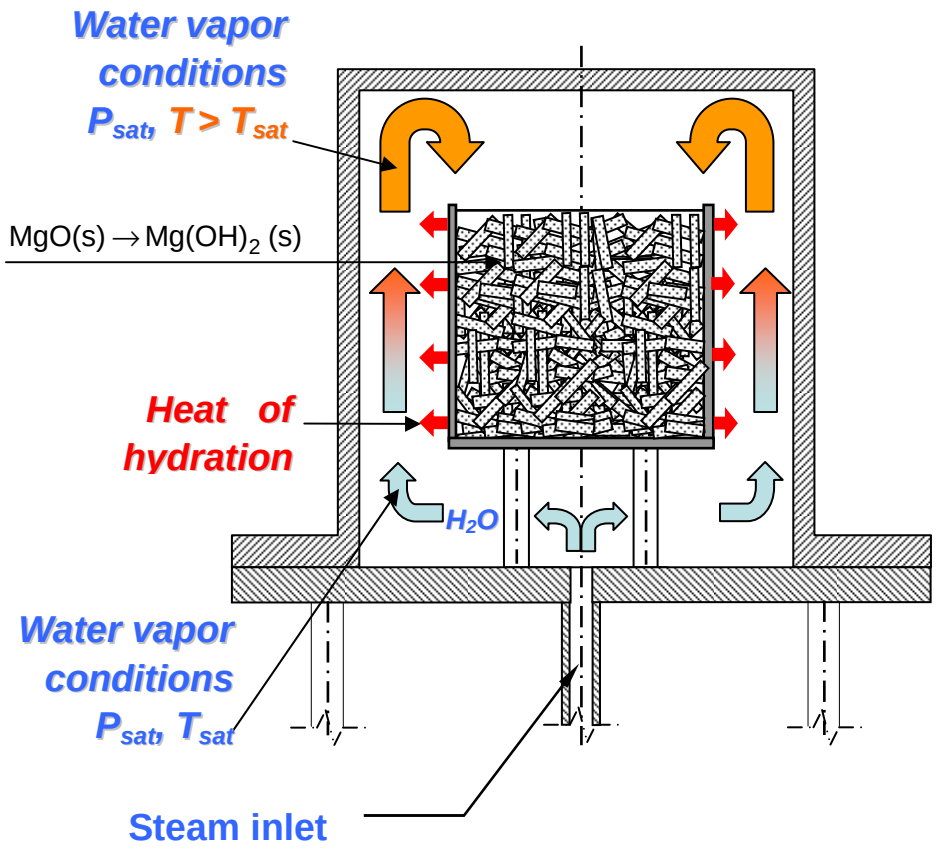

Fig. 5.9 Water vapor in the chamber during hydration exchanges heat with reactor and chamber's wall. Vapor pressure and temperature condition need to be calculated, as interacting both in chemical reaction and removing heat of hydration from the packed bed.

5.6. Note on chemical reaction model utilized in the numerical analysis

Despite fitting better with the experimental data on TG apparatus, the reaction rates of dehydration in function of temperature calculated with the contracting surface model could not be utilized in the numerical calculations. It was necessary to utilize the coefficients obtained from the 1st order analysis. This was decided after implementing the equations for the calculations of the coefficients $k_{i,j}$ for the nodes. Following the procedure already presented in section 5.2.3, we have that the $k_{i,j}$ is function of:

$$1-\sqrt{1-\alpha_{i,j}}=k_{i,j}\cdot\tau \qquad (5.21)$$

where $\alpha_{i,j}=1-x_{i,j}$

Equation 5.21 can be rewritten as:

$$1-\sqrt{x_{i,j}}=k_{i,j}\cdot\tau \qquad (5.21')$$

At time $\tau+\Delta\tau$ the equation 5.21' becomes:

$$1-\sqrt{x'_{i,j}} = k_{i,j}\cdot(\tau+\Delta\tau) \qquad (5.22)$$

By subtracting Eq.5.21' from 5.22, it is obtained:

$$\sqrt{x_{i,j}}-\sqrt{x'_{i,j}} = k_{i,j}\cdot\Delta\tau \qquad (5.23)$$

To express $x'_{i,j}$ in function of $x_{i,j}$ it is necessary to utilize the Taylor series. Finally it is possible to express

$$x'_{i,j} = x_{i,j} + 2\cdot k_{i,j}\cdot\Delta\tau$$

When running the numerical code, the calculations stopped for a failure of convergence. A comparison with Fig. 5.2 a) (results for bed of magnesium hydroxide pellets) is shown on Fig. 5.10.

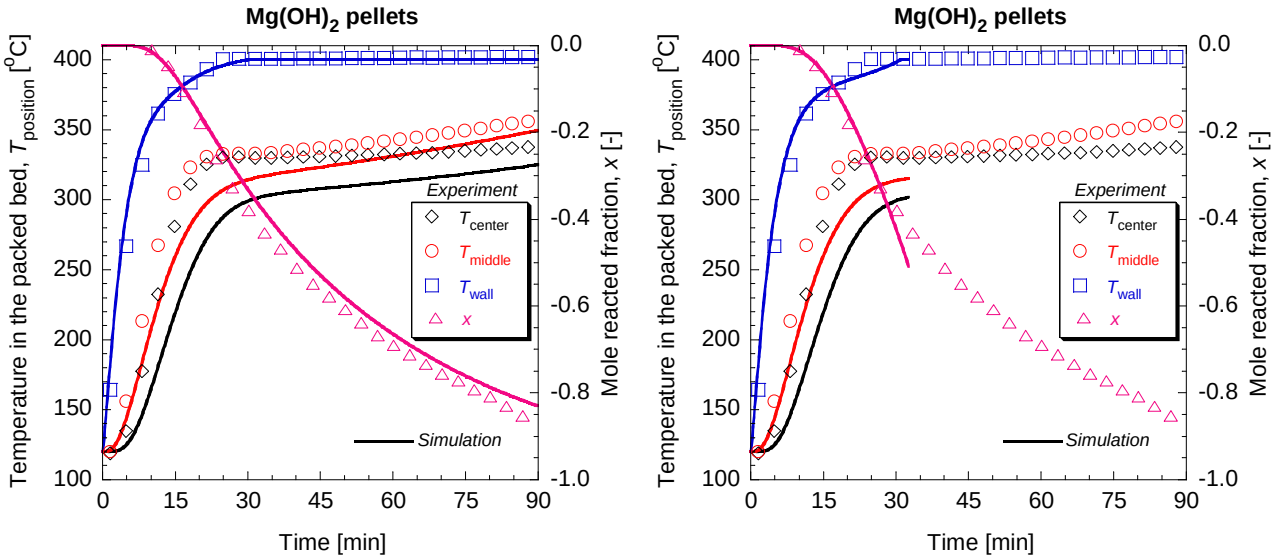

a) FIRST ORDER MODEL comparison between simulations and experimental results in a packed bed of $Mg(OH)_2$ pellets (T_{wall} = 400°C, P_{cond} = 2.3 kPa)

b) CONTRACTING SURFACE MODEL comparison between simulations and experimental results in a packed bed piled EM8-b blets (T_{wall} = 400°C, P_{cond} = 2.3 kPa)

Fig. 5.10 Comparison of numerical analysis using the first order reaction model and contracting surface model.

5.7. Conclusions

The numerical analysis of dehydration experiments agreed with experimental results. Local conversion of $Mg(OH)_2$ to MgO were calculated. In case of $Mg(OH)_2$ bed of pellets, the reaction could be completed only in the proximity of the wall, where heat was supplied. On the other hand, the results of EM8-b bed of piled tablets indicated that head could be transported rapidly through to the center of the bed. The temperature of the bed rose faster because of the larger thermal conductivity. At 7 minutes after starting bed heating, the EM8-b bed started to store heat also at the central position, but this was possible only after 15 minutes for the $Mg(OH)_2$ bed. Because the reaction could be completed more efficiently for EM8-b, the EM material resulted more practical for utilization in heat exchangers than

$Mg(OH)_2$ pellets. It ensured the same heat storage capacity of $Mg(OH)_2$ but dehydration could be completed in a shorter time.

5.8. References

[1] Heat transfer coefficients for forced convection through packed beds (Transport Phenomena, Bird-Stewart-Lightfoot, 2nd edition, chapter 14.5 and 6.4)

[2] Y. Kato et al., Kinetic study of the hydration of magnesium oxide for a chemical heat pump, Applied Thermal Engineering, 16 (11) (1996), 853-862

Massimiliano Zamengo, Y. Kato Laboratory, RLNR, Tokyo Institute of Technology

A Study on Heat Transfer-Enhanced Composites for a Magnesium Oxide/Water Chemical Heat Pump

Chapter 6
Utilization of the chemical heat storage for thermal load leveling in nuclear power plants

6. UTILIZATION OF THE CHEMICAL HEAT STORAGE FOR THERMAL LOAD LEVELING IN NUCLEAR POWER PLANTS

6.1. Introduction

Small nuclear cogenerating reactors may be suited to support existing process heat markets since their smaller sizes align well with the capacity requirements of process industries. Recently, there has been a renewed interest in small and medium-sized reactors (SMR) due to their low carbon generation, simpler design, more affordable economics, job creation, and possibility for new international market opportunities. These concepts are being pursued to support small utilities, countries with financing or infrastructure constraints, distributed power markets, and process heat customers. In a future energy mix with more small scale and intermittent production from renewable energy systems (RES), SMRs have the potential to become an important player (Ingersoll, 2009) [1], (Varquez 2010) [2]. The possibility to utilize a heat storage technology in a cogenerating nuclear power plant would make easier to manage the load variations caused by the industrial production cycles or to balance the RES variability, actively contributing to the operations of a 'smart grid'. This is particular advantageous because nuclear power station are generally more suitable for satisfying the base load rather than follow the demand continuously.

A Rankine cycle in the power station has been modified to include a chemical heat storage reactor. The range of admissible variation of electrical power output from the steam turbine was estimated from the enthalpy and mass balances under the heat storage and heat output operation modes, respectively. From the experimental results of heat storage capacity and heat power output, it was possible to estimate the amounts of $Mg(OH)_2$ pellets and EM8 block required for the peak shaving of electricity in a nuclear power station.

6.2. Rankine cycle including heat storage

In this section it is proposed an analysis of a Rankine cycle including the $Mg(OH)_2$ chemical heat storage. A schematic of the operations is shown on Figs.6.1, 6.2 and 6.3. They show respectively the design condition, the heat storage mode and the heat output node. The properties of steam at the inlet and at the outlet of the steam generator, together with the mass flow were taken from Terada *et al.*, which are the design values of steam generated by a small sized high temperature reactor (MHR-50) [3]. Because the design conditions of the Rankine cycle were not all available, some of them have been assumed: they lead to results not far from the declared design conditions in terms of thermal and electrical power generation (120 MWt and 50 MWe). Table 6.1 summarizes the main design parameters utilized for the heat mass balance calculations.

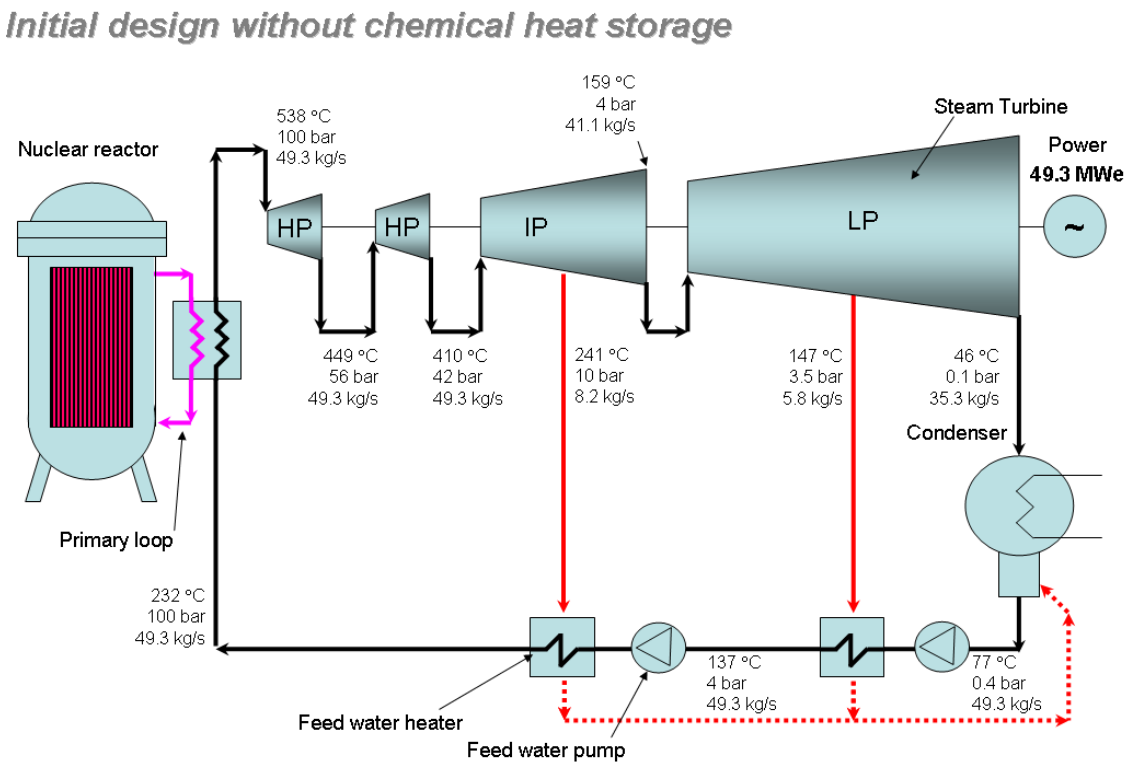

Fig. 6.1: System configuration and heat mass balance of the secondary loop (Rankine cycle)

Table 6.1 Basic plant specifications and assumptions

Item	Values
Reactor thermal power [3]	120 MWt
Gross electrical power [3]	49.2 MWe
Main steam temperature/ pressure (steam generator inlet) [3]	232°C / 100 bar
Main steam temperature/ pressure (steam generator outlet) [3]	538°C / 100 bar
Main steam flow rate [3]	49.3 kg/s
Isentropic efficiency of turbines (assumed) η_{is}	0.85
Mechanical efficiency (assumed) η_{m}	0.98
LP turbine inlet steam temperature / pressure (assumed)	159°C / 4 bar
Gross electrical power (from calculations)	49.3 MWe

The electrical power output from the turbine depends directly on the mass flow of steam produced by the steam generator and the enthalpy changes. When the demand of electricity decreases, the steam turbine has to rotate always at the same rotation speed, but the work from expansion of steam must be reduced. This can be accomplished by decreasing the mass flow in the steam generator; consequently, the operator has to decrease and control the generation of thermal power from the nuclear reactor. The utilization of heat storage allows keeping a constant mass flow in the steam generator, but thermal

energy of steam can be partially converted into work (and then electricity) by the turbine and partially stored via the dehydration. This is explained on Fig. 6.2 and 6.3: when the electricity demand decreases, some of the stages of the high pressure (HP) steam turbine can be partially (or totally) by-passed. The by-passed steam flows into the heat exchanger of the packed bed. In this way heat is stored via the dehydration. Then, steam returns to the turbine to complete its expansion. The dehydration condition have been chosen considering that a steam temperature larger than 420°C is necessary for operate dehydration at a rate of reaction comparable with the packed bed experiments. The condensation heat extracted from the water reservoir is reutilized for preheating the feed water. The heat output mode on Fig. 6.4 and 6.5 shows how heat can be released and reused in the Rankine cycle. Water vapor necessary for the hydration is produced in the water reservoir by using a part of steam extracted from the low pressure (LP) turbine. Heat released by hydration is used to reheat steam before it enters into the LP stages of the turbine. Reheat of steam is a well know practice for increasing efficiency in Rankine cycles: because of the larger difference between the reheated steam enthalpy and the enthalpy at the condenser, the power output from the turbine will be increased. Another advantage of reheating steam before entering the LP turbine is the increase of steam quality: it would be useful to prevent the condensation of water droplets which can damage the turbine's blades. The heat and mass balances have been calculated using the steam tables from the International Association for the Properties of Water and Steam (IAPWS-IF97). Table 6.2 shows the main results of the calculations.

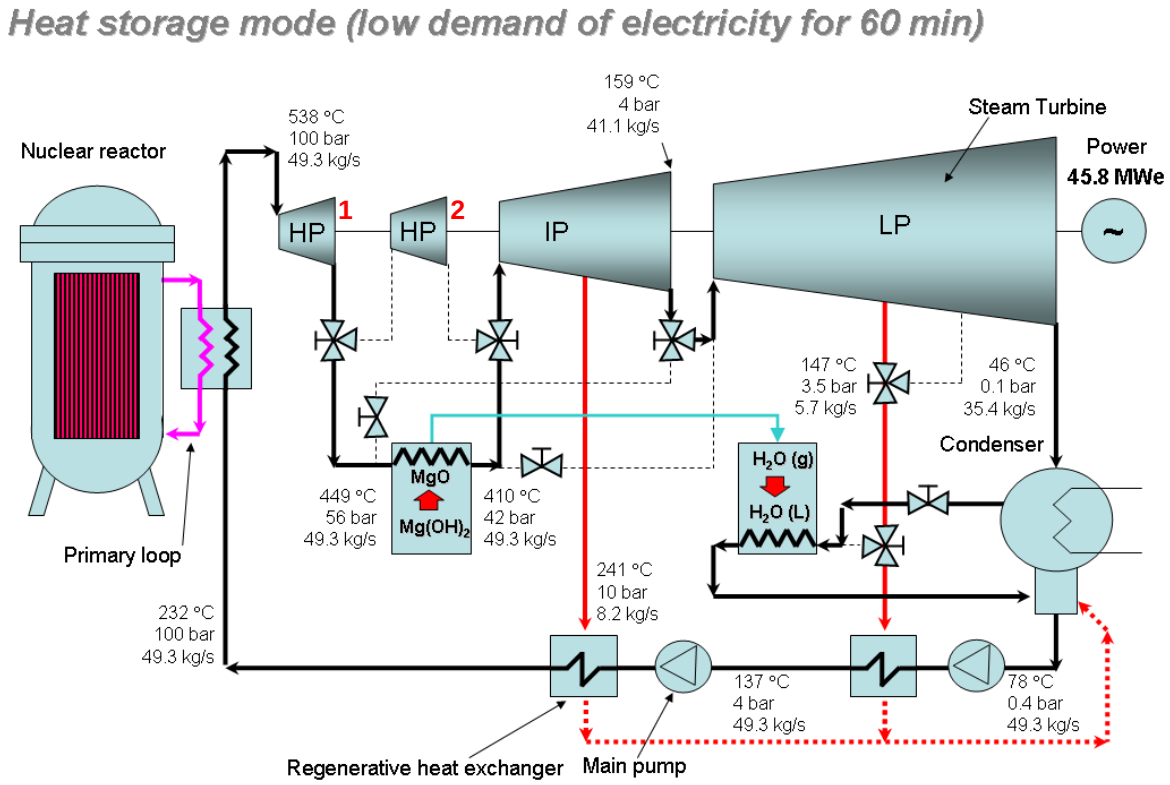

Fig. 6.2: System configuration and heat mass balance of the secondary loop including chemical heat storage operating the heat storage mode

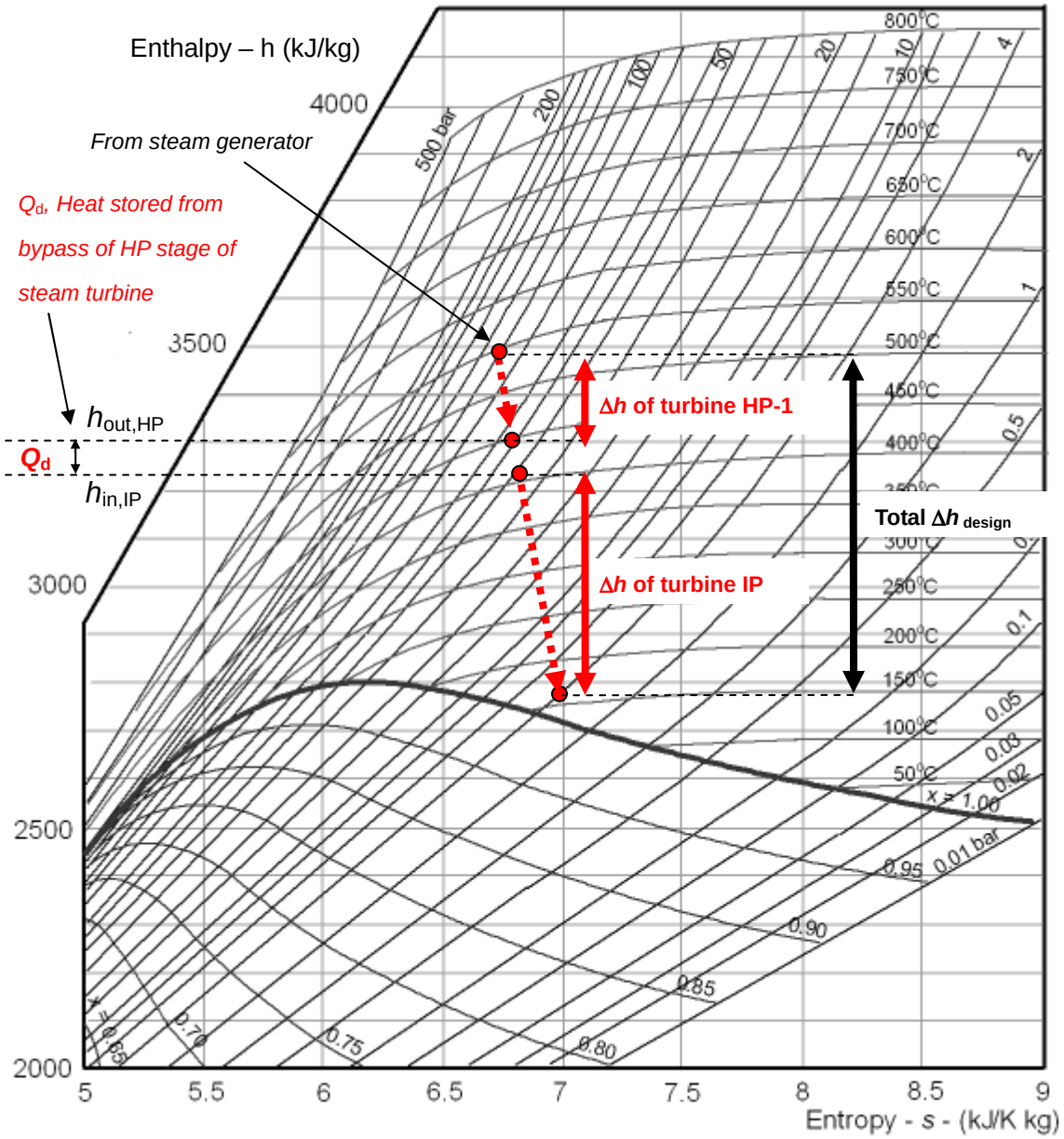

Fig. 6.4: Mollier diagram of steam, the amount of heat Q_d is by-passed from HP turbine and stored In the packed bed of chemical heat storage materials.

In this example, the maximum available thermal energy from the steam by-pass, Q_d [MJ], was calculated with Eq. 6.1:

$$Q_d = m' \cdot (h_{out,HP\text{-}2} - h_{in,HP\text{-}2}) \cdot t_d \qquad (6.1)$$

where m' is the mass flow of steam [kg s^{-1}], $h_{out,HP}$ and $h_{in,HP}$ [kJ kg^{-1}] are respectively the enthalpies of steam at the outlet and at the inlet of the HP stage of the turbine and t_d is the time of dehydration. The enthalpy difference $h_{out,HP} - h_{in,HP}$ in the second HP turbine is not used to generate power in the turbine

but stored in the packed bed reactor. Fig. 6.4 shows that summation of the two enthalpy differences of the turbines HP-1 and IP, respectively $\Delta h_{HP\text{-}1}$ and Δh_{IP} , is less than the design enthalpy difference Δh_{design}. The electrical power generated from the steam turbine, P_e, is calculated with Eq. 6.2:

$$P_e = \eta_m \cdot \left(m'_{HP-1} \cdot \Delta h_{HP-1} + m'_{HP-2} \cdot \Delta h_{HP-2} + m'_{IP} \cdot \Delta h_{IP} + m'_{LP} \cdot \Delta h_{LP} \right) \qquad (6.2)$$

where the m' is mass of steam flowing in the turbine stage, Δh the correspondent enthalpy difference between steam condition at outlet and inlet of the turbine stage and η_m the mechanical efficiency of the turbine. Hence, when operating the heat storage mode, the term $m'_{HP\text{-}2} \cdot \Delta h_{HP\text{-}2}$ in equation (6.2) becomes zero, consequently it results that the electrical power output can be decreased of –6.9% with respect to the design power. When t_d = 60 min, the amount of thermal energy that can be stored in the packed beds is Q_d = 12,816 MJ (corresponding to a thermal power of 3.6 MWt for 1 hour). From the experimental results given in Chapter 4 and reported on Fig. 6.5, the volumetric heat storage capacities $q_{d,v}$ of $Mg(OH)_2$ (bed of pellets randomly arranged) and EM8 (EM8 block fitting with the reactor diameter) resulted respectively 427 MJ m_{bed}^{-3} and 724 MJ m_{bed}^{-3}. Hence, the thermal energy Q_d can be stored in a bed of $Mg(OH)_2$ pellets having a volume $V_{Mg(OH)2}$ of 30.0 m^3 or in a bed of EM8 having a volume V_{EM8} of 17.7 m^3. In other words, the volume of EM8 bed is 41% smaller than the one of $Mg(OH)_2$ bed of pellets. The sensible heat available when heating or cooling the heat storage materials was not considered in these calculations, being smaller than the heat of chemical reactions.

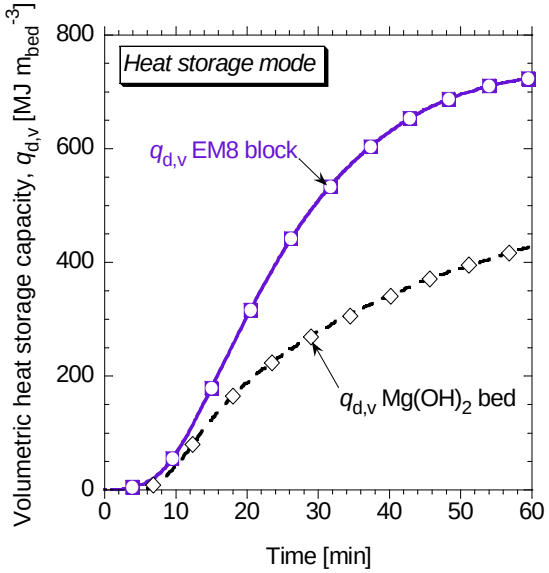

Fig. 6.5 Comparison of calculated volumetric heat-storage capacities, $q_{d,v}$ of packed beds (packed bed experiments)

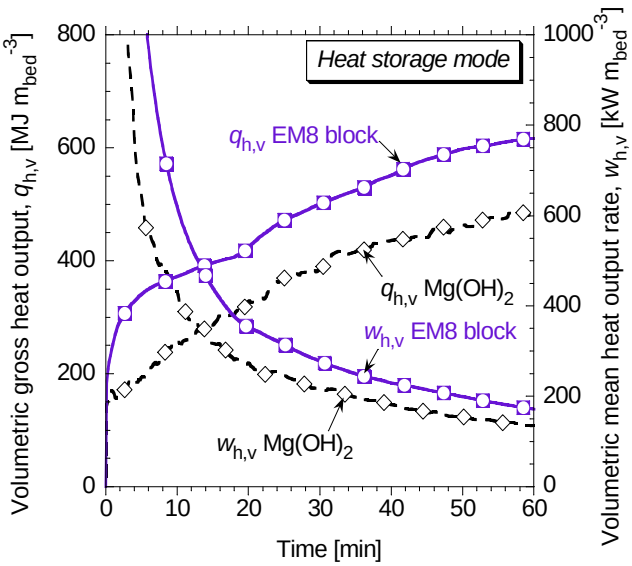

Fig. 6.6 Comparison of calculated volumetric gross heat output, $q_{h,v}$, and volumetric mean heat output rate $w_{h,v}$, of packed beds (P_h = 361 kPa, T_{evap} = 140°C)

Then, the electrical power output can be increased in a second time by operating the heat output mode. The heat output released by hydration of packed beds is used for reheat steam before it enters the LP turbine stages, as illustrated on Fig. 6.7 and Fig. 6.8. The new steam enthalpy ($h_{in,LP}$ [kJ kg^{-1}]) at

the inlet of the LP turbine stages was calculated with Eq. 6.3

$$h_{\text{in,LP}} = h_{\text{out,IP}} + \frac{q_{\text{h,v}} \cdot V}{t_{\text{h}} \cdot m'} = h_{\text{out,IP}} + \frac{w_{\text{h,v}} \cdot V}{m'} \qquad (6.3)$$

where V is the volume of the packed bed [m^3] previously calculated, t_h the time of hydration (30 min), m' is the mass flow of steam [kg s^{-1}], $h_{\text{out,IP}}$ and $h_{\text{in,LP}}$ [kJ kg^{-1}] are respectively the enthalpies of steam at the outlet of the IP turbine stages and at the inlet of the LP turbine stages.

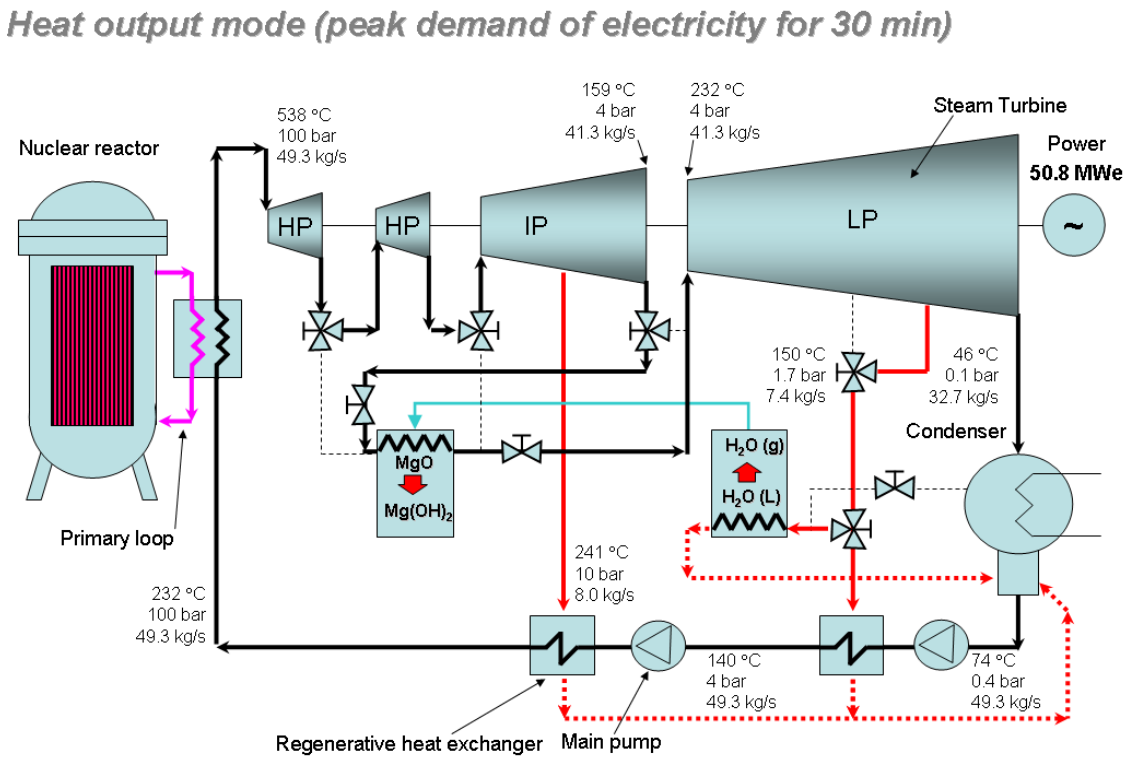

Fig. 6.7: System configuration and heat mass balance of the secondary loop including chemical heat storage operating the heat output mode

The gross thermal power output from the packed bed, W_t (= $w_{\text{h,v}} \cdot V$) [kW], results respectively 3.2 MWt for the $Mg(OH)_2$ bed and 3.6 MWt for the EM8 block. From the steam tables, for a given enthalpy and pressure (4 bar), it results that steam can be reheated to a temperature of 232°C in case of $Mg(OH)_2$ pellet and 240°C for EM8 block. However, this temperature is too close to the maximum temperature reached in the EM8 block experiments. In case of EM8 block, energy should be released at a lower rate; consequently, the time of heat output mode can be extended. By substituting in Eq. 6.3 the value of $h_{\text{in,LP}}$ of steam having a temperature of 232°C and pressure 4 bar and solving with respect of time t_h, it results that EM8 can operate for 33 min rather than 30 min. The larger value of steam enthalpy $h_{\text{in,LP}}$ permits to increase of the expansion work in the LP turbine stages and to increase the electrical power output (P_e) of +3.1% for 30 min (33 min in case of EM8) with respect of the design power. Histogram on Fig. 6.5 summarizes the average power output from the steam turbine in the three operation modes (design, heat storage mode and heat output mode, respectively). It refers to the results obtained when

storing and releasing thermal energy from in EM8 block. Because of its mold-ability, possibility to reduce the volume of the bed and enhanced thermochemical performances, EM8 demonstrated to be more practical than $Mg(OH)_2$ pellets for the utilization in a real reactor. EM8 can contribute actively to the management of thermal energy in the next generation of nuclear power stations.

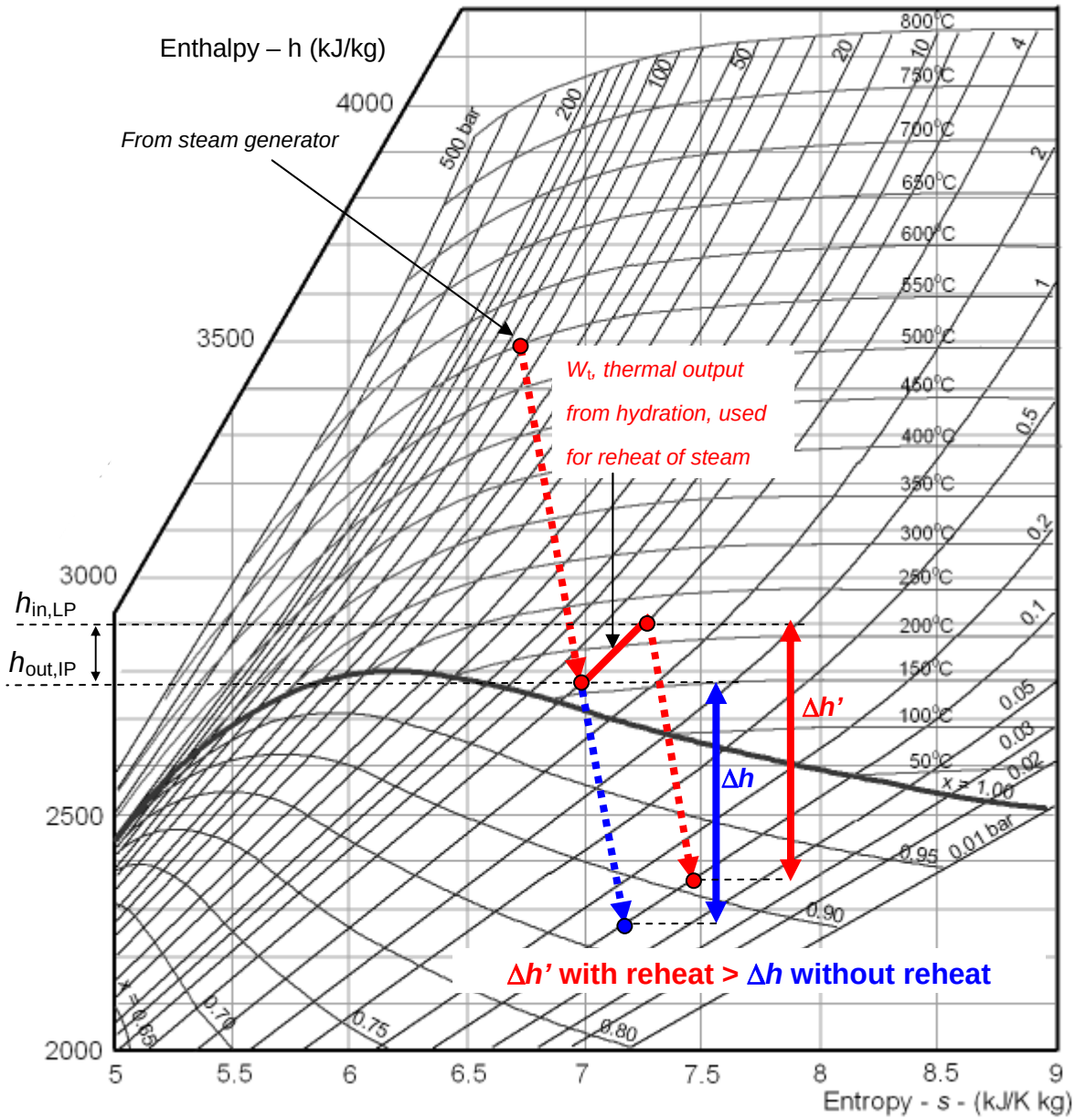

Fig. 6.8: Mollier diagram of steam, the amount of heat W_t (thermal power output from hydration) is utilized for steam reheating and increase the enthalpy at the end of the IP stage of the turbine.

Table 6.2 Results of the heat and mass balance calculations

Items	Values
Available thermal power from steam by-pass, $m' \cdot (h_{HP,out} - h_{HP,in})$	3.6 MWt
Available thermal energy from steam by-pass (in 1 hour)	12,816 MJ
Mole reacted fraction change of $Mg(OH)_2$ after 60 min, Δx_d	–0.49
Mole reacted fraction change of EM8 after 60 min, Δx_d	–0.55
Mole reacted fraction change of $Mg(OH)_2$ after 30 min, Δx_h	+0.44
Mole reacted fraction change of EM8 after 30 min, Δx_h	+0.55
Required volume of $Mg(OH)_2$, $V_{Mg(OH)2}$	30.0 m^3
Required volume of EM8, V_{EM}	17.7 m^3
Gross thermal power output from $Mg(OH)_2$ pellets, W_t (= $w_{h,Mg(OH)2} \cdot V_{Mg(OH)2}$)	3.2 MWt
Gross thermal power output from EM8, $w_{h,EM} \cdot V_{EM}$	3.6 MWt
LP turbine inlet steam temperature / pressure (reheated by the mean heat output of hydration)	232°C / 4 bar
Average electrical power output during heat storage mode	45.8 MWe
Average electrical power output during heat output mode(W_e)	50.8 MWe

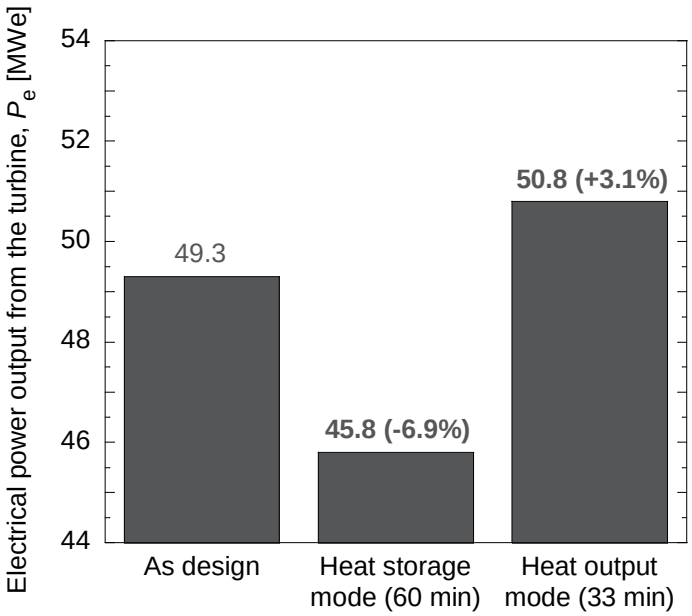

Fig. 6.5: Comparison of the gross electrical power output (P_e) from the turbine in three operation modes calculated from EM8 block experimental results.

6.3. Conclusions

Chemical heat storage materials have been applied for leveling the thermal and electric power output in a nuclear power station. The heat storage capacity and gross heat output calculated from the packed bed experiments have been utilized for a numerical analysis in a modified Rankine cycle of a nuclear power station. For a heat storage of 3.6 MWt in 1 hour, a bed filled with 17.7 m^3 of EM8 (block) was required, while the same amount of thermal energy could be stored in a $Mg(OH)_2$ bed of pellets of 30.0 m^3;. The volume of EM8 block required for storing the same amount of thermal energy of $Mg(OH)_2$ pellets resulted 41% smaller. It was estimated that the average electrical power output from the turbine could be decreased of –6.9% with respect of the design power when operating the heat storage mode for 60 minutes. By operating the heat output mode, the average electrical power output in 33 minutes resulted +3.1% higher than the design power. EM8 can contribute actively to the management of thermal energy in the next generation of nuclear power plants.

6.4. References

[1] D.T. Ingersoll, Deliberately small reactors and the second nuclear era, Progress in Nuclear Energy, 51 (2009) 589-603

[2] S. Vazquez, S. M. Lukic, E. Galvan, L.G. Franquelo, J.M. Carrasco, Energy Storage Systems for Transport and Grid Applications , IEEE Transactions on Industrial Electronics 2010, Vol. 57 (No. 12) 3881–95

[3] K. Shimizu, I. Minatsuki, K. Ujimori, Y. Mizokami, A. Terada, Small-sized high temperature reactor (MHR-50) for electricity generation: Plant concept and characteristics, Progress in Nuclear Energy, 53 (2011) 846-854

Massimiliano Zamengo, Y. Kato Laboratory, RLNR, Tokyo Institute of Technology

A Study on Heat Transfer-Enhanced Composites for a Magnesium Oxide/Water Chemical Heat Pump

Chapter 7

Conclusion

7. CONCLUSION

In order to cut emissions of CO_2 and pollutants from combustion of fossil fuels by utilizing small nuclear reactors for cogenerating purposes in industry, it would be difficult accept sudden load variations derived from the production cycles. The possibility to utilize a heat storage technology in a small cogenerating nuclear power plant would make easier to manage such variations. The magnesium oxide / water chemical heat pump (MgO/H_2O CHP) has been studied as a technology for heat storage and load leveling in cogeneration systems or for recovering unused heat from industrial processes at temperatures in the range between 350 and 450°C. Such a chemical heat storage technology is still difficult to be utilized in practical application because of the low values of thermal conductivity of $Mg(OH)_2$ and MgO and the contact resistance between material and heat exchanger surface. This research aimed to develop a high performance material which could be used in practical application. It is required that such a material has the ability to respond promptly to load variations, therefore exchange large quantities of heat in a short time. Expanded graphite (EG) was utilized for enhancing the heat transfer properties. A composite material of EG and $Mg(OH)_2$ was developed. It was compressed in order to increase thermal conductivity and heat storage capacity. The volume of chemical heat storage materials for load leveling in a cogeneration power plant was determined.

In **Chapter 1**, “Introduction”, the background of the research and the current status were reviewed. The principles of MgO / H_2O chemical heat pump and the importance of chemical heat storage were illustrated. The main issues of the technology were presented and the objectives of research were listed.

In **Chapter 2**, “Experimental apparatus and procedures”, the apparatuses and instruments used in this research were described. Thermo-gravimetric apparatus (TG) was used for studying the reaction kinetics and evaluate the reaction rate constants. Thermal conductivities were measured with a thermal conductivity meter. The main results were obtained on a unique of a kind packed bed reactor apparatus. It allowed studying the effects of heat transfer and conducting hydration reactions at pressure larger than in the TG apparatus. The definition and the equations for calculating the thermochemical performances parameters were given.

In **Chapter 3**, “Materials and evaluation of their properties”, the materials used in the experiments were described. The preparation method of the Expanded graphite (EG) and Magnesium hydroxide composite ($Mg(OH)_2$), called EM, was explained. EM showed mold-ability, high thermal conductivity and endurance to repetitive cyclic reactions. SEM photographs showed the effective attachment between $Mg(OH)_2$ and EG before and after cyclic experiments. Three kind of EM composite were prepared, characterized by a different mass mixing ratio $Mg(OH)_2$ to EG, r_{mix} [-], respectively 16:1, 8:1 and 4:1. They were called respectively EM16, EM8 and EM4. Thermal conductivity of EMs was

measured. It was observed that thermal conductivity of EM slabs had anisotropic behavior. Thermal conductivity of EM4 resulted 1.9 W m^{-1} K^{-1}, which is more than 10 times larger than the thermal conductivity of a packed bed of $Mg(OH)_2$ pellets (0.16 W m^{-1} K^{-1}). Kinetic analysis was conducted using TG apparatus on those EM materials, previously compressed in tablet shape (diameter ϕ = 7.0 mm, average thickness *l* = 3.5-4.5 mm). It showed that EG did not change sensitively the reaction rate of dehydration in such a small scale experiments. The results of materials characterization were used in Chapter 5 for the numerical analysis of dehydration in the packed bed reactor apparatus.

In **Chapter 4**, "Packed bed reactor experiments", the results obtained from the packed bed reactor experiments (dehydration and hydration) were shown. Under identical dehydration conditions, the higher thermal conductivities of packed beds comprising EM tablets made it possible to reach higher and more homogeneous temperatures, leading to an enhancement of the reaction rate. Compared with pure $Mg(OH)_2$ bed of pellets, the dehydration reaction in the EM packed beds was completed in a shorter time. The heat-storage capacity, q_d, per unit mass of $Mg(OH)_2$ was higher for the EM beds in the chemical heat pump experiments. The use of EG as a thermal conductivity enhancer also proved advantageous for the hydration reaction; the EM beds of tablets showed a larger change in the mole reacted fraction than did the pure $Mg(OH)_2$ bed of pellets. The temperature observed during hydration indicated that the removal of reaction heat progressively improved with the addition of EG. Additionally, the calculated gross heat output, q_h, and mean heat-output rate, w_{mean}, of the EM beds were greater than the corresponding values for pure $Mg(OH)_2$ bed. EM8, which corresponds to a mass ratio r_{mix} = 8:1, performed better than EM16 and EM4. EM8 dehydrated as fast as EM4, but the power output from hydration of the former was larger than the latter. EM8 was then utilized for other experiments, in which the volumetric heat storage capacity was increased by decreasing the void fraction of the bed. Finally, the reactor was filled completely with an EM8 block, which ensured an improved contact with the heater's surface. The EM8 block had a mean heat output rate in 30 minutes of hydration at 361 kPa of 407 kW m_{bed}^{-3}, which is almost two times larger than 218 kW m_{bed}^{-3} obtained the $Mg(OH)_2$ bed of pellets. EM8 block demonstrated to be the optimal solution as chemical heat storage material and heat output at temperatures of 230-240°C. In case of hydration at low pressure (47 kPa) EM8 block has still better performance than $Mg(OH)_2$, but it is necessary to improve the diffusion of water vapor in order to let the hydration to be conducted with higher rates of reaction.

In **Chapter 5**, "Numerical analysis of packed bed reactor", a transient heat transfer problem with chemical reaction has been solved by compiling a FORTRAN code. The results of simulations agreed with experimental results. It could explain that the larger thermal conductivity of a bed containing EM8 tablets (diameter ϕ = 10.0 mm, average thickness *l* = 6.5 mm, arranged in piles into the reactor) enhanced heat transport in the packed bed from the heated wall through to the center. Local conversion of $Mg(OH)_2$ to MgO were calculated in several positions of the packed bed and indicated that 7 minutes after starting bed heating, the bed of EM8 piled tablets started to store heat also at the central

position, but this was possible only after 15 minutes for the $Mg(OH)_2$ bed. The model was useful to understand in detail the reaction in the packed bed reactor and can be utilized in future for further investigations or design of new reactors.

In **Chapter 6**, "Utilization of the chemical heat storage for thermal load leveling in nuclear power plants", the utilization of the chemical heat storage for thermal load leveling in power station was discussed. A model of a system including the Rankine cycle of a nuclear power plant and a chemical heat storage reactor was proposed. The system would accumulate heat rather than convert it into electricity during the low demand periods. When electricity demand reaches peak, heat would be released and reused for reheating steam and increase the electrical power production from the turbine. The heat storage capacity and gross heat output calculated from the packed bed experiments were utilized for the numerical analysis. For a heat storage of 3.6 MWt in 1 hour, a bed filled with 17.7 m^3 of EM8 (block) was required, while the same amount of thermal energy could be stored in a $Mg(OH)_2$ bed of pellets of 30.0 m^3. The volume of EM8 block required for storing the same amount of thermal energy of $Mg(OH)_2$ pellets resulted 41% smaller. It was estimated that the average electrical power output from the turbine could be decreased of –6.9% with respect of the design power when operating the heat storage mode for 60 minutes. By operating the heat output mode, the average electrical power output in 33 minutes resulted +3.1% higher than the design power.

It was demonstrated experimentally that an EM8 composite block had superior performances for chemical heat storage and chemical heat pump operations than of a packed bed of $Mg(OH)_2$ pellets. The employment of EG made it possible to overcome the heat transfer issues typical of the packed bed of $Mg(OH)_2$ pellets developed in previous studies. The EM8 composite is expected to be utilized for harvesting, storing and reutilizing surplus amounts of heat at temperatures of 350–450°C from nuclear reactors, cogeneration systems and industrial processes. Its utilization for the management of thermal and electrical energy demands would contribute actively to an efficient and sustainable utilization of primary energy sources.

Nomenclature

h: enthalpy of steam [kJ kg^{-1}]

M: molecular weight [g mol^{-1}]

m: initial charged material weight [g]

m': mass flow of water / steam in the Rankine cycle [kg s^{-1}]

P: pressure [kPa]

q_d: dehydration heat storage capacity per unit mass of reactant [kJ $kg_{Mg(OH)2}^{-1}$]

q_h: hydration gross heat output per unit mass of reactant [kJ $kg_{Mg(OH)2}^{-1}$]

$q_{d,v}$: dehydration heat storage capacity per unit volume of packed bed [kJ m_{bed}^{-3}]

r_{mix} mass mixing ratio $Mg(OH)_2$:EG [g of $Mg(OH)_2$:g of EG]

s: pellet thickness [m]

P_e: Electrical power output from the steam turbine [MW]

Q_d: Heat stored during the dehydration [MJ]

R: radius of packed bed [m]

s: Heat stored per unit time per unit volume during dehydration [kJ s^{-1} m^{-3}]

T: temperature [°C]

t: reaction time [min]

x reacted fraction [-]

x_{ini} initial reacted fraction at reaction cycle onset [-]

w_{mean}: hydration mean heat output rate per unit mass of reactant [W $kg_{Mg(OH)2}^{-1}$]

$w_{mean,v}$: hydration mean heat output rate per unit volume of packed bed [W m_{bed}^{-3}]

W_t Thermal power output of hydration [MW]

Z: height of packed bed [m]

ΔH: standard enthalpy change of reaction [J mol^{-1}]

Δm: weight change of reactor [g]

Δx: mole reacted fraction change [-]

α: mole unreacted fraction [-]

ε: void fraction of the packed bed [-]

ϕ: pellet diameter [m]

γ: shape coefficients for pellets [-]

ρ: density [g cm^{-3}]

ξ: local concentration of $Mg(OH)_2$ in the packed bed reactor [%]

ψ: mass mixing ratio $Mg(OH)_2$:EG [g of $Mg(OH)_2$:g of EG]

Subscripts

bed packed bed

bound boundary

center	center of the packed bed
d	dehydration
EG	expanded graphite
EM	composite material (Expanded graphite mixed with Magnesium hydroxide)
h	hydration
in	inlet
$Mg(OH)_2$	Magnesium hydroxide
middle	position *R*/2 along the radius of the packed bed
out	outlet
pc	phase change of water system
pellet	pellet
r	Magnesium oxide/water reaction system
v	volumetric, expressed per unit volume
wall	reactor's wall
1–7	indexes of thermocouple positions

Acknowledgments

I would like to express my deep gratitude to Professor Kato and Professor Ryu, for their encouragement, suggestions and discussion for this research work. I would also like to thank Dr. Fujioka, for her questions and advice received while at Conferences. I am particularly grateful for the assistance given by Atsumi Foundation, providing me the scholarship for this last final year of Doctoral Course.
I wish to acknowledge the help provided by the students I met at Kato Laboratory in these years, in particular Dr. Ishitobi, Dr. Kim, Ms. Odko and Mr. Kariya, especially with the TG experiments.
I would also like to extend my thanks to the technician of the laboratory of the RLNR for his help in the preparation of molds used in the experiments.
Last but not least, I wish to thank my Family for their encouragement throughout my study.